R-Mode implementation on VHF

Issue: 2.0
Issue Status: Approved
Issue Date: 22/10/2021

	Name	Partner	Signature
Provided	Armin Dammann	DLR	
Review	Armin Dammann	DLR	
Approval	Stefan Gewies	DLR	

Document Information

Project Title	R-Mode Baltic
Work Package No.	GA 5.3
Document Title	R-Mode implementation on VHF
Description	Report which covers the results of this GA5.3: • VHF ranging signal design and performance results • The proposed R-Mode ranging signal for application within the VHF digital exchange system. • A description of experiments and corresponding results regarding ranging and positioning using the designed R-Mode VHF signals.
Date	22.10.2021
Lead Author	Armin Dammann
Lead Author's Contact Information	German Aerospace Center (DLR) Institute of Communication and Navigation Department of Communication Systems Telephone: +49 8153 28 2871 E-mail: Armin.Dammann@DLR.de
Contributing Author(s)	Krzysztof Bronk, Magdalena Januszewska, Adam Lipka, Patryk Koncicki, Rafał Niski, Błażej Wereszko (all NIT) Markus Wirsing, Ronald Raulefs (all DLR)
Approval	Yes

Track Changes

Issue	Date	Pages	Change	Author, Company
1.0	17/09/2021	111	Initial version	Armin Dammann (DLR)
2.0	22/10/2021	112	Minor changes by NIT included	Armin Dammann (DLR) Krzysztof Bronk (NIT)

This report was created within the framework of the **R-Mode Baltic** project, which aims to develop and demonstrate a new maritime backup system for Position, Navigation and Time (PNT) purposes based on R-Mode technology. Within the project life time of three years the project consortium develops solutions for R-Mode transmitter and receiver prototypes, for independent time synchronizations of broadcasting stations and for a testbed concept and its deployment. The dissemination of R-Mode technology is supported by work in international standardization bodies. The world's first operational testbed for a transnational R-Mode system will be completed by the project in 2020.

The R-Mode Baltic project is co-financed by the European Regional Development Fund within the Interreg Baltic Sea Region Programme.

This report is available for download on the project website www.r-mode-baltic.eu.

Executive Summary

The original aim of this Group of Activities was to work on the development and verification of the R-Mode implementation for an accurate estimation of (pseudo-) ranges between an AIS transmitter and receiver.

Therefore, work in GA5.3 started with developing ranging signals, which are tailored to be transmitted within the AIS channels. Signal designs coming from the ACCSEAS project have been the basis and benchmark for the R-Mode Baltic ranging signal designs.

The R-Mode Baltic signal design performance criteria has been the R-Mode signals' time-of-arrival (ToA) estimation variances, which consequently provide (pseudo-) range estimates. For designing R-Mode signals with respect to ToA estimation performance estimation theoretic tools like the Cramer-Rao and Ziv-Zakai lower bounds have been used. The designs have been verified by simulations. Evaluations have shown that transmitting ranging signals coherently in both of the AIS channels, either parallel in time or sequentially with known time offset, provides more than one order of magnitude gain in ranging performance compared to using only a single AIS channel for ranging. For the case of coherently using 2 AIS channels for ranging, the additional transmission of CW signal components provides negligible performance gains only, but comes with additional implementation complexity and an increased PAPR compared to a coherent sequential use of the 2 AIS channels. The ranging performance, predicted by theory and simulation, for coherently using 2 AIS channels for one AIS time slot is in the order of 1 meter for a receiver input power of -100 … -90 dBm.

During the lifetime of the R-Mode Baltic project the focus of a R-Mode implementation in the VHF band has been changed. Instead of an implementation in the AIS channels, an R-mode implementation within the VHF Digital Exchange System (VDES) has been foreseen in standardization. VDES covers a continuous downlink spectrum of 100 kHz, and therefore, provides an additional ranging performance gain compared to using 2 AIS channels as mentioned above, such that sub-meter accuracy is predicted at receiver input power levels of -100 … -90 dBm. In order to be compliant with the modulation scheme of VDES, the VDES ranging signal design in this GA has been focused of optimizing ranging bit sequences. These ranging bit sequences provide, when fed into a VDES modulator, the VDES ranging baseband signal. The proposed R-Mode Baltic VDES ranging signal consists of two components which are a pseudo-noise Gold sequence and a so-called alternating sequence. The alternating sequence is designed such that the equivalent bandwidth of the corresponding VDES ranging signal is increased, thus providing ranging performance improvements at higher signal-to-noise ratios (SNRs) at the receiver compared to a pseudo-noise Gold sequence which predicts better performance at lower SNRs. The VDES R-Mode Baltic ranging sequence is a combination of both components mentioned above. The combination is a timely sequential multiplex of the 2 components, where the ratio between the duration of the two components can be controlled by a single parameter. With this VDES R-Mode ranging signal construction, the transmitted ranging signal can be adapted to the SNR in different environments. The signal designed proposed by R-Mode Baltic GA5.3 has been included into the VDES R-Mode IALA guideline G1139.

For sequence-by-sequence (snapshot) ToA estimation cross-correlation based approaches have been used for simulations and for signal processing in experiments. Assuming line-of-sight and additive white Gaussian noise (AWGN) propagation conditions, such an approach is known to provide maximum likelihood ToA estimation. For sequential ToA estimation Kalman filters have been used for exploiting ToA correlations in time.

Several experiments at the Baltic Sea near Gdynia, Poland, and at Lake Ammer, Germany, were performed to validate the proposed R-mode Baltic VDES ranging sequences. Using Bayesian position estimation approaches, such as Kalman filtering, showed that positioning accuracy in the order of 10 meter is possible with the proposed signal design.

With the activities described above, GA5.3 has completed the planned work, including adjustments to reflect advances in ongoing VDES R-Mode standardization. GA5.3 results have been published at scientific conferences and journals.

Contents

List of Tables

List of Figures

Abbreviations

AIS	Automatic Identification System
A/D	Analog/Digital
ASM	Application Message Service
AWGN	Additive White Gaussian Noise
BER	Bit Error Rate
BLER	Block Error Rate
BPSK	Binary Phase Shift Keying
CDF	Cumulative Distribution Function
CDMA	Code Division Multiple Access
CRB	Cramér-Rao-Bound
CRC	Cyclic Redundancy Check
CRLB	Cramér-Rao Lower Bound
CW	Continuous Wave
D1, D2	Distances between pairs of samples in a multicorrelator
DFT	Discrete Fourier Transform
DLL	Delay Locked Loop
DLR	Deutsches Zentrum für Luft- und Raumfahrt (German Aerospace Center)
DOP	Dilution of Precision
EGNOS	European Geostationary Navigation Overlay Service
EIRP	Effective Isotropic Radiated Power
ERP	Effective Radiated Power
FD	Frequency Domain
FDMA	Frequency-Division Multiple Access
FEC	Forward Error Correction
GA	Group Activity
GDOP	Geometric Dilution of Precision
GMSK	Gaussian Minimum Shift Keying
GNSS	Global Navigation Satellite System
GPS	Global Positioning System
GPSDO	GPS Disciplined Oscillator
IALA	International Association of Lighthouse Authorities
I&D	Integration and Dump
INS	Inertial Navigation System
I/Q	Inphase/Quadrature
ITDMA	Incremental Division Multiple Access

LNA	Low Noise Amplifier
LoS	Line of Sight
LPF	Low-pass filter
L1,L2,E1,E2	Sample positions in a multicorrelator
MAC	Media Access Control
MCS	Modulation and Coding Scheme
MOG	Maritime Office in Gdynia
NCO	Numerically Controlled Oscillators
NIT	National Institute of Telecommunications, Poland
NLoS	Non Line of Sight
NRZI	Non Return to Zero Inverted
MF	Medium Frequency
PAPR	Peak-to-Average Power Ratio
PLL	Phase Locked Loop
PN	Pseudo Noise
PNT	Position, Navigation and Time
PPS	Pulse Per Second
PRN	Pseudorandom noise
PSD	Power Spectrum Density
PSK	Phase Shift Keying
QAM	Quadrature Amplitude Modulation
QPSK	Quadrature Phase Shift Keying
R-Mode	Ranging Mode
RMS	Root Mean Square
RMSE	Root Mean Square Error
RRC	Root Raised Cosine
RTK	Real Time Kinematic
RX	Receiver
SDR	Software Defined Radio
SNR	Signal to Noise Ratio
SOTDMA	Self-organized time-division multiple access
SWR	Standing Wave Ratio
TD	Time Domain
ToA	Time of Arrival
TX	Transmitter
UKF	Unscented Kalman Filter

UMTS	Universal Mobile Telecommunication System
USRP	Universal Software Radio Peripheral
UTC	Coordinated Universal Time
VDE	VHF Data Exchange
VDES	VHF Data Exchange System
VDE-TER	VHF Data Exchange Terrestrial
VHF	Very High Frequency
VSWR	Voltage Standing Wave Ratio
ZZB	Ziv-Zakai Bound

1 Introduction

Current position information of vessels is relevant for safety and navigation applications. The Automatic Identification System (AIS) utilizes the information by broadcasting it together with heading, current velocity and more detailed information about the vessel itself. The Global Navigation Satellite Systems (GNSSs) are the primary systems determining positions and its derivatives, such as velocity and heading. Recent events, such as the Galileo outage in July 2019, have shown that the satellite-based systems cannot always be relied on to determine the location. Therefore, it is desirable to have an additional implementation method of localization for monitoring the integrity of the GNSS and as well as for navigation in case the satellite system fails. Such failure could be a solar storm which primarily affects space-based systems, but could also be a local event in case of intentional jamming or even spoofing.

Therefore, the International Association of Marine Aids to Navigation and Lighthouse Authorities (IALA) discusses the need of a contingency or even backup system for GNSS. A backup system requires fulfilling similar performance requirements as the primary system, such as GPS. A contingency system has weaker performance requirements, especially the holdover time until the clock of the transmitters causes significant errors in determining the position. However, system requirements shall assure a safe travel of a vessel back to the harbor in case of a significant GNSS failure. The proposal is called Ranging-Mode or R-Mode. R-Mode intends to utilize the shore-based communication infrastructure, like AIS base stations [JS14] with the existing housing infrastructure. The accuracy of ranges between the base station on land and the vessel at sea, measured by means of the received radio signal, depends on the utilized bandwidth and on the received signal power versus the power of other noise sources. AIS offers 25 kHz of bandwidth and uses a Gaussian Minimum Shift Keying (GMSK) modulated signal. Currently, IALA defines the VHF data exchange system (VDES) that comprises of the existing AIS, and an additional application message service (ASM) and the VHF data exchange (VDE). VDE has a terrestrial and a satellite component. The terrestrial component offers in the up- and downlink 25 kHz each. AIS and VDE have already been investigated regarding R-Mode. The authors in [HJZSZ15] investigated the AIS system and its existing infrastructure and how it could be used for ranging and positioning. A key aspect that was stressed is the impact of the Geometric Dilution of Precision (GDOP) and is limited to coastal areas. It was concluded that because of cost issues that a precise clock on the vessel seems unfeasible. An additional secondary factor was applied which increased the performance by an order of magnitude. However, the proposed site requirements are challenging to cope with the limited bandwidth of AIS to achieve 10m ranging accuracy. The concept of using AIS as a ranging source was further proposed and addressed in [GDZB+18]. The concept described the application of R-Mode in the Baltic Sea which covers relevant areas with a favorable GDOP. The concept is expanded further to the MF frequency band to increase the coverage of individual transmitter sites. Therefore, a joint R- Mode system concept utilizing AIS and MF was proposed. The MF-R-Mode has significant advantages by using only limited infrastructure as the propagation conditions during day time can reach several hundred km. However, during the night the skywave effect causes severe multipath errors which prohibit a night-time use of MF-R-Mode. In [SGWW20] the authors derived the Cramér-Rao bounds for AIS, ASM and VDE considering the different bandwidths of all three systems. They also considered five successive time slots in AIS and three successive time slots for ASM to improve the ranging performance and to compete with the terrestrial 100 kHz VDE system. The authors applied the ITU-R P.1546-5 channel model with distinct antenna heights to provide realistic assessments about the expected range. The authors concluded that the focus should be on VDE because of the superior performance results.

2 R-Mode Range and Position Estimation

2.1 Range Estimation

Since VDES R-mode is based on multi-lateration, it is necessary to estimate the ranges between the receiver and several base stations. This is done by estimating the time of arrival of a signal sent from the base station with a known time of transmission. Thus, the performance of the time of arrival estimator is important to the overall accuracy of the VDES R-Mode system.

In order to evaluate this performance, we consider a signal at the receiver that can be modeled as a time delayed version of the transmitted signal corrupted by additive white Gaussian noise. In this paper, we assume that the clocks at the base station and the receiver are synchronized. Under these conditions, the received signal can be modeled as

$$x(t) = s(t-\tau) + w(t), \tag{2-1}$$

where $s(t)$ is the transmitted signal, and $w(t)$ is the additive white Gaussian noise with a noise power spectral density of N_0. We are interested in estimating the parameter τ which is the delay between the transmission of the signal and its arrival at the receiver. Together with the propagation speed c_0 of the signal, an estimation

$$\hat{r} = c_0 \cdot \hat{\tau} \tag{2-2}$$

for the distance between transmitter and receiver, i.e., the range r, can then easily be calculated from a time estimate $\hat{\tau}$.

2.1.1 Cramér-Rao-Bound

The first bound which we consider is the Cramér-Rao-Bound (CRB). For the given problem of estimating the time of arrival of a ranging signal, the CRB for an unbiased estimator states that [Kay93]

$$\mathrm{var}(\hat{r}) = {c_0}^2 \,\mathrm{var}(\hat{\tau}) \geq \frac{{c_0}^2}{8\pi^2 \frac{E_s}{N_0} \overline{F^2}}, \tag{2-3}$$

where $\mathrm{var}(\hat{r})$ denotes the variance of the range estimate $\hat{r}$, $E_s = \int_{-\infty}^{\infty} |s(t)|^2 \,\mathrm{d}t = \int_{-\infty}^{\infty} |S(F)|^2 \,\mathrm{d}F$ is the energy of the ranging signal, N_0 is the noise power density, and

$$\overline{F^2} = \frac{\int_{-\infty}^{\infty} F^2 \,|S(F)|^2 \mathrm{d}F}{\int_{-\infty}^{\infty} |S(F)|^2 \,\mathrm{d}F} \tag{2-4}$$

is mean square bandwidth of the signal [Kay93]. This indicates that an important signal parameter for range estimation is its bandwidth So according to the CRB, the signal's energy should be located at the edges of the available spectrum for maximizing ranging performance.

2.1.2 Ziv-Zakai Bound

For a given signal, the CRB is often a fairly good indicator for achievable estimation performance at sufficiently high signal-to-noise ratios (SNR). At low SNR values, however, the

achievable estimation performance is usually much lower than indicated by the CRB. Up to a certain SNR value, reliable range estimation is hard to achieve. This is known as the threshold effect. To take this phenomenon into account, we also consider the Ziv-Zakai Bound (ZZB), which, unlike the CRB, takes this phenomenon into account. The ZZB is based on a comparison of the estimation problem with a detection problem.

The ZZB for time of arrival estimation is given by [CZZ75]

$$\mathrm{var}(\hat{r}) = {c_0}^2\,\mathrm{var}(\hat{\tau}) \geq {c_0}^2 \int_0^T h \cdot \left(1 - \frac{h}{T}\right) \cdot P_e(h)\,\mathrm{d}h \qquad 2\text{-}5$$

where the integration interval $[0, T]$ represents an a-priori time interval, within which τ is assumed to be uniformly distributed, and $P_e(h)$ is the error probability of an optimal detector deciding between the two signal hypotheses $s(t)$ and $s(t-h)$. This probability can be expressed by

$$P_e(h) = \mathrm{Q}\left(\sqrt{\frac{E_s}{2N_0}(1 - \mathrm{real}(\rho(h)))}\right) \qquad 2\text{-}6$$

where $\rho(h)$ is the autocorrelation function of signal $s(t)$, normalized to the signal's energy E_s and given by

$$\rho(h) = \frac{1}{E_s}\int_{-\infty}^{\infty} s\,(t)\,s^*(t-h)\,\mathrm{d}t. \qquad 2\text{-}7$$

The Q-function is defined as $\mathrm{Q}(x) = \frac{1}{\sqrt{2\pi}}\int_x^\infty e^{-\frac{u^2}{2}}\,\mathrm{d}u$.

To calculate the ZZB according to Eq. 2-5 of this kind of signal, we need to determine its normalized autocorrelation function according to Eq. 2-7. This can be achieved by creating a sampled representation of the signal $s[n] = s(nT_s)$ with a sufficiently high sampling rate $f_\mathrm{s} = \frac{1}{T_\mathrm{s}}$.

Figure 2-1 shows the ZZB for range estimation standard deviation for a signal with $\gamma = \frac{1}{3}$ and corresponding simulation results for an a-priori integration interval of $\mathrm{T} = 12.5\,\mathrm{T_{sym}} = 162.8\,\mu s$. At an SNR range of $10 \ldots 15\,dB$, both, ZZB and simulation results show the threshold effect mentioned above as a severely degrading ranging performance.

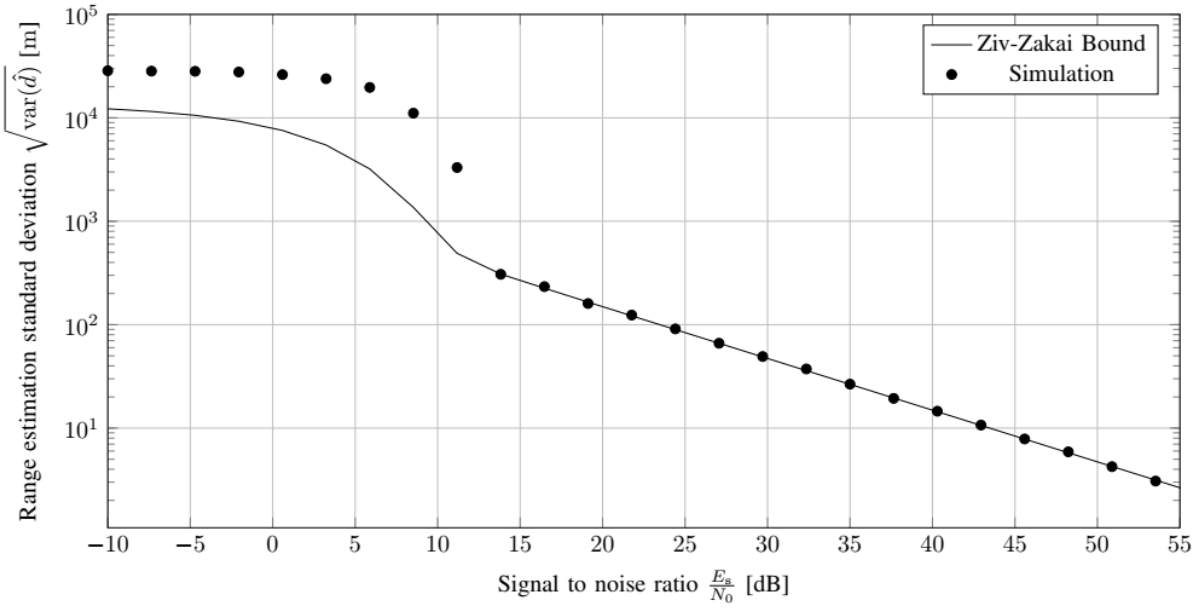

Figure 2-1: Ziv-Zakai Bound for ToA based range estimation.

2.2 Velocity Estimation

In addition to the distance between the transmitter and the receiver, it is possible to determine the radial velocity v_r as well by taking the Doppler effect into account. Due to the radial velocity between transmitter and receiver, a Doppler shift

$$\Delta f = -\frac{v_\mathrm{r}}{c_0} f_0 \qquad \text{2-8}$$

is observed at the receiver side. Note a positive radial velocity results from an increasing transmitter-receiver-distance and causes a negative Doppler shift. The ZZB for Doppler frequency estimation can be derived in a similar way to the ZZB for ToA estimation. The time domain autocorrelation function that was needed for the ToA case, needs to be replaced by a frequency domain autocorrelation function

$$\rho(\Delta f) = \frac{1}{E_s} \int_{-\infty}^{\infty} S\,(f) S^*(f - \Delta f)\,\mathrm{d}f, \qquad \text{2-9}$$

or equivalently by

$$\rho(\Delta f) = \frac{1}{E_s} \int_{-\infty}^{\infty} |s(t)|^2 \cdot \mathrm{e}^{\mathrm{j}2\pi\Delta f t}\,\mathrm{d}t. \qquad \text{2-10}$$

using Fourier transformation properties. If we consider a sampled representation $s(kT_s)$ of the signal, can be rewritten as

$$\rho(\Delta\,\mathrm{f}) = \frac{\sum_k |s(kT_s)|^2 e^{\mathrm{j}2\pi\Delta f k T_s}}{\sum_k |s(kT_s)|^2} \qquad \text{2-11}$$

which can be evaluated by numerical means. The ZZB for velocity estimation is given by

$$\begin{aligned}\mathrm{var}(\hat{v}_\mathrm{r}) &= \left(\frac{c_0}{f_0}\right)^2 \mathrm{var}(\Delta\hat{f}) \\ &\geq \left(\frac{c_0}{f_0}\right)^2 \int_0^{f_\mathrm{max}} \Delta f \cdot \left(1-\frac{\Delta f}{f_\mathrm{max}}\right) \cdot \mathrm{Q}\left(\sqrt{\frac{E_s}{2N_0}\left(1-\mathrm{real}(\rho(\Delta f))\right)}\right) \mathrm{d}\Delta f\end{aligned} \quad 2\text{-}12$$

where $\mathrm{var}(\hat{v}_\mathrm{r})$ denotes the variance of the velocity estimate $\hat{v}_\mathrm{r}$ and the integration interval $[0, f_\mathrm{max}]$ represents an a-priori frequency interval, within which Δf is assumed to be uniformly distributed. The ZZB according to and corresponding simulation results are shown in Figure 2-2 for an a-priori interval of $f_\mathrm{max} = 100\,Hz$. Compared to the results in Figure 2-1, the threshold effect is less pronounced because the autocorrelation function given by exhibits lower sidelobes than the time domain ranging signal autocorrelation function.

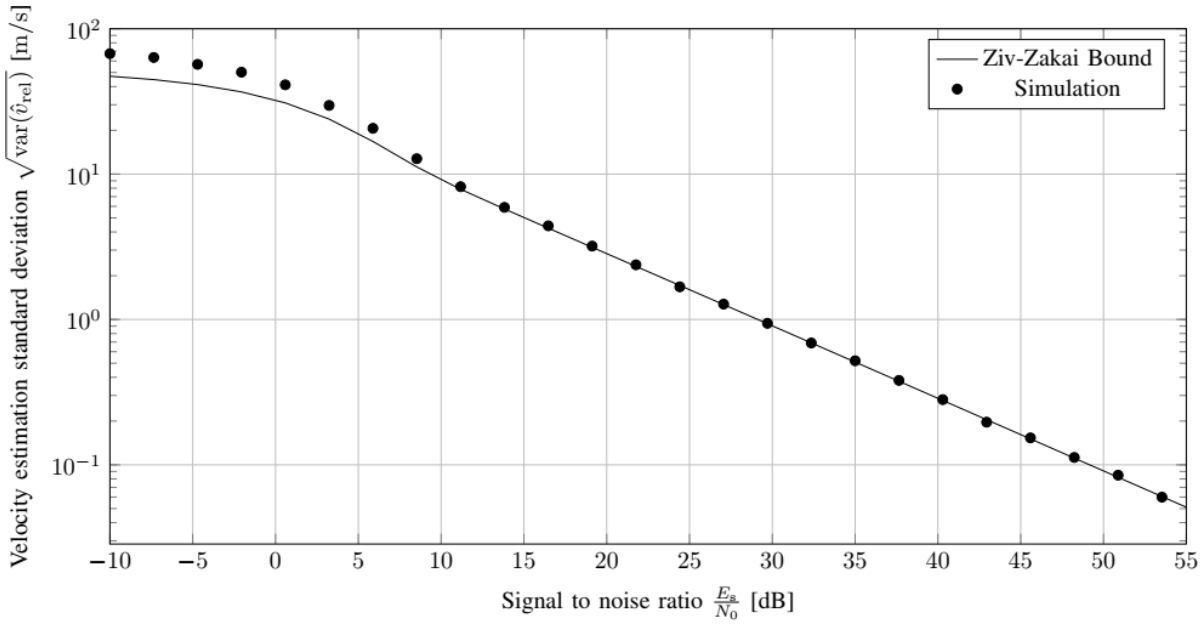

Figure 2-2: Ziv-Zakai Bound for Doppler based velocity estimation.

2.3 Position Estimation and Tracking using an Unscented Kalman Filter

To determine the position information, it is necessary to combine multiple range measurements into one position estimate. For the range estimates, as described in Sec. 2.1, this can be done on a snapshot basis for each individual set of measurements. In order to utilize the radial velocities, as described in Sec. 2.2, it is necessary to consider the receiver as a dynamic system.

A good tool to use for estimating the state of a dynamic system is the Kalman filter [Kay93]. The unmodified Kalman filter is applicable for linear systems only. The positioning problem though is nonlinear since the measured ranges and radial velocities cannot be expressed as a linear function of the receiver position. For this reason, we use an unscented Kalman filter (UKF), which is applicable to nonlinear problems as well [JU97]. The general working principle of a Kalman filter as well as a description of the unscented transform, which is the basis of the UKF, can be found in the literature [Kay93, JU97].

Thus, we present the UKF implementation, specific to the R-Mode system. The state vector that we use for the UKF is

$$\mathbf{x} = \begin{pmatrix} x \\ y \\ v_x \\ v_y \\ a_x \\ a_y \end{pmatrix}. \tag{2-13}$$

It contains the 2D-position consisting of x and y in a local Cartesian coordinate system, as well as 2D velocity and acceleration. The height is not considered, since we're dealing with a maritime system and the receiver is assumed to be at a constant height above the water. The clock bias and drift are also not considered here, however, they would need to be tracked as well for a practical implementation where the receiver does not have a highly accurate clock. The dynamics of the boat are modelled by a constant acceleration model, given by the differential equation

$$\frac{\mathrm{d}}{\mathrm{d}t}\mathbf{x} = \mathbf{A}\,\mathbf{x} \tag{2-14}$$

with

$$\mathbf{A} = \begin{pmatrix} 0 & 0 & 1 & 0 & 0 & 0 \\ 0 & 0 & 0 & 1 & 0 & 0 \\ 0 & 0 & 0 & 0 & 1 & 0 \\ 0 & 0 & 0 & 0 & 0 & 1 \\ 0 & 0 & 0 & 0 & 0 & 0 \\ 0 & 0 & 0 & 0 & 0 & 0 \end{pmatrix}. \tag{2-15}$$

The state transition matrix is then given by

$$\mathbf{F} = \mathrm{e}^{\Delta t \cdot \mathbf{A}} = \begin{pmatrix} 1 & 0 & \Delta t & 0 & \frac{\Delta t^2}{2} & 0 \\ 0 & 1 & 0 & \Delta t & 0 & \frac{\Delta t^2}{2} \\ 0 & 0 & 1 & 0 & \Delta t & 0 \\ 0 & 0 & 0 & 1 & 0 & \Delta t \\ 0 & 0 & 0 & 0 & 1 & 0 \\ 0 & 0 & 0 & 0 & 0 & 1 \end{pmatrix}, \tag{2-16}$$

where Δt is the time difference between the state updates. The system noise covariance matrix $\mathbf{Q}$ is assumed to be

$$\mathbf{Q} = q \begin{pmatrix} \frac{\Delta t^5}{20} & 0 & \frac{\Delta t^4}{8} & 0 & \frac{\Delta t^3}{6} & 0 \\ 0 & \frac{\Delta t^5}{20} & 0 & \frac{\Delta t^4}{8} & 0 & \frac{\Delta t^3}{6} \\ \frac{\Delta t^4}{8} & 0 & \frac{\Delta t^3}{3} & 0 & \frac{\Delta t^2}{2} & 0 \\ 0 & \frac{\Delta t^4}{8} & 0 & \frac{\Delta t^3}{3} & 0 & \frac{\Delta t^2}{2} \\ \frac{\Delta t^3}{6} & 0 & \frac{\Delta t^2}{2} & 0 & \Delta t & 0 \\ 0 & \frac{\Delta t^3}{6} & 0 & \frac{\Delta t^2}{2} & 0 & \Delta t \end{pmatrix}, \quad \text{2-17}$$

which corresponds to a white noise with variance q that only affects the acceleration of the receiver. The UKF allows to update the current position estimate with each new observation of a signal that is received from VDES R-Mode base stations. As the velocity of the ship is tracked in the UKF, it is easy to incorporate the measurements of the radial velocities into the evaluation. The observation vector $\mathbf{z}$ consists of the ranges r_n and the radial velocities $v_{\mathrm{r},n}$ to the respective base stations:

$$\mathbf{z} = \begin{pmatrix} r_1 \\ \vdots \\ r_N \\ v_{\mathrm{r},1} \\ \vdots \\ v_{\mathrm{r},N} \end{pmatrix}. \quad \text{2-18}$$

The expected observations $\mathbf{z}$ depending on the state vector $\mathbf{x}$ can be expressed by the nonlinear expressions

$$r_n = \sqrt{(x - x_n)^2 + (y - y_n)^2} \quad \text{2-19}$$

$$\mathrm{v_{r,n}} = \frac{\mathrm{v_x(x - x_n) + v_y(y - y_n)}}{\mathrm{r_n}} \quad \text{2-20}$$

with $n = 1, \ldots N$, where r_n and $v_{r,n}$ represent the range and radial velocity with respect to the n-th base station and x_n together with y_n represents the position of that base station.

Using a UKF allows us to utilize the Doppler measurements to track the ship's position. Notably, if a good estimate of the ship's velocity is known, such as tracked from a previous measurement, the radial velocity as defined in Eq. 2-20 still depends on the position and thus can be used for position estimates. Especially for small distances r_n, this effect is considerable. The computational complexity of the UKF is also suitable for real time tracking.

3 Spectrum Options

The original aim of this Group of Activities was to work on the development and verification of the R-Mode implementation for an accurate estimation of (pseudo-) ranges between an AIS transmitter and receiver.

Therefore, work in GA5.3 started with developing ranging signals, which are tailored to be transmitted within the AIS channels. Signal designs coming from the ACCSEAS project have been the basis and benchmark for the R-Mode Baltic ranging signal designs.

During the lifetime of the R-Mode Baltic project the focus of a R-Mode implementation in the VHF band has been changed. Instead of an implementation in the AIS channels, an R-mode implementation within the VHF Digital Exchange System (VDES) has been foreseen

3.1 Using the AIS Spectrum for R-Mode

3.1.1 R-Mode using a single AIS channel

As a benchmark for R-Mode ranging, we use one time slot of length $T_s = 26.7$ ms in one AIS channel having a channel bandwidth of 25 kHz. Within this time slot we transmit a ranging signal, which is a GMSK modulated random 256-bit sequence. We use GMSK modulation parameters as defined in the AIS standard [AIS14], which means a bit rate of $9600\ bit/s$ and a GMSK transmitter BT-product of 0.4.

Figure 3-1 shows the R-Mode ranging performance using a 1-slot ranging signal in 1 AIS Channel when applying a GMSK modulated random 256-bit sequence as ranging signal. As lower bounds we provide the Cramer-Rao (CRB) and Ziv-Zakai (ZZB) lower bounds for the ranging error standard deviation. Compared to these bounds simulation results are shown for different range estimation approaches.

- Time Domain (TD) estimation
  Range estimation is done in time domain (TD) by applying cross-correlation between the sampled received baseband signal and the sampled ranging baseband signal, which is transmitted. Since we are using time discrete sampled signals we get Time of Arrival (ToA) and consequently range estimated which are discrete in time. This leads to an error floor at high SNR values as it can be seen from Figure 3-1.
- Frequency Domain (FD) estimation
  In order to avoid the error floor of the TD simulation approach, we need an interpolation method to provide ToA estimates which are continuous in time. For that, we have implemented ToA estimation using cross correlation in frequency domain (FD). For this approach we apply a discrete Fourier transform to the received baseband signal and the sampled ranging baseband signal, which is transmitted. In frequency domain, signal delays correspond to a phase shift, which can be implemented using real, and therefore, continuous numbers.
- Non-Coherent estimation
  In practice, we usually observe a carrier phase shift at the receiver side, which is unknown, and therefore, has to be estimated in addition to the ToA. With this approach we apply a minimum mean-square error approach for estimation of the carrier phase offset. This results in maximizing the magnitude of the cross-correlation function

- Coherent estimation
  With this approach we assume that the carrier phase offset for ToA estimation is known. This assumption is a best case compared to the non-coherent case, described above. From simulation results we observe that the performance differences between coherent and non-coherent simulation approaches are negligible.

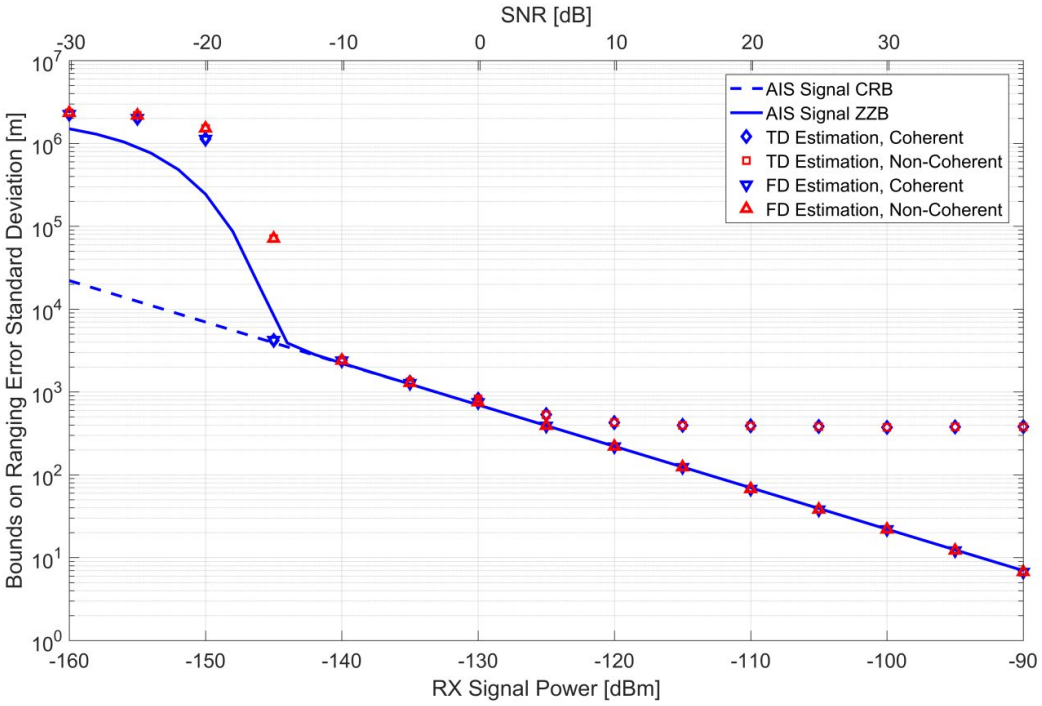

Figure 3-1: R-Mode ranging performance bounds and simulation results using a 1-slot ranging signal in 1 AIS Channel. The ranging signal is a GMSK modulated random 256-bit sequence.

At typical AIS operation ranges (RX signal power ≥ -110 dBm) the pseudo ranging standard deviation is in the order of 10…100m.

As discussed in Sec. 2.1.1, the mean square signal bandwidth determines the ranging performance. Using a GMSK modulated random 256-bit sequence as a ranging signal shows an average mean square signal bandwidth of 1.91 kHz. In order to increase the mean square bandwidth of the ranging signal we superimpose a continuous wave (CW) signal

$$s_{CW}(t) = \sin(2\pi f_r t), \quad for \quad t \in [0, T_s] \qquad 3\text{-}1$$

to our GMSK modulated random 256-bit sequence. We choose the CW signal's frequency $f_r = 6.9375\ Hz$ such that it coincides with the spectral notch of the GMSK signal component. With that we minimize interference between CW and the GMSK signal components. We transmit this hybrid signal in one AIS time slot with duration $T_s = 26.7$ ms. In case both signal components are transmitted with equal power the mean square signal bandwidth of this hybrid ranging signal is 5.1 kHz.

Special attention must be paid to the spectral characteristics of the hybrid range signal described above. Just adding a CW signal burst according to Eq. 3-1 without power ramp-up/down (roll-off = 0) results in non-negligible out-of-band emission, and consequently in a

violation of the AIS spectrum mask [AIS14]. Figure 3-2 shows the power spectrum density of the hybrid ranging signal's components together with the AIS channel boundary and the AIS spectrum mask.

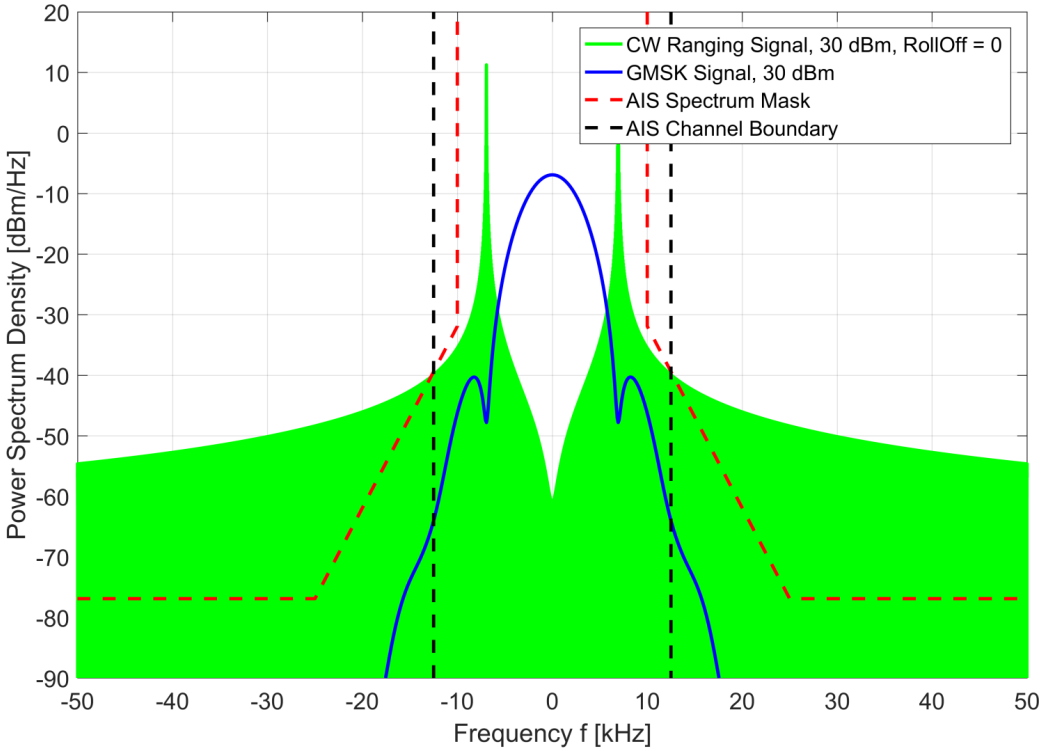

Figure 3-2: Power spectrum density of a GMSK modulated random bit sequence and a CW signal.

In order to prevent out-of-band emission, we apply power ramp-up/down by windowing the CW ranging signal component

$$s_{\mathrm{CW}}(t) = w\left(\frac{t}{T_s}\right)\sin(2\pi f_r t), \quad for \quad t \in [0, T_s] \tag{3-2}$$

using a Tukey window

$$\mathrm{w(x)} = \begin{cases} \frac{1}{2}\left(1+\cos\left(\frac{2\pi}{r}\left(x-\frac{r}{2}\right)\right)\right) & 0 \le x < \frac{r}{2} \\ 1 & \frac{r}{2} \le x < 1-\frac{r}{2} \\ \frac{1}{2}\left(1+\cos\left(\frac{2\pi}{r}\left(x-1+\frac{r}{2}\right)\right)\right) & 1-\frac{r}{2} \le x < 1 \end{cases} \tag{3-3}$$

The amplitude of the Tukey window and its energy spectrum density are shown in Figure 3-3 resp. Figure 3-4. Applying Tukey windowing with a roll-off factor of $r = 0.05$ provides a significantly denser spectrum of the CW signal component as shown in Figure 3-5, where we have evaluated the power spectrum density analytically and Figure 3-6, which shows the power spectrum density obtained by simulation. Note the peak-to-average power ratio (PAPR)

increases from 0 dB for using a GMSK ranging signal to about 4.7 dB for the hybrid GMSK/CW ranging signal because of signal superposition.

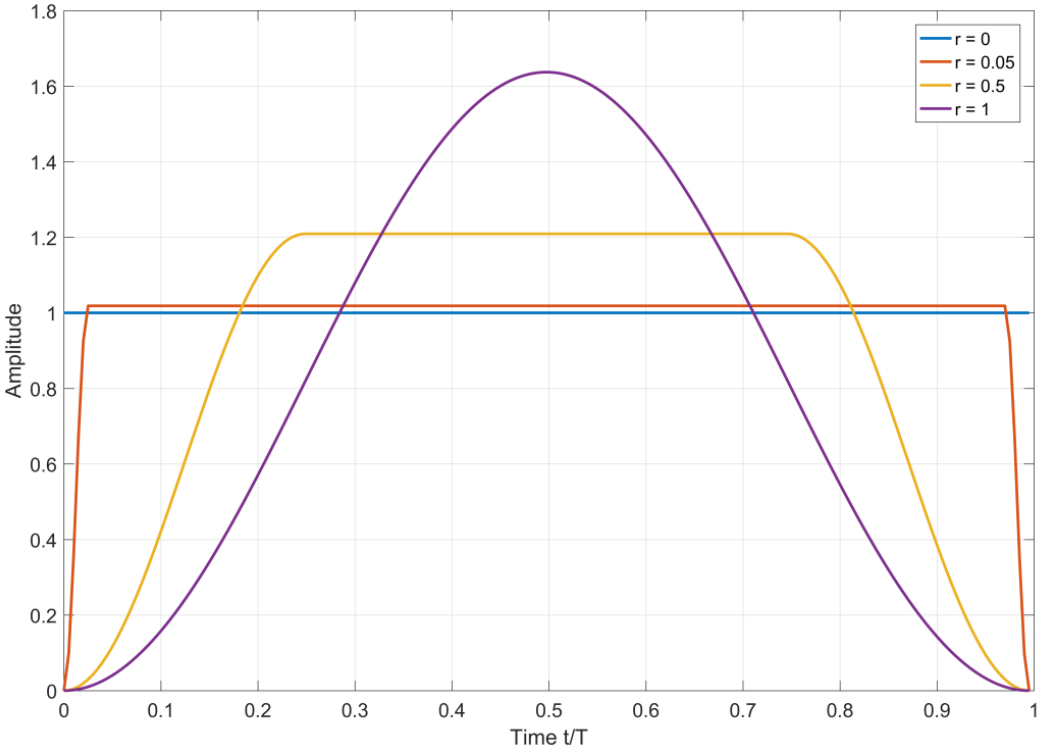

Figure 3-3: Tukey window for different roll-off values r.

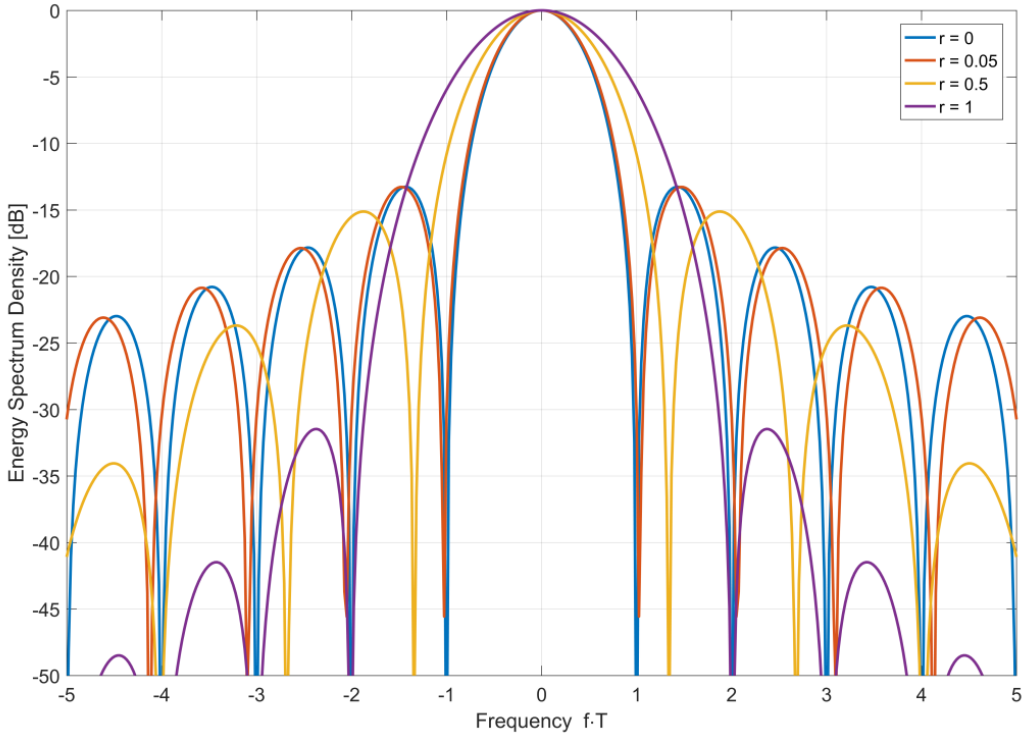

Figure 3-4: Energy density spectrum of the Tukey window for different roll-off values r.

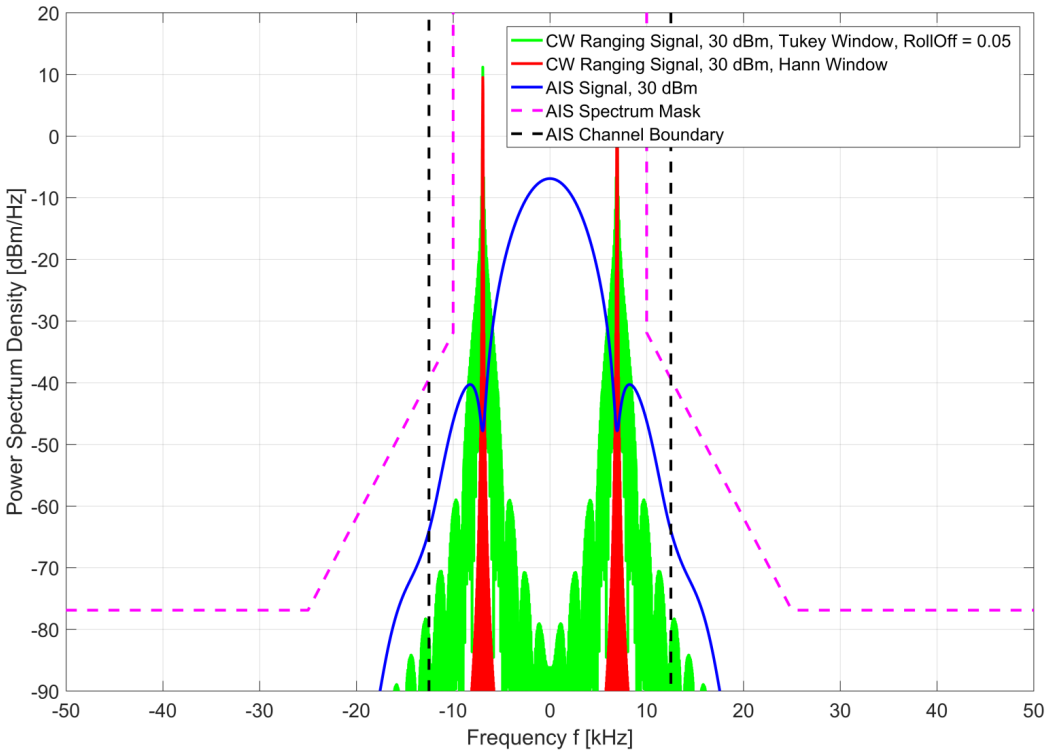

Figure 3-5: Power spectrum density of a GMSK modulated random bit sequence and a Tukey windowed CW signal.

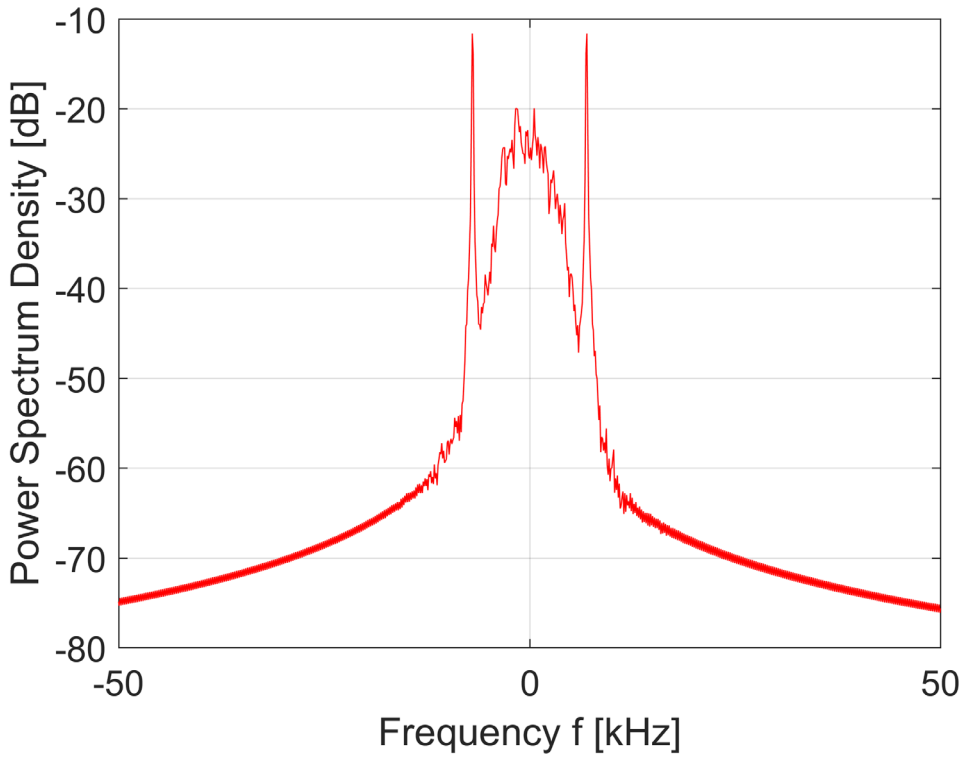

Figure 3-6: Power spectrum density, obtained by simulation, of a hybrid ranging signal of duration $T_s = 26.7$ ms (1 AIS time slot), which consists of a GMSK modulated random bit sequence and a Tukey windowed CW signal.

The ranging performance bounds and simulation results for a hybrid GMSK and Tukey windowed CW ranging signal are shown in Figure 3-7. Both ranging signal components are transmitted with equal power. Compared to the results shown in Figure 3-1, the ranging standard deviation at sufficiently high SNRs decreases by a factor of about 2.7, which is the ratio of the mean square bandwidths of the considered ranging signals.

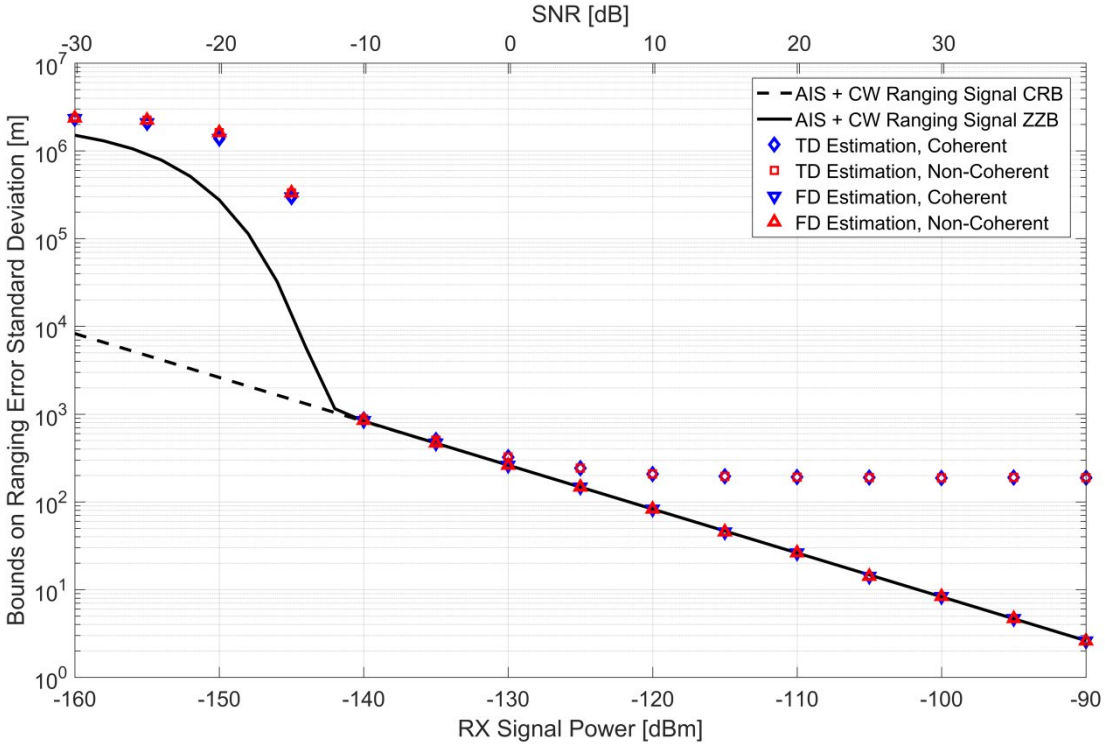

Figure 3-7: R-Mode ranging performance bounds and simulation results using a 1-slot ranging signal in 1 AIS Channel. The ranging signal consists of a GMSK modulated random bit sequence and a Tukey windowed CW signal, transmitted with equal power.

3.1.2 R-Mode using both AIS channels

Two AIS channels of bandwidth $25\ \mathrm{kHz}$ are allocated in the VHF spectrum at carrier center frequencies $161.975\ \mathrm{MHz}$ and $162.025\ \mathrm{MHz}$. Note there is another $25\ \mathrm{kHz}$ channel in between these 2 AIS channels. In order to further increase the mean square bandwidth of the ranging signal we use the 2 AIS channels coherently. We obtain such a ranging signal

$$\mathrm{s(t)} = s_{\mathrm{GMSK}}(\mathrm{t})\cos(2\pi f_{\mathrm{sc}} t)\,, \quad for \quad t \in [0, T_{\mathrm{s}}] \qquad 3\text{-}4$$

by multiplying a GMSK ranging signal $s_{\mathrm{GMSK}}(\mathrm{t})$ as we have used in Sec. 3.1.1 with a cosine subcarrier of frequency $f_{\mathrm{sc}} = 25\ \mathrm{kHz}$. The PSD, obtained by simulation, of this signal design is shown in Figure 3-8. The corresponding ranging performance results are shown in Figure 3-9. This signal construction shows a mean square bandwidth of $25.07\ \mathrm{kHz}$. This mean square bandwidth is dominated by the frequency shift of the GMSK signal by $\pm 25\ \mathrm{kHz}$ due to the cosine subcarrier. Consequently, we observe a ranging error reduction by a factor of about 13 compared to using a single AIS channel at sufficiently high SNRs. The PAPR of a 2-AIS channel GMSK ranging signal design is $3\ \mathrm{dB}$.

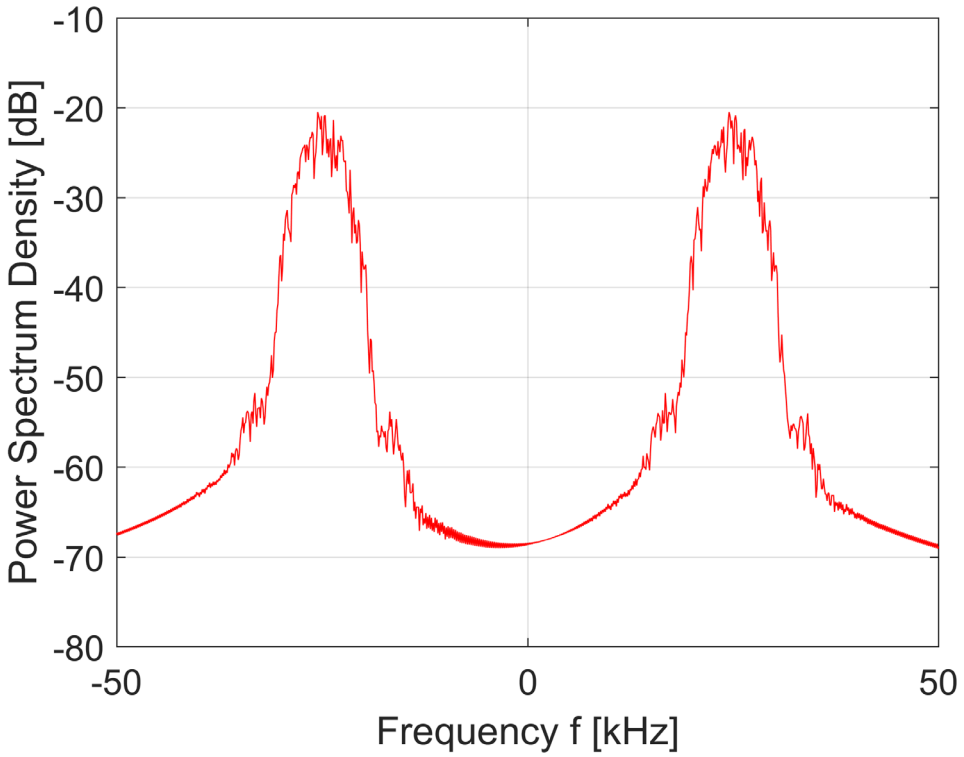

Figure 3-8: Power spectrum density, obtained by simulation, of GMSK modulated random bit sequence of duration $T_s = 26.7$ ms (1 AIS time slot) shifted in frequency domain by ± 25 kHz to cover both AIS channels coherently.

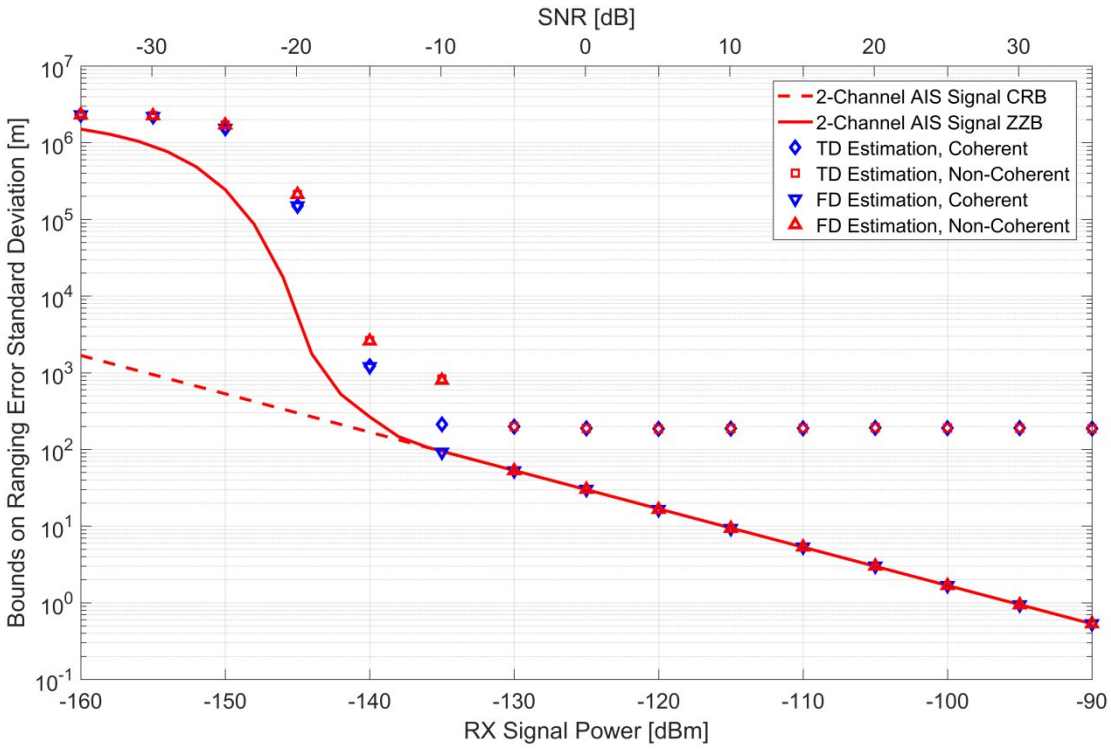

Figure 3-9: R-Mode ranging performance bounds and simulation results using a 1-slot GMSK ranging signal covering 2 AIS Channels coherently.

3.2 Using the VDES Spectrum for R-Mode

As the VDES standard allows different bandwidths to be used, a few options are available.

- Using a single 25 kHz channel: This option would make use of the possibility in the VDES standard to utilize a lower bandwidth with 4 channels instead of one wider channel. This way, the three other channels would still be available for communication while a ranging signal is being transmitted. It also serves as a useful reference, as it would occupy the same amount of frequency spectrum as an AIS signal.
- Using two 25 kHz channels coherently: Using the two outermost 25 kHz channels available in VDE, allows to achieve a high effective bandwidth, while possibly still leaving two channels available for communication purposes. Conformance to the VDE standard however needs to be determined.
- Using 100 kHz: In this case, a signal is broadcasted using the full available bandwidth of the VDE system. Transmitting a data sequence which, under the constraints of the used $\frac{\pi}{4}$–QPSK, maximises the effective bandwidth, allows this option to reach good ranging performance.

The different options are visualized in Figure 3-10.

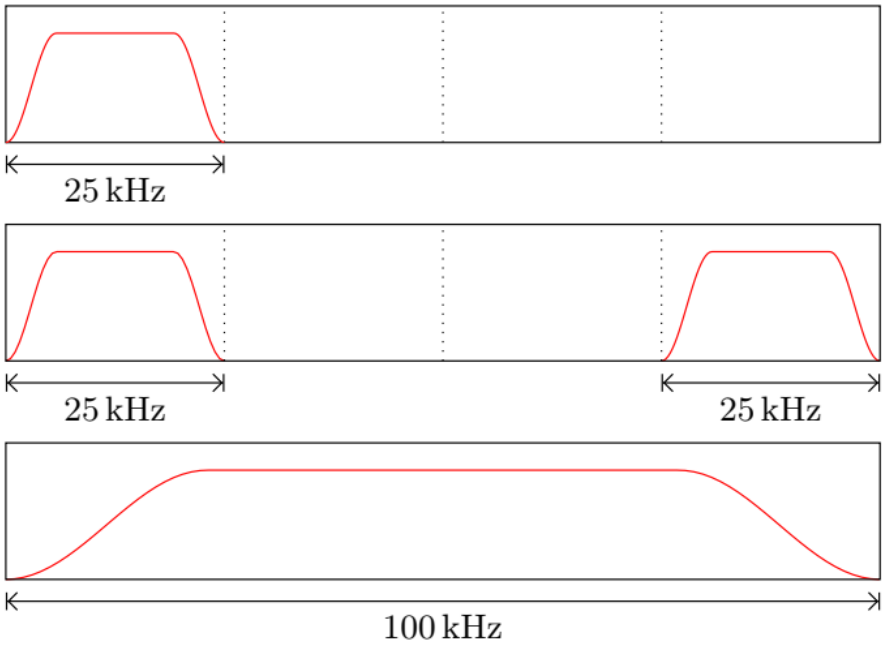

Figure 3-10: Different options for utilizing the available bandwidth. Schematically showing the power spectral density of average VDES link signals.

In order to evaluate the possible performance of the different options, lower bounds on the estimation error for time of arrival estimation are used. Specifically, the Cramér-Rao bound and the Ziv-Zakai bound are evaluated for the different signals. For a fair comparison between the different options, it is assumed that all of the considered signals have the same total energy. The results of the Ziv-Zakai bound are shown in Figure 3-11. The Ziv-Zakai bound converges to the Cramér-Rao bound four high signal energies, but gives results closer to reality at low signal energies.

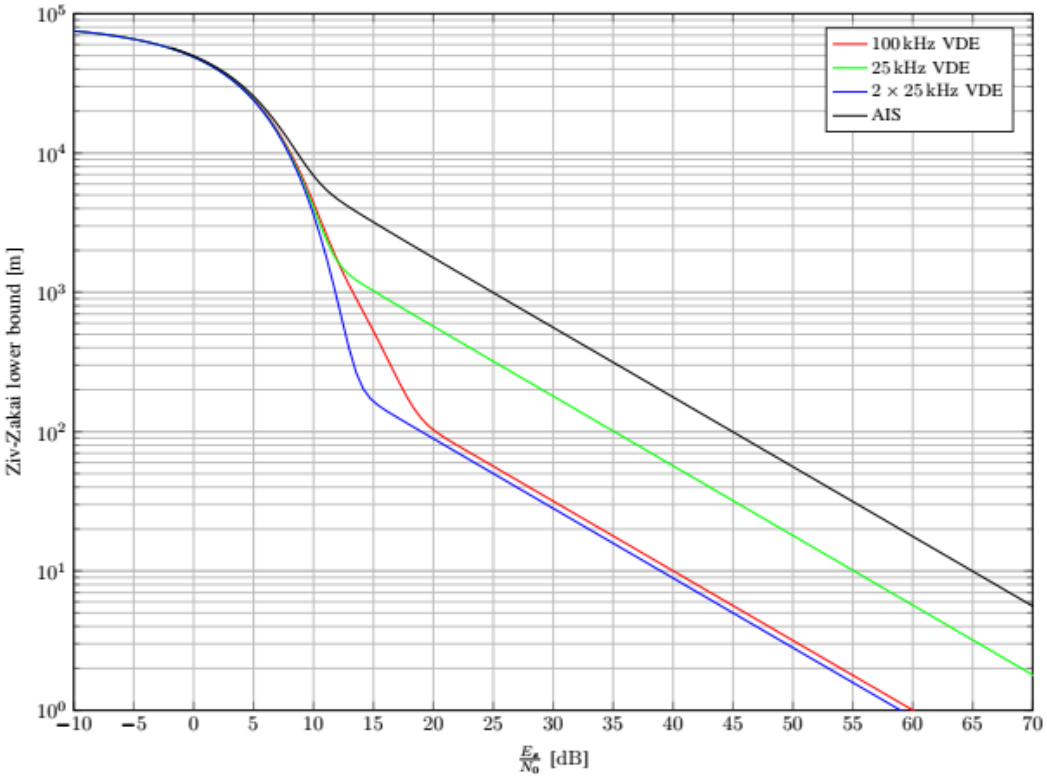

Figure 3-11: Lower bounds on the time of arrival estimation error.

Already the use of a single VDES channel results in a significant improvement in ranging performance compared to AIS. This is due to the energy of the AIS signal being mostly located close to the center of the spectrum, thus resulting in a lower effective bandwidth. Utilizing two 25 kHz channels results in further significant improvements over using only one channel, providing about six times better results than a signal with the same total energy but only 25 kHz of bandwidth. Using the entire 100 kHz bandwidth gives similar results when an optimized transmit sequence is chosen which puts most of the signal energy in the outer regions of the spectrum. Two 25 kHz channels offer the option to use the remaining bandwidth for communication purposes. Implementation issues however might favor the use of the 100 kHz channel.

Compared to AIS, the required signal energy for the same ranging performance can be reduced by about 24 dB by making use of two 25 kHz VDES link channels. In case of constant transmitted signal energy, this would result in about 15 times more range, for the same ranging performance, when only free space coverage is considered.

4 Proposed R-Mode Sequences

In order to be compliant with the modulation scheme of VDES, the VDES ranging signal design in this GA has been focused of optimizing ranging bit sequences.

4.1 Component Sequences

As Eq. 2-3 states, the mean square bandwidth is the defining factor for good time of arrival estimation. Therefore, it is desirable to maximize this parameter. The signal with the highest

possible mean square bandwidth for a given amount of spectrum available, would be a continuous wave signal. In frequency domain, this would correspond to two Dirac impulses at the edges of the available channel. According to Eq. 2-4, such a signal has a mean square bandwidth of

$$\bar{F}^2 = 4\pi^2 f_0^2, \tag{4-1}$$

where f_0 is the frequency of the continuous wave signal. For a total available bandwidth of B, the maximum frequency that can be chosen is $f_0 = \frac{B}{2}$.

The VDES utilizes a linear single carrier modulation scheme. Thus, the transmitted signal $s(t)$ can be described by

$$s(t) = \sum_{n=0}^{N-1} d_n \cdot g(t - nT_{\mathrm{sym}}), \tag{4-2}$$

where d_n is the transmitted data symbol and $g(t)$ is the root raised cosine pulse shape with T_{sym} being the duration of one data symbol.

To calculate the ZZB according to Eq. 2-5 of this kind of signal, we need to determine its normalized autocorrelation as given in Eq. 2-7:

$$\rho_s(h) = \frac{1}{E_s}\int_{-\infty}^{\infty}\left(\sum_{n=0}^{N-1} d_n \cdot g(t - nT_{\mathrm{sym}})\right)\cdot\left(\sum_{n=0}^{N-1} d_n \cdot g(t - nT_{\mathrm{sym}} - h)\right)^{*} \mathrm{d}t \tag{4-3}$$

Since the individual root raised cosine pulses are orthogonal to each other, the signal Energy E_s can be calculated by

$$E_s = \left(\sum_{n=0}^{N-1} |\, d_n|^2\right)\cdot\int_{-\infty}^{\infty} |\, g(t)|^2 \mathrm{d}t \tag{4-4}$$

As we are using a PSK signal $|d_n| = 1$ for all possible symbols, and $g(t)$ is normalised, such that $\int_{-\infty}^{\infty} |\, g(t)|^2 \mathrm{d}t = 1$. Therefore Eq. 4-4 simplifies to $E_s = N$. Eq. 4-3 can also be simplified further, resulting in:

$$\begin{aligned}\rho_s(h) &= \frac{1}{N}\sum_{k=0}^{N-1}\sum_{n=0}^{N-1} d_k\, d_n^{*}\int_{-\infty}^{\infty} \mathrm{g}\left(t - kT_{\mathrm{sym}}\right) g^{*}\left(t - nT_{\mathrm{sym}} - h\right)\mathrm{d}t \\ &= \frac{1}{N}\sum_{k=0}^{N-1}\sum_{n=0}^{N-1} d_k\, d_n^{*}\cdot\rho_g\left(h - (k-n)T_{\mathrm{sym}}\right).\end{aligned} \tag{4-5}$$

where $\rho_g(h)$ is the autocorrelation of the pulse shape $g(t)$. As $g(t)$ is a root raised cosine pulse, its autocorrelation is a raised cosine pulse. As Eq. 2-6 requires only the real part of the normalized autocorrelation, we can simplify this further by grouping the summation differently:

$$\begin{aligned}\mathrm{Re}(\rho_s(h)) &= \frac{1}{N}\sum_{k=0}^{N-1}\sum_{n=0}^{N-1}\mathrm{Re}\left(d_k d_n^*\right)\cdot\rho_g(h-(k-n)T_{\mathrm{sym}}) \\ &= \frac{1}{N}\sum_{l=-(N-1)}^{N-1}\rho_g\left(h-lT_{\mathrm{sym}}\right)\left(\sum_{m=|l|}^{N-1}\mathrm{Re}\left(d_m d_{m-|l|}^*\right)\right) \\ &= \rho_g(h)+\frac{1}{N}\sum_{l=1}^{N-1}\left(\rho_g(h-lT_{\mathrm{sym}})+\rho_g(h+lT_{\mathrm{sym}})\right) \\ &\cdot\sum_{m=l}^{N-1}\mathrm{Re}\left(d_m d_{m-l}^*\right).\end{aligned} \quad 4\text{-}6$$

This form of the signals normalized autocorrelation can be evaluated numerically without having to perform numerical integration. The resulting ZZB according to Eq. 2-5 depends on the transmitted data symbols d_n and the parameters of the root raised cosine pulse. As the pulse parameters are given by the VDES standard to be a roll of factor of $\beta = 0.3$ and a symbol duration of $T_{\mathrm{sym}} = 13.021$ µs, they cannot be changed. To influence the ranging performance, the data symbols d_n have to be used.

4.1.1 Alternating Sequence

The VDES standard specifies π/4-QPSK modulation. Therefore, simply alternating between opposite constellation points is not possible. To achieve a high mean square bandwidth under the constraints of the π/4-QPSK modulation, it is possible to approximate this alternating pattern. This approximated alternating data sequence $d_{\mathrm{alt},n}$ consists of multiple repetitions of the constellation points j, (-1-j)/√2, j, (1-j)/√2. This is visualized in Figure 4-1.

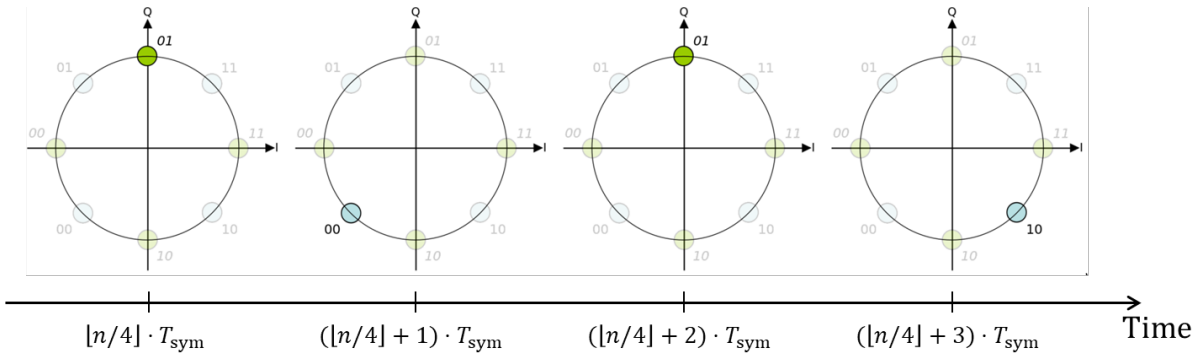

Figure 4-1: Alternating R-Mode Sequence

4.1.2 Pseudo Noise Gold Sequence

When searching for the appropriate synchronization code, it was decided to use the Gold's sequences and the long uplink scrambling code generator defined for the UMTS system [UMTS]. The code generator is constructed of two generator polynomials of degree 25: $X^{25}+X^3+1$ and $X^{25}+X^3+X^2+X+1$. The two output scrambling sequences are constructed from modulo 2-sum of two binary sequences generated by those polynomials. The resulting sequences have bipolar values (+1 and -1) and constitute segments of a set of the Gold sequences. The construction of the UMTS uplink scrambling code generator is shown in

figure 2-1. Nominally the length of the scrambling code is 38400 chips, so it can be easily shortened.

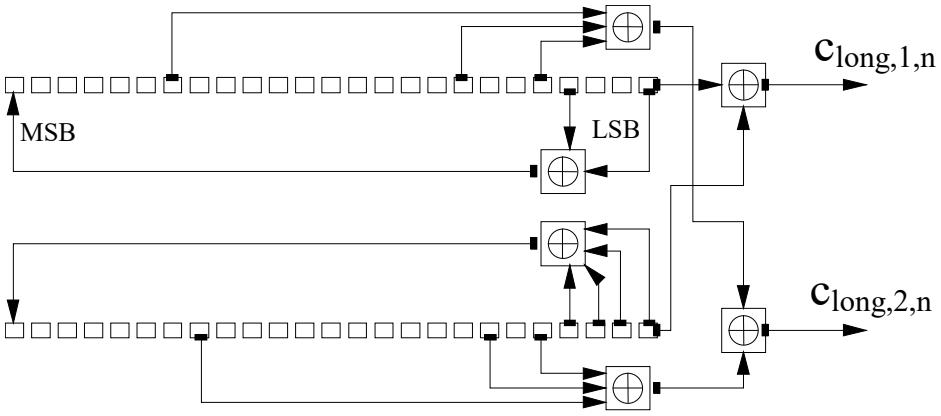

Figure 4-2: Configuration of the UMTS uplink scrambling sequence generator [UMTS]

Finally, the complex-valued long scrambling sequence is defined as [UMTS]:

$$C_n(i) = c_{long,1,n}(i) \cdot \left[1 + j \cdot (-1)^i \cdot c_{long,2,n}\left(2\left\lfloor {}^{i}/_{2} \right\rfloor\right)\right] \qquad 4\text{-}7$$

where:

i is the number of consecutive bits of the sequence,

n is the 24 bit binary representation of the scrambling sequence number,

[ ] denotes rounding to the nearest lower integer.

In order to determine the maximum length of Gold's code obtained using UMTS generator, which will not require the insertion of additional bits by the AIS bit stuffing mechanism, the simulation tests were carried out for all 2^{24} (over 16.7 million) possible combinations of initial states of the generator (scrambling sequence number).

As it was mentioned, the sequence generated by this method is originally bipolar, so in the first step, a code was searched that would correspond to the binary sequence coded by the NRZI encoder. In that case the longest code that meets the bit stuffing criteria (there is no five consecutive “+1” and no five consecutive “-1” bit values) has a length of 463 bits and there is only one such code (initial state 8 889 334) and it is the imaginary part of the generated Gold code.

In the second step the bipolar code sequence has been converted to the binary form (bipolar “1” denotes binary “0” and bipolar “-1” denotes binary “1”). As a result, it was established that the longest code that meets the bit stuffing criteria (there is no five consecutive “1”) has a length of 885 bits and there are 2 such codes (initial states 4 731 302 and 12 862 768) and they are also the imaginary part of the generated Gold code.

In the third step the bipolar code sequence has been converted to the negative binary form (bipolar “1” denotes binary “1” and bipolar “-1” denotes binary “0”). As a result, it was established that the longest code that meets the bit stuffing criteria (there is no five consecutive “1”) has a length of 968 bits and there is only one such code (initial state 702 948) and it is also the imaginary part of the generated Gold code.

Since the code obtained in the third stage is the longest one, it was decided to use that code in further considerations.

The selected synchronization code with initial state 702 948 and length 968 bits is:

0,0,0,0,0,1,1,0,0,1,1,0,1,0,1,1,0,0,0,0,0,0,0,1,1,1,1,0,1,1,0,0,1,0,1,1,0,1,1,1,0,1,1,0,0,0,1,1,1,
1,0,0,1,1,1,0,1,0,0,0,0,0,0,0,0,1,0,0,1,0,0,1,1,0,0,1,0,1,1,0,0,0,1,1,0,0,0,1,0,1,0,0,1,0,1,0,1,1,
0,0,1,1,1,0,1,1,0,0,1,1,0,1,0,0,1,1,1,1,0,1,1,0,1,1,1,1,0,0,1,1,0,0,0,0,1,0,0,0,0,0,0,1,1,1,1,0,0,
1,0,1,1,0,1,1,0,0,0,1,0,0,0,1,0,1,0,1,0,0,0,1,0,1,0,0,0,1,1,0,1,1,0,0,1,0,0,1,1,0,1,1,1,0,0,0,1,0,
0,1,0,0,0,1,0,0,1,1,0,0,0,0,0,0,0,1,1,0,1,0,0,0,1,0,1,1,0,1,0,0,1,0,0,1,1,1,0,1,0,0,0,0,0,0,0,0,1,
1,0,0,1,1,0,0,1,0,1,1,1,0,1,1,0,0,1,0,1,1,0,0,1,0,0,1,1,1,0,1,0,0,1,0,1,0,1,0,0,1,1,0,1,1,0,0,0,0,
0,1,1,0,0,1,0,0,1,1,0,1,0,1,0,1,0,1,0,0,1,0,1,0,1,0,0,0,1,0,0,1,0,0,1,0,1,0,0,0,0,1,0,1,0,1,0,1,1,
1,1,0,1,0,0,1,0,0,0,0,0,1,1,0,0,1,0,1,0,0,0,1,0,0,0,0,0,0,0,0,0,1,0,1,0,1,1,0,1,1,0,0,1,0,1,0,0,0,0,
1,1,0,0,0,1,0,1,0,1,0,1,0,0,0,1,1,1,0,0,0,0,1,1,0,1,1,0,1,1,1,0,0,0,0,1,0,0,0,1,1,0,0,1,1,0,0,1,0,
0,0,1,0,0,1,1,0,1,1,0,0,0,1,1,1,0,1,0,0,1,1,1,0,0,0,0,1,1,1,0,0,1,1,0,1,1,0,0,0,0,0,0,1,1,1,0,0,1,
0,1,1,1,0,0,1,0,1,1,1,0,0,0,1,0,1,1,1,1,0,1,0,1,1,0,1,0,1,0,1,1,1,1,0,0,1,0,0,1,0,1,1,1,1,0,1,1,1,0,
0,1,1,1,1,0,0,0,0,1,0,0,1,0,0,1,0,1,0,1,1,1,1,1,0,0,0,1,1,1,0,0,0,0,0,0,0,0,0,0,0,0,0,1,1,0,0,1,0,
1,0,1,0,1,1,0,0,0,0,1,1,1,1,0,1,0,0,0,1,0,1,1,0,0,1,0,0,1,0,0,0,0,0,0,0,0,0,0,1,1,1,0,0,0,1,1,1,0,
0,0,0,1,0,1,0,1,1,1,0,0,1,0,0,0,1,1,1,0,1,1,0,0,1,1,0,1,0,1,0,0,1,1,0,0,1,0,0,0,1,0,1,1,0,0,0,0,1,0,1,
0,1,0,1,1,1,1,1,0,1,0,1,1,0,0,0,0,1,1,1,0,0,1,0,1,0,1,1,0,1,0,0,1,0,1,0,1,0,1,0,1,0,1,1,1,0,0,1,1,1,
0,1,0,0,0,0,1,1,0,1,0,0,1,1,1,0,0,1,1,1,1,0,1,1,0,0,0,0,0,1,1,1,0,1,0,0,1,1,0,1,1,1,1,0,1,1,1,0,0,
1,0,0,1,1,0,1,0,1,1,0,1,0,0,1,1,0,1,0,1,1,0,1,1,0,1,0,1,1,1,0,1,1,1,1,0,1,0,1,0,0,0,1,0,1,0,1,0,1,
1,0,0,0,1,1,0,0,1,1,0,0,0,1,0,0,1,1,1,0,1,0,1,1,0,1,1,1,0,0,1,1,0,1,0,1,0,1,0,1,1,0,0,1,0,0,0,1,1,
0,0,1,0,1,0,0,0,1,1,0,0,1,1,1,0,0,0,1,1,1,0,1,0,0,0,0,0,1,0,0,1,1,1,0,0,1,1,1,1,0,0,1,1,0,0,0,0,0,0,
0,1,1,1,1,0,0,0,0,0,1,0,0,0,1,0,1,1,1,0,1,1,1,1,0,1,0,1,1,0,1,0,1,1,1,1,1

In the next stage the selected synchronization code was NRZI coded and its autocorrelation function has been determined and compared with the autocorrelation function before coding. Both autocorrelation functions are presented in figure 2-2.

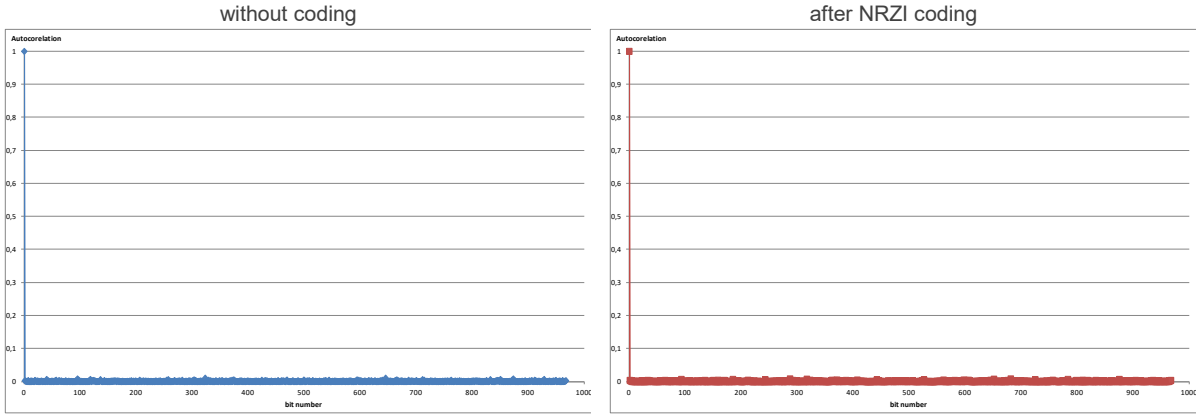

Figure 4-3: The autocorrelation function of the selected synchronisation code before and after NRZI coding

As can be seen, the NRZI coding does not affect the correlation properties of the selected synchronization code, and after coding, the second highest value has even decreased from 0,01067 for the uncoded synchronisation code to 0.00826 for the NRZI coded code.

The same procedure was carried out to search codes of length 300 and 80 bits, which meet the bit stuffing criteria. Over 200 000 usable codes of length 300 bits have been found, and among them, the one (initial state 1 174 014), whose autocorrelation function has the best

properties, has been selected. This code is negative binary conversion (bipolar “1” denotes binary “1” and bipolar “-1” denotes binary “0”) of the imaginary part of the generated Gold code. For this code, the second highest value is 0.01138 for the NRZI coded code.

The selected synchronization code with initial state 1 174 014 and length 300 bits is:

0,1,0,1,1,0,0,1,1,0,0,1,0,0,1,0,1,0,1,0,0,0,1,0,1,1,0,1,1,0,0,1,0,1,1,0,1,1,1,1,0,1,0,1,0,1,1,0,1,
1,1,0,0,1,1,0,1,1,1,0,0,1,0,0,0,0,0,1,0,0,1,0,0,0,0,0,0,1,1,0,1,1,0,0,0,1,0,0,0,0,0,1,0,1,0,1,0,0,
0,0,0,0,1,0,1,0,0,1,0,0,0,1,1,0,0,1,0,0,1,0,0,1,0,1,0,1,1,1,1,1,0,1,0,1,0,1,0,1,0,1,0,1,1,0,0,1,0,1,
0,0,0,0,0,0,0,0,1,1,0,0,1,1,0,0,0,0,0,0,1,0,0,0,1,1,1,0,1,1,1,1,0,0,0,1,0,1,1,1,1,0,1,1,1,1,0,0,0,
0,1,0,0,0,0,1,0,0,1,1,0,0,0,1,0,0,1,1,1,0,0,0,1,1,1,0,1,0,1,0,1,0,1,0,0,0,1,1,0,1,1,0,0,0,1,1,0,0,
0,1,0,0,1,1,1,0,0,1,1,0,0,1,0,0,0,1,1,1,1,0,0,1,1,0,1,1,0,0,0,1,1,1,0,0,0,0,0,1,1,1,1,0,0,1,1,0,0,
0,1,1,0,1,1

For the codes of length 80 bits, over 10 000 000 codes have been found which meet the bit stuffing criteria. Once again, among them, the one (initial state 4 872 582), whose autocorrelation function has the best properties, has been selected. This code is also negative binary conversion (bipolar “1” denotes binary “1” and bipolar “-1” denotes binary “0”) of the imaginary part of the generated Gold code. For this code, the second highest value is 0.01000 for the NRZI coded code.

The selected synchronization code with initial state 4 872 582 and length 80 bits is:

1,0,0,1,0,1,0,1,0,1,1,0,0,1,1,1,0,1,1,1,0,0,1,1,1,1,0,1,1,1,1,0,1,1,0,0,0,1,0,0,0,1,1,0,0,1,1,1,1,
0,0,1,1,0,1,0,1,0,0,0,0,1,0,0,0,1,1,1,0,1,1,0,0,0,1,1,1,1,0,1

4.2 The R-Mode Sequence Composed of Alternating and Pseudo Noise Gold Sequence

While the mean square bandwidth determines the ranging performance at good signal to noise ratios, the performance at lower signal to noise ratios is determined by the sidelobes of the signal’s autocorrelation level, as it is likely that a sidelobe is mistaken for the main correlation peak. The previously mentioned approximated alternating signal however has very high correlation sidelobes, as the signal shifted by one symbol period strongly correlates with the original signal. To reduce the level of sidelobes in the signal’s autocorrelation function, a pseudo-noise sequence can be chosen for its good autocorrelation properties. The pseudo-noise sequence, however, has a lower mean square bandwidth, and therefore performs worse at higher signal to noise ratios than the previously described signal.

In Figure 4-4, the normalized autocorrelation for both types of signal are being shown. It can be seen that the pseudo-noise signal has much lower sidelobes, and thus a much lower sidelobes that could be confused for the main lobe at lower SNRs. But the approximated alternating signal has a narrower correlation peak, which can be estimated with higher accuracy at good SNRs.

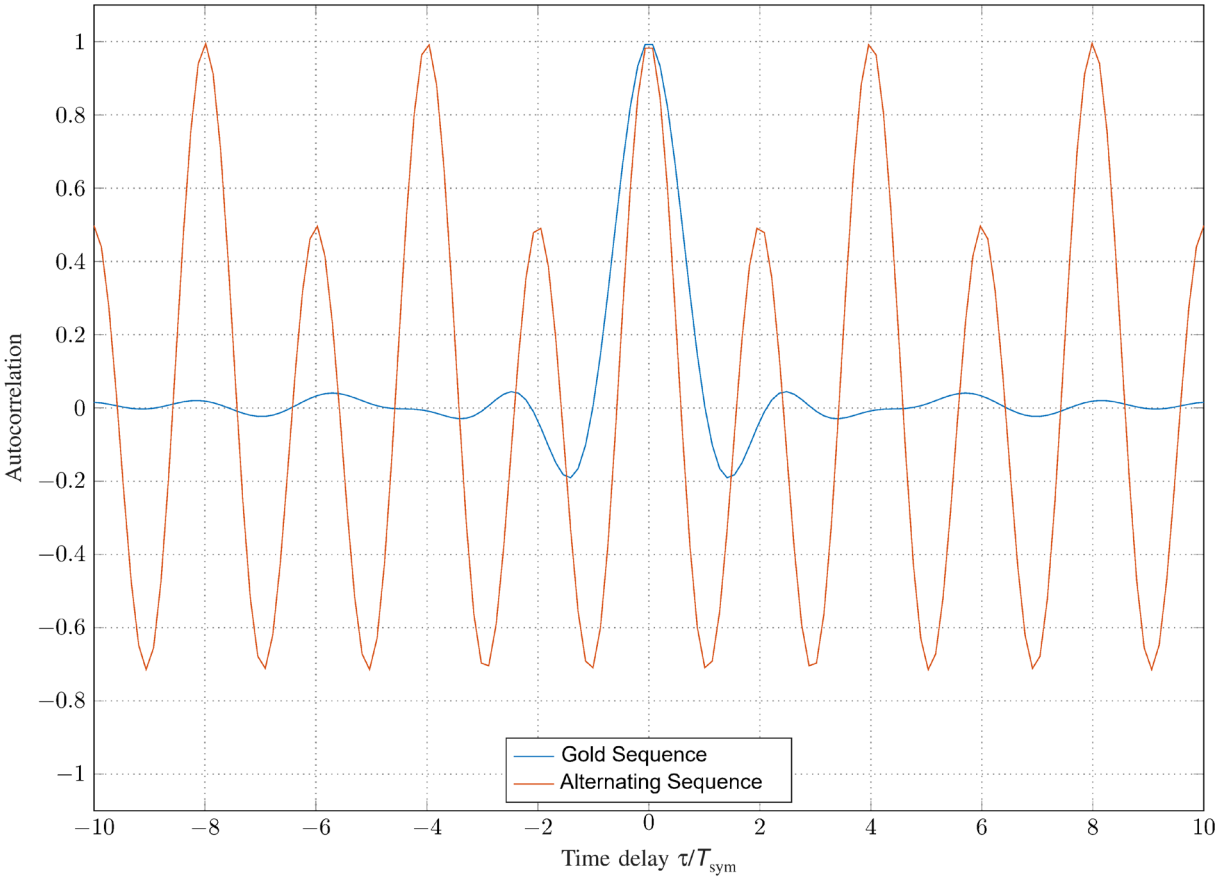

Figure 4-4: Autocorrelation functions of the R-Mode component sequences

To find a compromise between these two design goals, a combination of the two signals can be used. The most straightforward way of combining both signals would consist of a weighted linear combination, such that

$$s(t) = \sqrt{\gamma} \cdot s_{alt}(t) + \sqrt{1-\gamma} \cdot s_{pn}(t), \quad 4\text{-}8$$

where $\gamma \in [0;1]$ controls the power ration between the alternating sequence $s_{alt}(t)$ and the pseudo-noise Gold sequence $s_{pn}(t)$.

This simple superposition of the two signals would not be conforming to the requirements of the VDES Standard anymore. The resulting transmitted data symbols would not conform to the allowed modulation alphabet anymore. Furthermore, the PAPR would increase, which might necessitate a lower transmit power. Therefore, we investigate a concatenation of the approximate alternating signal and a pseudo-noise sequence, as shown in Figure 4-5, such that

$$d_n = \begin{cases} d_{alt,n} & \frac{n}{N} < \gamma \\ d_{pn,n} & \text{otherwise} \end{cases} \quad 4\text{-}9$$

where $d_{pn,n}$ is a pseudo-noise Gold sequence, and $d_{alt,n}$ is the approximated alternating sequence as described in Sec. 4.1.1.

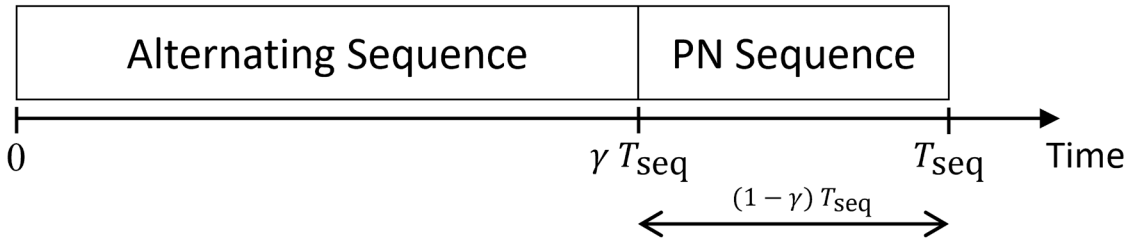

Figure 4-5: The ranging sequence is split into two parts consisting of an alternating sequence part and a Gold code (pseudo-noise (PN)) sequence part. The ratio of both sequence parts in a VDES time slot of $T_{\text{seq}} = 26.67\ \text{ms}$ is determined by the ranging sequence ratio $\gamma \in [0; 1]$.

Depending on the ratio of the lengths of the two concatenated signals, the resulting signal's power spectral density changes from almost uniform over the given spectrum of 100 kHz, for the case of the pseudo-noise sequence, to concentrated mostly at the edges of the spectrum, in the case of the approximated alternating data sequence. This relationship is shown in Figure 4-6. Even for $\gamma = 1$, the signal has noticeable components in the middle of the spectrum. This is caused by the approximation necessitated by $\frac{\pi}{4}$-QPSK.

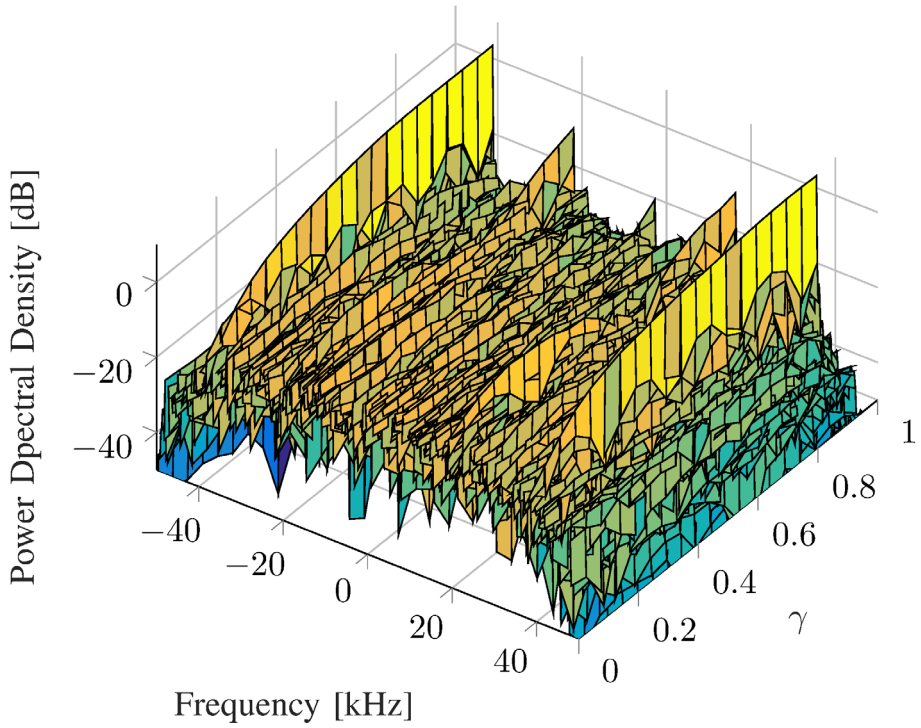

Figure 4-6: Power spectral density of the signal for different values of γ.

The influence of ranging sequence ratio γ on the autocorrelation function is shown in Figure 4-7. A narrow autocorrelation main lobe comes with high sidelobes that cause ambiguity. In contrast an autocorrelation function with low sidelobes shows a wider main lobe which degrades the ranging performance at high SNRs.

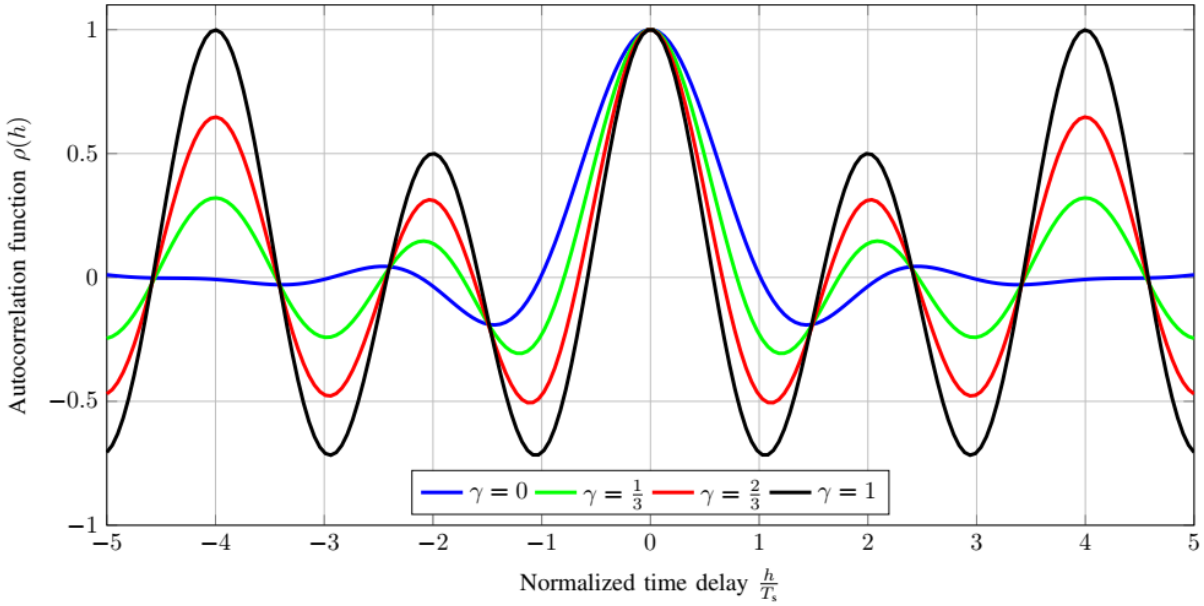

Figure 4-7: Normalized autocorrelation function $\rho(h)$ for the proposed VDES R-Mode sequences for different values of ranging sequence ratio γ versus time delay h, normalized to the symbol duration T_{sym}.

To evaluate the suitability of the R-Mode ranging signal, the ZZB as described in Sec. 2.1.2 was evaluated for multiple values of the ranging sequence ratio γ. The resulting bounds on the square root of the minimum ranging variance are shown in Figure 4-8 for a several values of γ. The parameter T that is required in Eq. 2-5 was chosen as 1 ms.

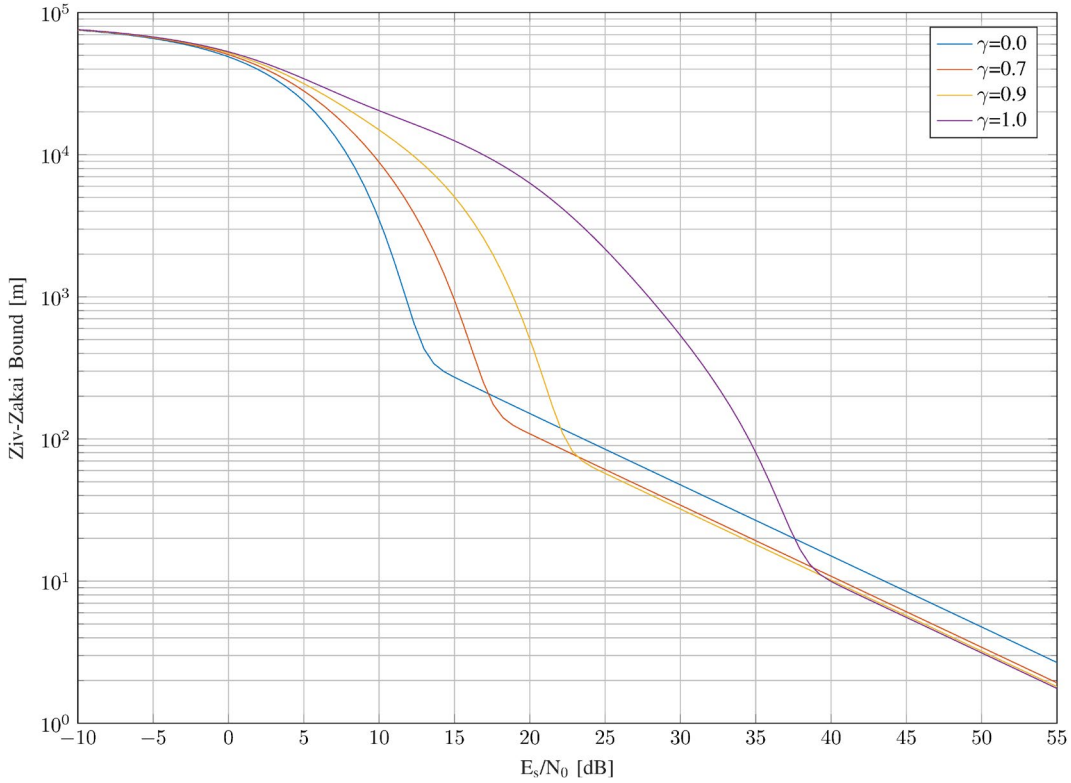

Figure 4-8: Ziv-Zakai bounds on range estimation for different values of ranging sequence ratio γ

It can be seen from Figure 4-8 that for high SNRs, the curves with a high value of γ allow a higher accuracy than those with a lower γ, while at low SNRs lower values of γ give better results. Thus, for optimal performance, the parameter γ has to be chosen depending on the SNR of the signal at the receiver. In Figure 4-9, the optimal value depending on the SNR is shown.

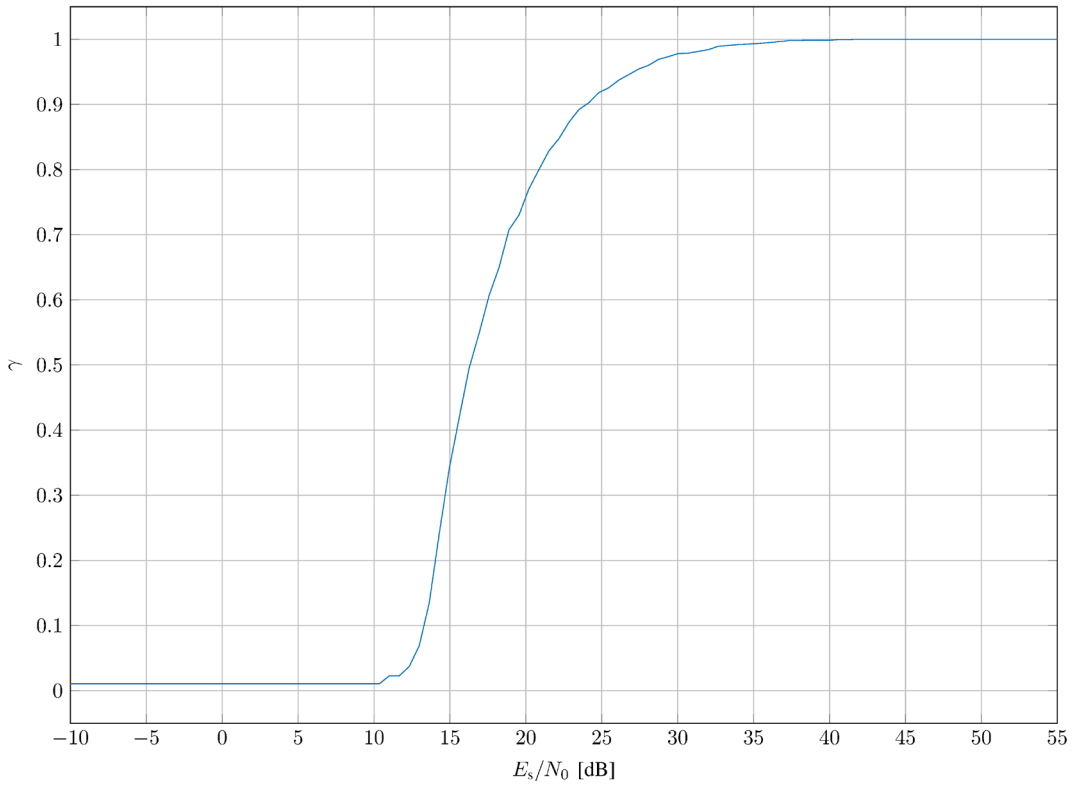

Figure 4-9: Optimal values of ranging sequence ratio γ for a given E_s/N_0

5 R-Mode Experiments at Lake Ammer

5.1 Single Link Ranging Experiment

5.1.1 Measurement Setup

To validate the results obtained by considering estimator bounds, a measurement campaign was performed.

The measurement setup consisted of a transmitter on the land side and a receiver on a vessel on the lake. Both sides utilized Software Defined Radio (SDR) hardware to transmit or receive the different signals to be evaluated.

The location of the measurement was the Lake Ammer in Germany.

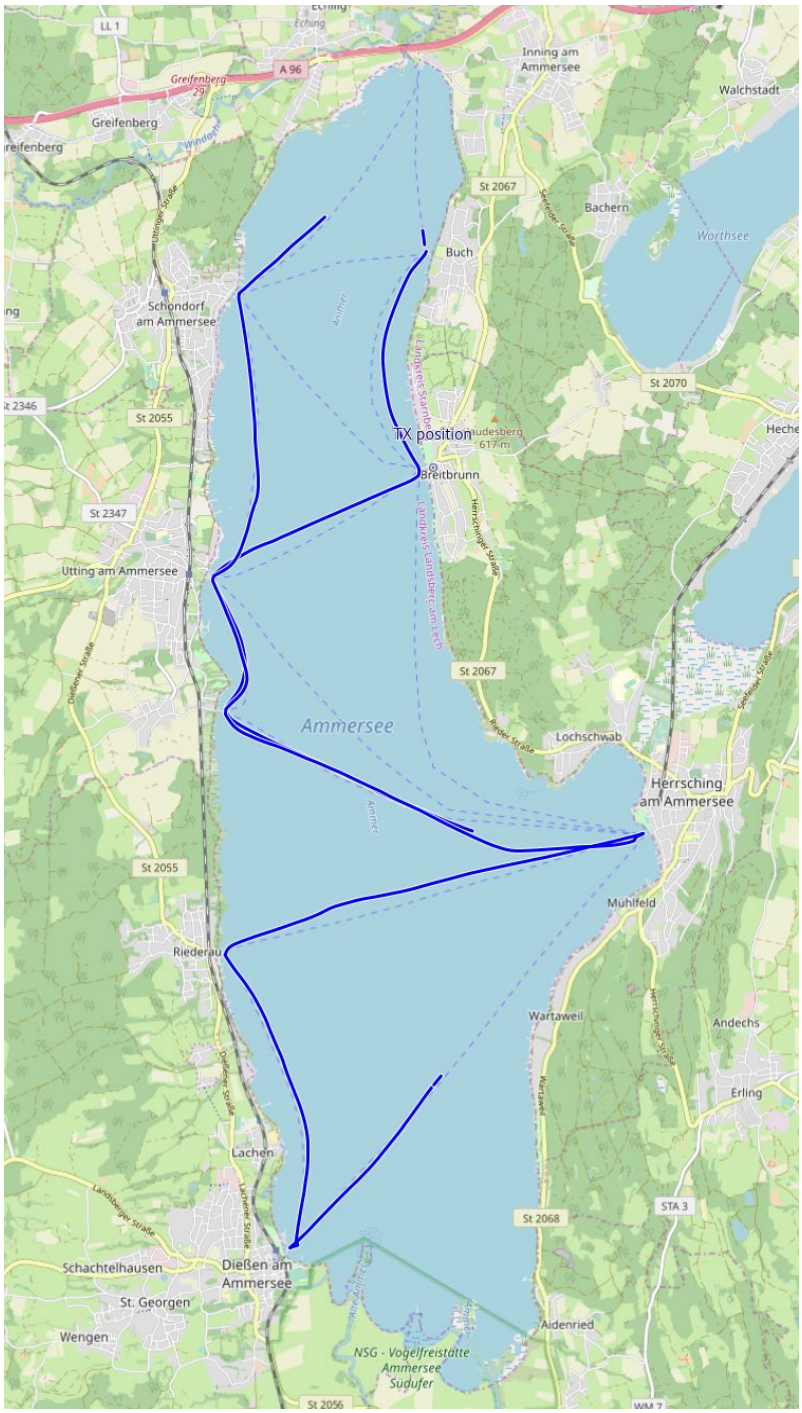

Figure 5-1: Map of the Lake Ammer where the measurements were performed.

As usage of motorboats is highly restricted on the lake, the measurement was performed on board of a commercial passenger ship. The antenna of RX side SDR, as well as the GNSS antenna can be seen in Figure 5-3.

In addition to the same SDR hardware, as used on the receiver side, the TX side setup also included a power amplifier to allow transmission of the signal with a power of 1 Watt. A higher power was not approved by the regulatory agency. The transmitter antenna was mounted on top of a car, as is shown in Figure 5-2. However, the car remained stationary during the entire measurement.

Figure 5-2: Transmitter antenna next to the Lake

Figure 5-3: Receiver antenna and GNSS antenna on the ship.

5.1.2 Measurement Methods

In order to allow a fair comparison between the different ranging signals, they should be transmitted in close temporal proximity, such that the channel conditions are comparable. In our measurement, this was done by transmitting each signal of interest in succession with a guard interval in between.

Each block of transmitted signals was sent at the full second mark. Thus, the update rate for the measured range was 1 Hz. A reference Pulse-Per-Second (PPS) for precise timing of the transmitted signal was provided by a GPS disciplined oscillator (GPSDO) module in the SDR hardware. The carrier frequency was also derived by a 10 MHz signal provided by the GPSDO.

On the receiver side, the same type of SDR and GPSDO was utilized. This way, both sides had access to a common GNSS based time base. While the purpose of R-Mode is to be independent of satellite-based systems, the purpose of this measurement was only to evaluate the possible ranging signals. After the reception of each signal block, it was tagged with a time stamp and written to disk in the form of I/Q baseband samples.

As a reference for the true range between transmitter and receiver, both sides were equipped with GNSS receivers.

Evaluation of the recorded signals was done in a postprocessing step. As each signal was tagged with the time of reception, the data could be associated with the appropriate position as recorded by the GNSS equipment. The true range could then be calculated. To determine the range from the measurements, first the appropriate time slot within the one second block of recorded samples was cut out. Then a coarse synchronization was performed by determining the maximum of the cross correlation of the received signal with the transmitted signal:

$$\hat{\tau} = T_s \cdot \text{argmax}_m \left| \sum_{n=0}^{N-1} r\,(n) \cdot s^*(n-m) \right|^2 \qquad 5\text{-}1$$

Where N is the number of samples within one timeslot, $r(n)$ denotes the received samples and $s(n)$ is the transmitted signal.

As a sampling frequency f_s of 612.5 kHz was used, the result of this estimation is quantized to steps of 1.63 µs, which corresponds to a range of 489.5 m. This is obviously unsatisfactory for the purpose of a ranging system. Therefore, an additional fine estimation step is necessary.

As the fine synchronization needs to determine the time of arrival of the signal with a better accuracy than the sampling time, it is necessary to interpolate between the recorded samples. This can be achieved by the means of a Discrete Fourier Transform (DFT). A cyclic shift in time domain corresponds to a multiplication with the complex exponential function in frequency domain. Thus, a time shift can be achieved by multiplying the frequency domain representation of a sufficiently zero padded signal with an exponential function, and transforming the signal back to time domain. For the purpose of determining the maximum correlation, it is possible to omit the inverse DFT and do the correlation in frequency domain.

$$\hat{\tau} = \text{argmax}_\tau \left| \sum_{k=0}^{K-1} R\,(k) \cdot \left(S(k) \cdot \exp\left(-j2\pi \frac{\tau}{T_s} k \right) \right)^* \right|^2 \qquad 5\text{-}2$$

Where R(k) and S(k) are the DFT of the received and the transmitted signal. The maximum in Eq. 5-2 has to be found by numerical methods, as there are no analytical methods possible for the measured signal.

5.1.3 Measurement Results

As a first step, the data collected on the way from Breitbrunn to Utting was evaluated. The path of the ship can be seen on the map in Figure 5-1 The result of the distance estimation plotted over time is shown in Figure 5-4.

In Figure 5-4, it can already be seen, that the VDES signals provide a better estimate of the actual distance. However, the measurement also exhibits some artefacts at about 10:37 UTC. It is not yet understood what causes this, however multipath effects could be an explanation. As the RX antenna, was not mounted at the highest point of the ship, parts of the ship itself could act as a reflector and cause the signal from a stronger path to arrive at the antenna.

As the graph in Figure 5-4 does not allow a good comparison between the different signals, Figure 5-5 shows the RMSE of the estimated ranges over a sliding window of 30 seconds. It can be seen that the signals with 100 kHz of bandwidth perform noticeably better than AIS or VDES with 25 kHz.

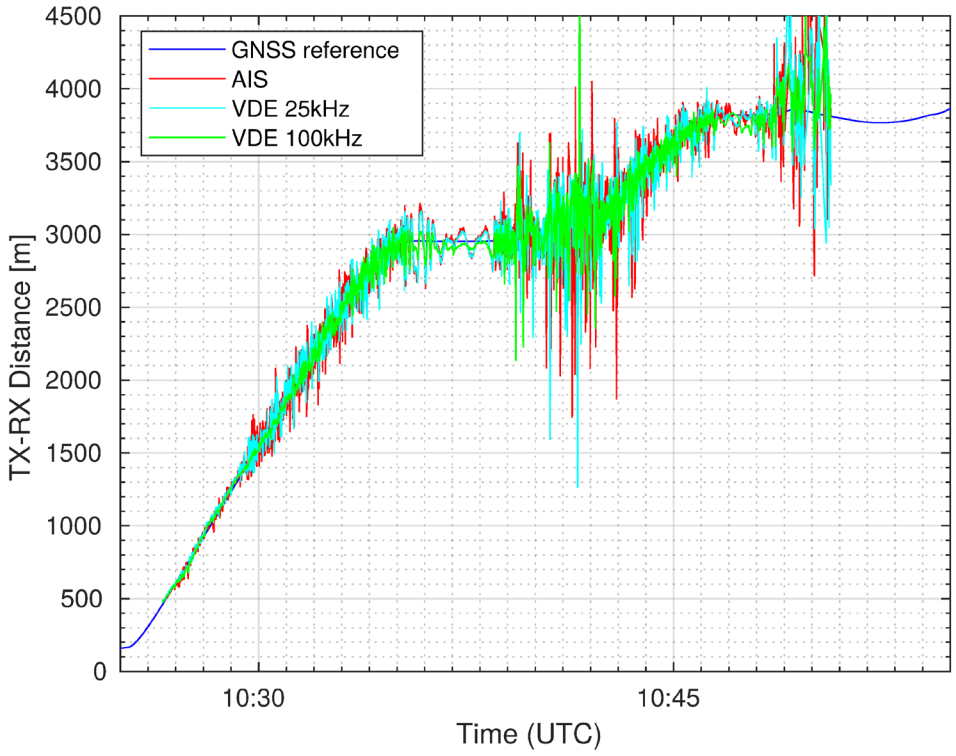

Figure 5-4: Ranging performance plotted over time.

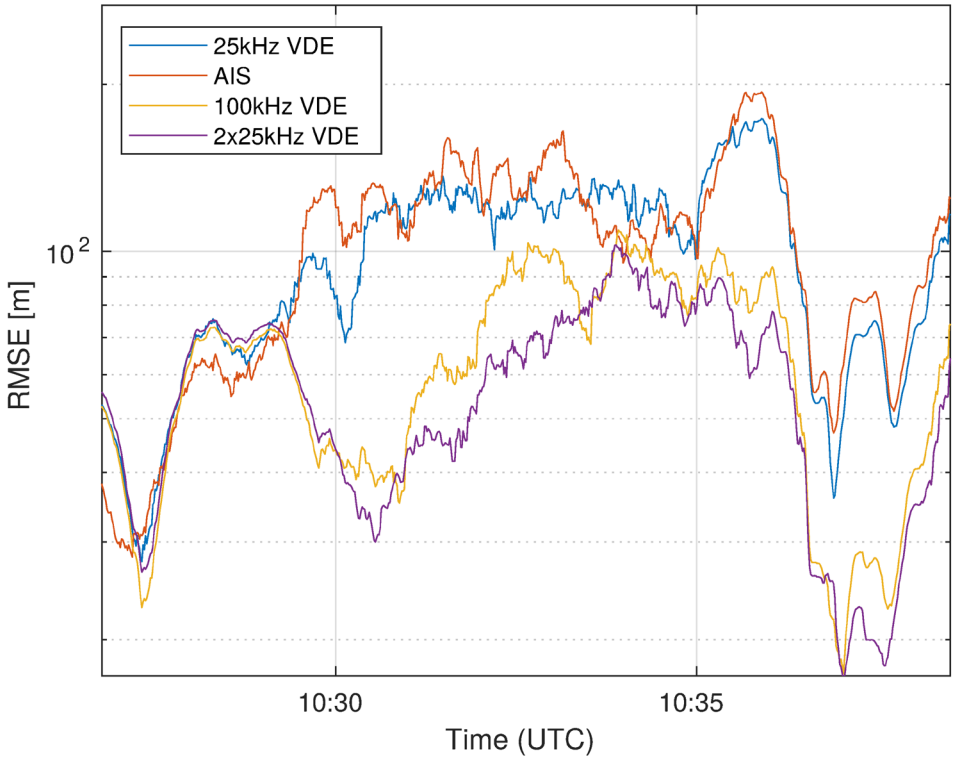

Figure 5-5: RMSE in a sliding 30 second window.

5.1.4 Summary

For the purpose of measuring ranges and calculating a position based on these ranges, significant improvements can be expected from the upcoming VDES system compared to the existing AIS. Theoretical considerations based on estimation theory and bounds on estimator errors suggest that using either a 100 kHz channel or two 25 kHz channels coherently provide the best results. The measurements that were performed, support this theory. However, further analysis of the measurement data is required, in particular considering signal propagation effects.

5.2 Positioning Experiment

In order to test the practical implementation of a VDES R-Mode system, we performed and assessed measurements on Lake Ammer near Munich in Bavaria. These measurements were the first experimental results of VDES R-Mode that resulted in a successfully estimated position. The measurement setup consisted of three land-based stations that transmitted a VDES R-Mode ranging signal as defined in Sec. 4.2, and a mobile transceiver unit that was placed on a boat.

5.2.1 Measurement Setup

The land side of the measurement setup consisted of three temporarily erected masts that were located on the shore of Lake Ammer, with the antennas at a height of approximately 10 m above the water. Each of the transmitters consisted of a laptop, a USRP B210 software defined radio, an amplifier, and a Septentrio PolaRx5TR GNSS receiver. The GNSS receiver was used to provide precise position information and accurate timing information to each of the base stations. The setup of one of the land stations can be seen in Figure 5-6(a).

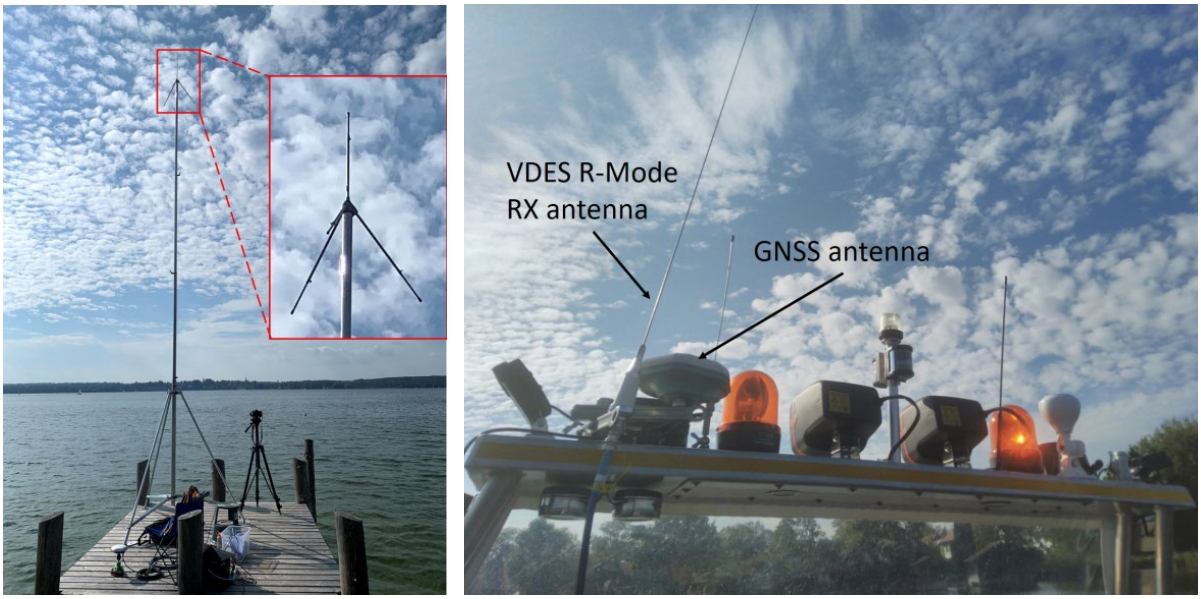

(a) Transmitter station with VDES transmitter antenna

(b) VDES R-Mode receive antenna and GNSS receiver antenna on the boat

Figure 5-6: Transmitter and receiver setup at Lake Ammer.

To coordinate the transmissions of different base stations, each base station was assigned a specific time slot, relative to the full second following the Media Access Control (MAC) layer allocation defined in the VDES standard [VDES15]. While the intended transmit power of a VDES base station, according to the standard, is 12.5 W without antenna gain, we were limited to a transmit power of 1 W EIRP based on the license of the German regulatory agency. Due to the use of a TX/RX switch, each of the land stations was also able to receive while not transmitting.

The positions of the transmitters were chosen in a way that sets up a good geometry for positioning estimation in the northern part of Lake Ammer. Specifically, the three transmitters were located at the waterside of the villages Utting, Buch and Schondorf. Their location, and the outline of the lake can be seen in Figure 5-10.

The mobile setup was similar to the setup of the land stations. Since the land stations are able to receive outside of their assigned transmit time slot, the mobile station was assigned a transmit time slot, too. However, this data set is foreseen for future evaluations. Like the land-based stations, the mobile station was equipped with a GNSS receiver to provide precise position information as reference and an accurate timing signal for the SDR. This is a deviation from the R-Mode system design that envisages clocks with lower accuracy at the receiver. However, investigating the effects of a less accurate clock was not in the scope of this experiment.

The Wasserwacht Bayern (Water Rescue Bavaria) supported us by driving our mobile station with a motorized boat. The antenna setup on the boat is shown in Figure 5-6(b).

As VDES only provides a single 100 kHz channel, it was not possible to assign each transmitter its own frequency. Thus, a time multiplexed setup was chosen. Each transmitter was assigned a 250 ms time slot, within which it could transmit without interference from the other transmitters. Figure 5-7 illustrates this approach.

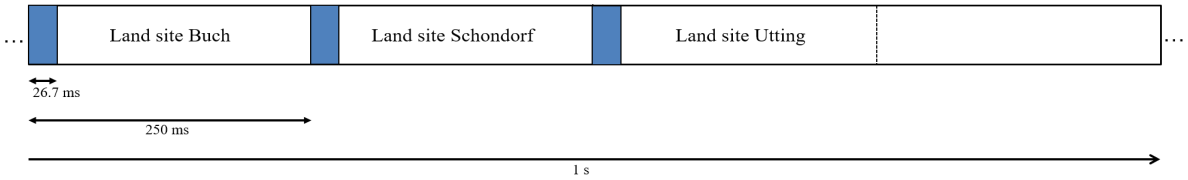

Figure 5-7: Time scheduling of the different land transmitters. The blue colored area represents the ranging sequence of length $T_{seq} = 26.67\text{ms}$ or one VDES time slot.

5.2.2 Measurement Results

The setup during the measurement was recording all data samples. Data evaluation itself was done in postprocessing. In order to obtain estimates for the ranges and for the radial velocities, a maximum likelihood approach was used. This means that the delay τ and the Doppler shift Δf were estimated by

$$(\hat{\tau}, \Delta\hat{f}) = \arg\max_{\tau,\Delta f} \sum_{k} x[k] s^*(k\,T_s - \tau)\, e^{j2\pi k T_s \Delta f} \qquad 5\text{-}3$$

with $x[k]$ being the received samples from the USRP, and $s(t)$ being the transmitted signal. A numerical optimizer was used to evaluate the $\arg\max$ operation. Since the signal delay from the SDR was not calibrated, all of the range measurements had a constant offset and the range estimate $\hat{r}$ was obtained as:

$$\hat{r} = c_0 \cdot (\hat{\tau} - \tau_{\text{offset}}). \qquad 5\text{-}4$$

The offset parameter τ_{offset} was obtained by comparing the estimated values with reference values from the GNSS receiver. The range measurements obtained this way are shown in for each base station, along with the corresponding reference values from the GNSS receiver.

For the Doppler frequency based estimation of the radial velocity, no such measures were necessary. The estimate for the radial velocity $\hat{v}_r$ was easily obtainable by

$$\hat{v}_r = -\Delta\hat{f}\,\frac{c_0}{f_0}.$$

The estimated velocities and their reference values are shown in Figure 5-9. Each plot shows the estimated values for all three base stations, as well as the reference values obtained from the GNSS data.

We implemented an Unscented Kalman Filter in Matlab, as described in Sec. 2.3, in order to track the boat's position and the boat's velocity. This tracking was done in a local Cartesian coordinate system. The zero coordinate was chosen as the mean position of the three base stations. The noise parameters in the Kalman filter were determined empirically. The evaluation was performed twice. Once with only the range measurements, and once with the measurements of the radial velocity in addition. The resulting estimated track of the ship for both evaluations is shown in Figure 5-10. The results for the estimated speed are shown in Figure 5-11.

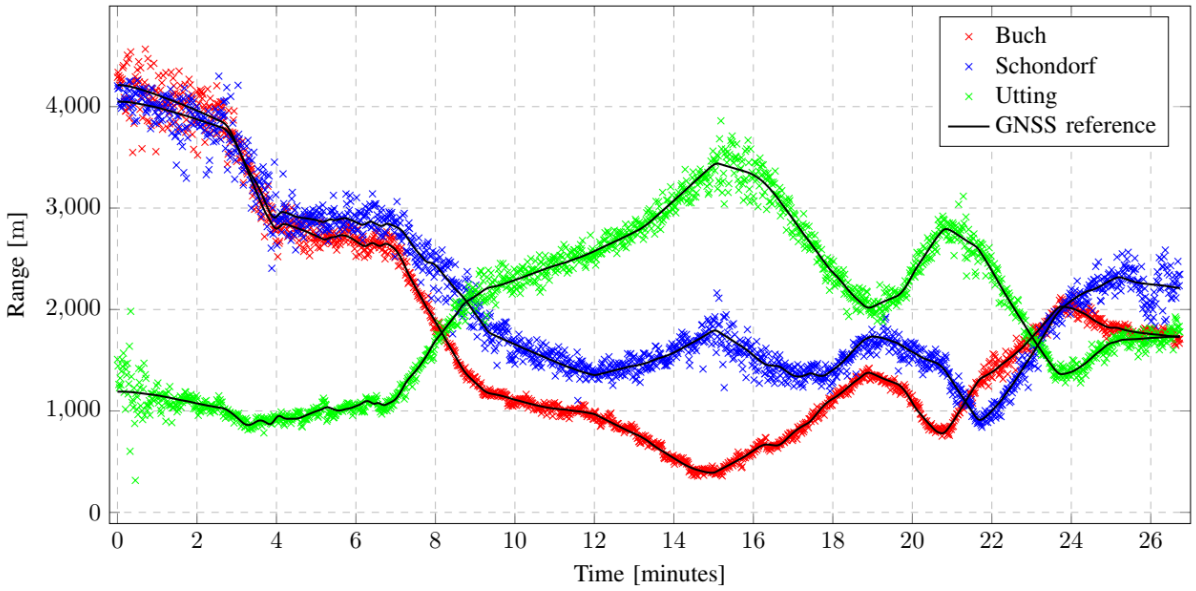

Figure 5-8: Estimated ranges and the GNSS reference.

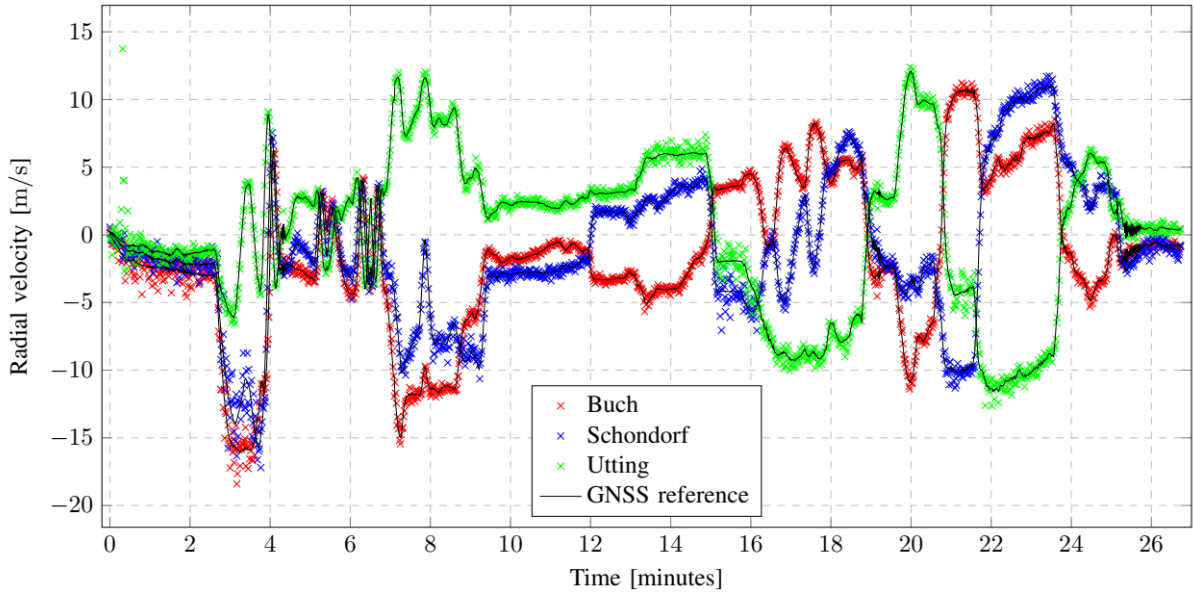

Figure 5-9: Estimated radial velocity.

It can be seen in that plot, that the addition of the radial velocity measurements to the evaluation significantly improved the positioning performance. To illustrate this further, the absolute difference of the tracked position to the GNSS reference position is being shown in Figure 5-12 for both evaluations. Figure 5-13 shows the empirical Cumulative Distribution Function (CDF) of the positioning error with and without the Doppler observations under line of sight conditions. The first 5 min of the recorded data were omitted from the computation of the CDF due to the non-line-of-sight conditions between the boat and the Utting land station. From this plot, we can see that the positioning accuracy that was achieved 95 % was 145 m without the Doppler observations, and 22 m with them. The effect of the Doppler observations on the estimated velocity is also considerable, as can be seen in Figure 5-14.

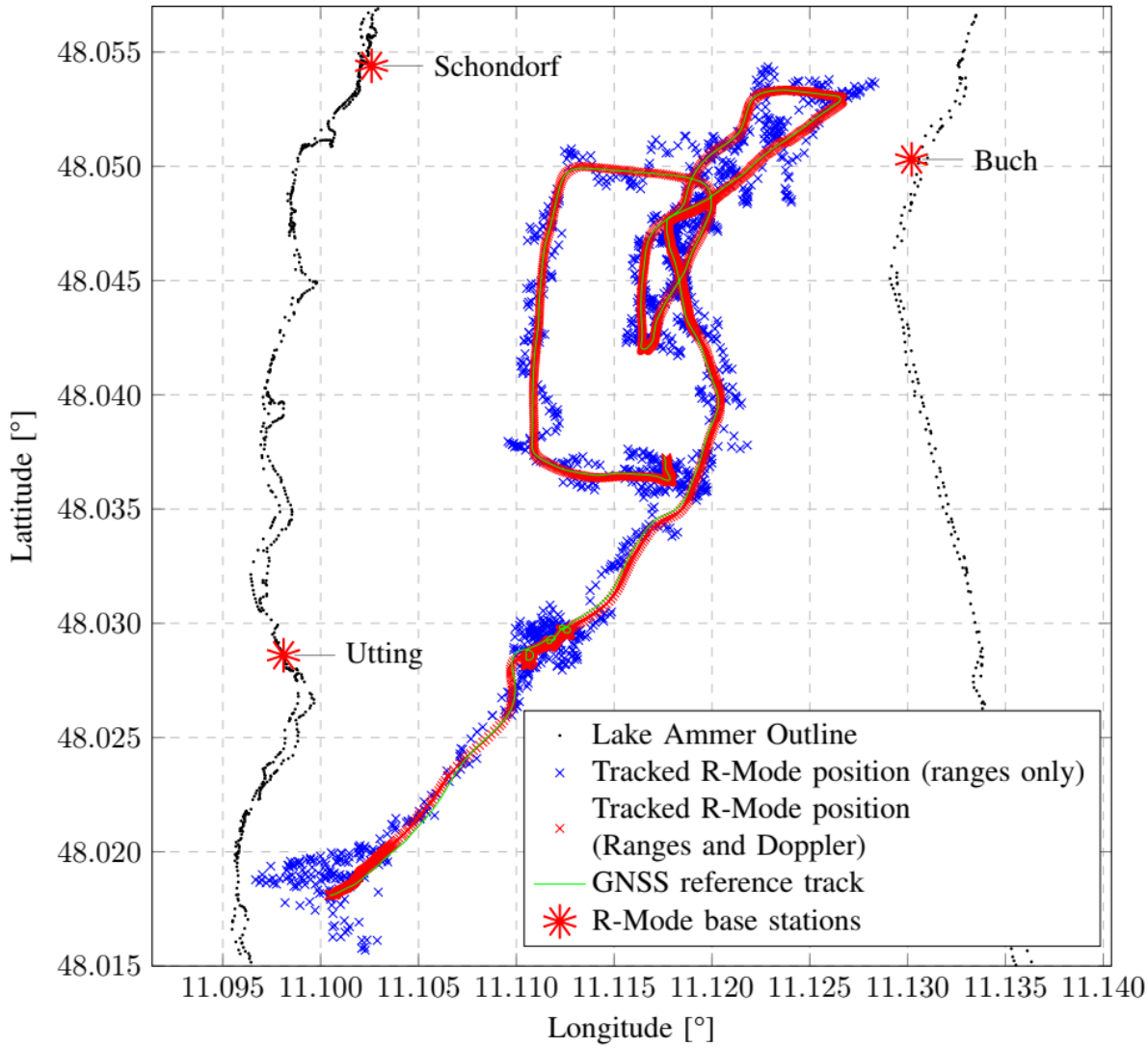

Figure 5-10: Positioning results of the Lake Ammer measurement.

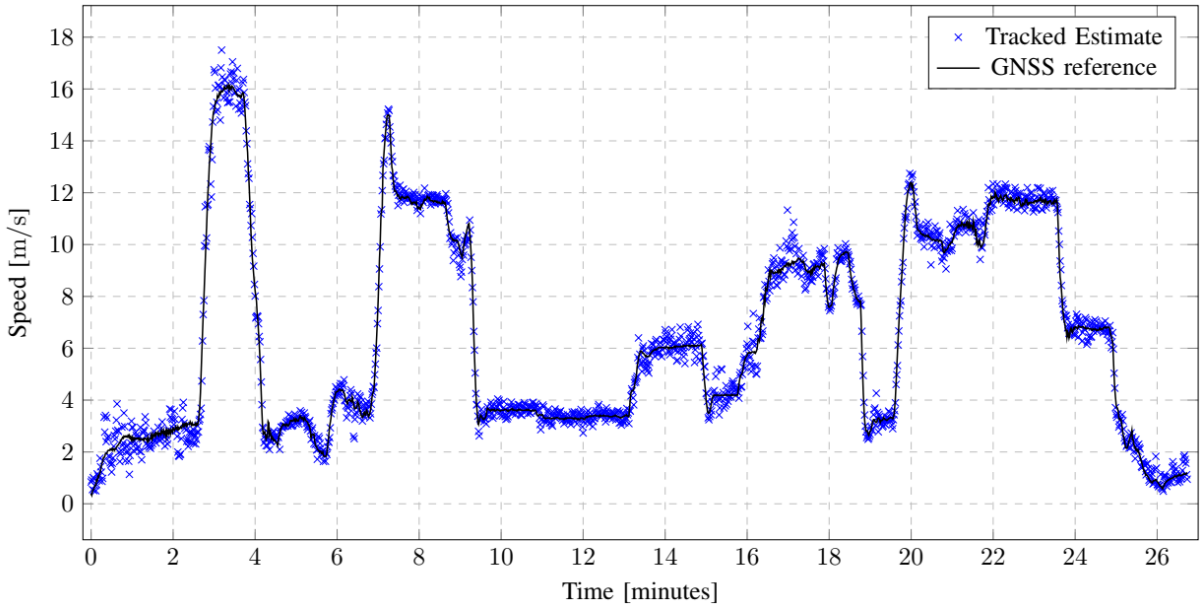

Figure 5-11: Estimated speed and reference speed obtained by GNSS.

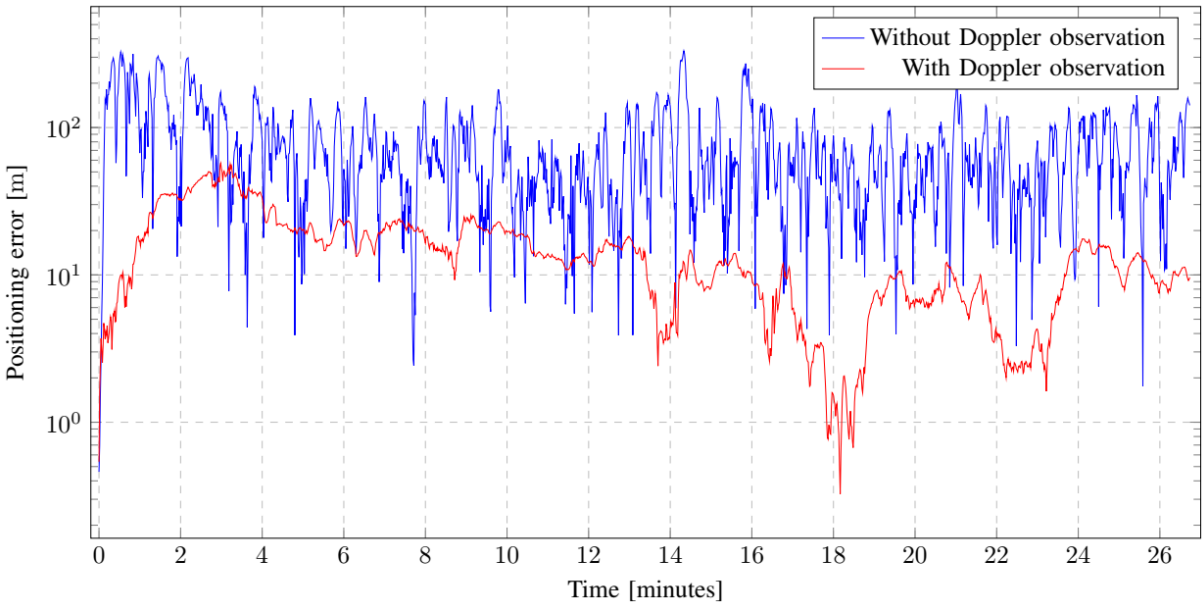

Figure 5-12: Positioning error after Kalman filtering.

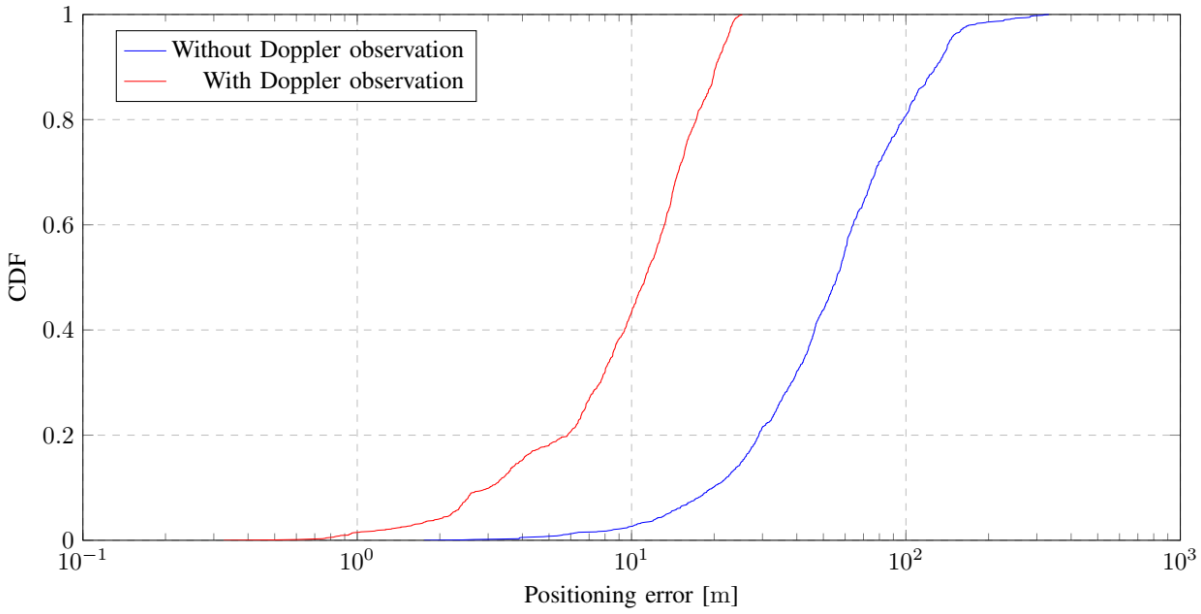

Figure 5-13: Positioning error CDF under line of sight conditions.

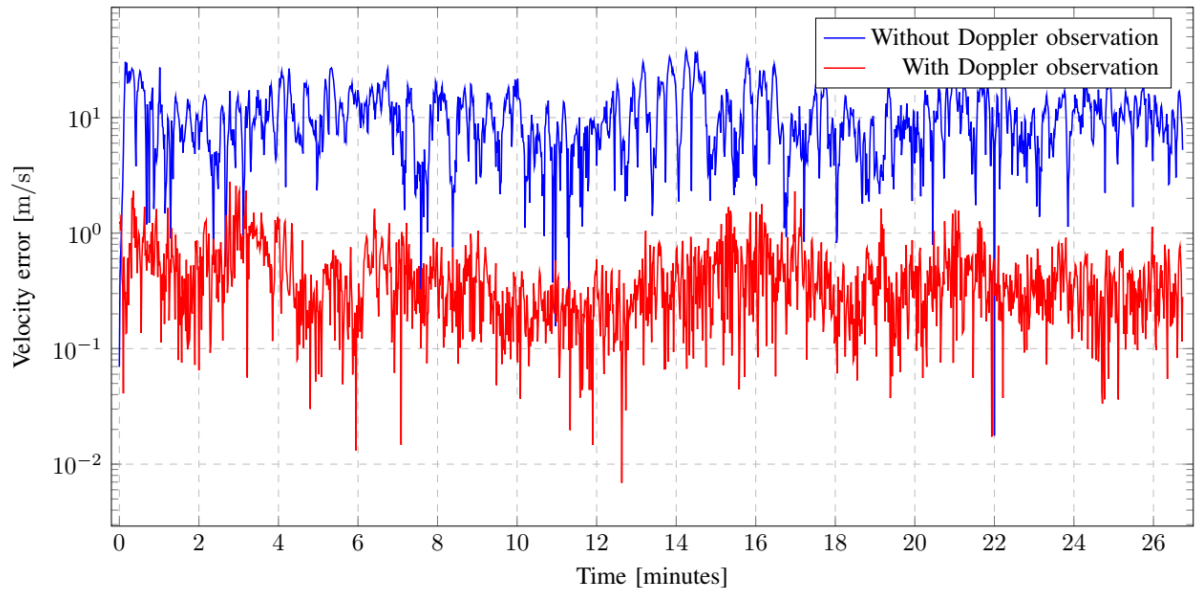

Figure 5-14: Absolute error of the estimated velocity after Kalman tracking.

5.2.3 Discussion

The measurement results show that estimating a position by utilizing VDES R-Mode signals is possible and that an accuracy of about 10 m can be achieved under good conditions where the line of sight between transmitter and receiver is unobstructed and the geometry of the base stations corresponds to small Dilution of Precision (DOP) values. Our measurements took place on Lake Ammer. Due to the limited distances between the base stations and the boat, the scenario represents a situation that could occur close to the coast, such as when approaching a harbour. As the density of maritime traffic is highest close to the harbour, resulting in high requirements on the positioning, this is an important use case of the R-Mode system. Since the transmit power in our experiments was only 1 W, which is 11 dB below the

12.5 W intended by the standard, it is plausible that, using the full power, similar results can be achieved at higher distances as well.

While existing literature on VDES R-Mode focuses on the range estimation aspect, our experimental results show that using the Doppler shift to estimate the radial velocity of the vehicle can greatly improve the accuracy of the tracked position estimate. As described in Sec. 2.1, the ranging performance depends on the bandwidth of the signal. The VDE system however offers only 100 kHz bandwidth, which limits the ranging performance. In contrast to that, the Doppler estimation performance depends on the duration of the signal, which could be increased further by utilizing multiple time slots of the VDE system coherently. This approach would increase the load on the VDE system. Since VDES is primarily a communication system, any resources that are solely dedicated to R-Mode will decrease the system's capacity for data transmission. Further research of how much performance can be gained by improving the Doppler estimation should be performed.

5.2.4 Conclusion

We have addressed system design aspects and evaluated the positioning performance of VDES R-Mode. The VDES R-mode positioning performance has been evaluated using both estimation theoretic and experimental methods. Including Doppler observations, in addition to range estimates, for position and velocity tracking at the VDES R-Mode receiver improves the positioning accuracy significantly. Experimental results show that VDES R-Mode is capable of achieving a 95th-percentile horizontal position error of 22 m under line of sight conditions with good geometry. Thus, VDES R-Mode is a promising approach for a maritime GNSS backup system which can fulfil the accuracy requirements of IALA, as defined in [IALA R-129].

6 Experiments at the Baltic Sea near Gdynia

6.1 Analysis of the 2020 Measurement Campaign Results

This chapter focuses on the analysis of the results of the VDES measurement campaign that took place in 2020. This was the third measurement campaign during the R-Mode project. As part of detailed analyzes, the following charts were obtained, thanks to which it was possible to explain and understand many interesting phenomena along the measurement route:

- measurement chart for the route to Karlskrona,
- measurement chart for the route to Gdynia,
- SNR measurement chart,
- graph of measurements of the main-peak-to-side-peaks ratio,
- accuracy error graph,
- RMS curves for all measurements,
- RMS curves for the water environment,
- RMS curves for the terrestrial environment,
- impact of the width of the Hel peninsula on the RMS,
- map with accuracy errors in the measurement campaign,
- comparison of results from the AIS campaign with the VDES campaign.

6.1.1 VDES R-Mode campaign preparations

National Institute of Telecommunications (NIT) organized two measurement campaigns of the VDES R-mode System. Both took place on the Baltic Sea waters, i.e. in the target environment of the future system.

For the purpose of the measurements, the Maritime Office in Gdynia (MOG) provided its VHF antenna installation located on the tower near the entrance to the port in Gdynia. It was the localization of the R-Mode testbed's transmitter (Tx) which was designed, built and installed by the NIT.

The testbed receiver (Rx) – also built by the NIT – was located aboard the Stena Line ferry operating between Gdynia and Karlskrona

The main goal of the measurements was the analysis of the impact of the maritime radio VHF channel on the ranging accuracy when using time-based methods (this analysis will be performed for different weather conditions).

In order to eliminate some sources of errors, the rubidium oscillators were installed on both ends of the radio link. Additionally, the exact locations of the transmitting/receiving stations were determined via RTK measurements and using GNSS+EGNOS.

The configuration for which the measurements were performed is shown below:

- Modulation: π/4-QPSK
- RRC filter and 100 kHz bandwidth,
- Data rate: 76,8 ksym/s,
- New USRP modules (higher sampling rate and better A/D converter resolution),
- Gold Code length: 1877 symbols,
- compared to the second measurement campaign, the Hann Window was not used this time,
- VDES physical layer will allow to achieve 8-fold increase of the data rate (consequently, the correlation's peak width will decrease 8 times). Additionally, VDE-TER modulation schemes and filtering mechanisms make the signal more suitable for both correlation and, consequently, also for navigation purposes,
- No filter on the transmitting side,
- Amplifier with higher output power levels (greater range of the station!),
- Different LNA and filter configuration on receiver side.

One week before the planned measurement campaign, calibration measurements were carried out. They were aimed at thorough preparation of the measuring equipment and checking all measuring modules. The Table 6-1 contains information on the number of recorded files, which were later processed in the signal correlation application and during the validation of data reception.

Table 6-1: List of the number of files recorded during calibration

Route	Number of files	File size
The first point is 30 meters from the broadcasting station	1790	39,9 GB
The second point is located 450 meters from the broadcasting station	1690	39,2 GB
The NiT building is 17450 meters away from the broadcasting station	1908	42,2 GB

The graph below shows the results for the processed part of the files (Figure 6-1):

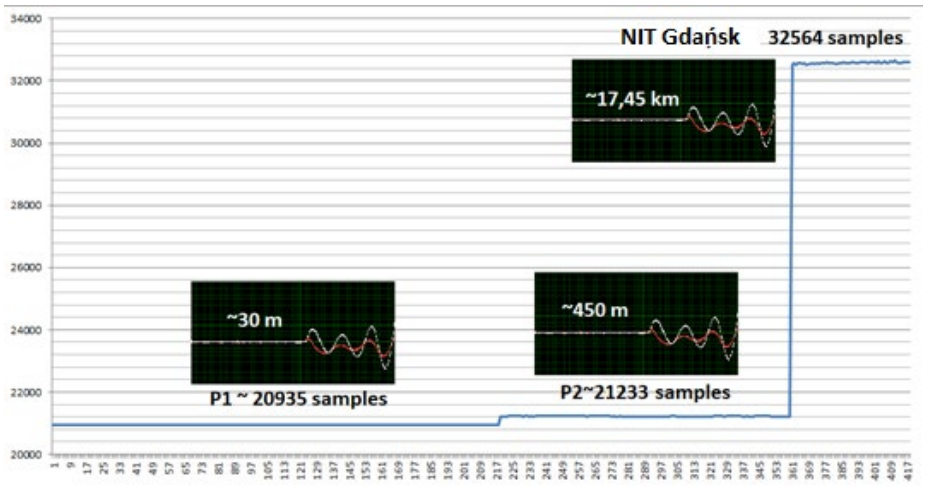

Figure 6-1: Processed calibration files

From the graph above, we can see that the calibration measurements ended with a positive result. The recorded sample files have been processed in the signal correlation application. All signals were correctly received and correlated. The obtained results allowed for the selection of a constant value of the number of samples that should be subtracted during the measurements. This correcting factor considers all cable delays and all other delays introduced by the samples' recording application. By subtracting the correctly calculated delay, the exact distances that are the result of a signal correlation application can be obtained.

Pictures from the calibration measurements that took place in the port of Gdynia are presented below (Figure 6-2 to Figure 6-7).

Figure 6-2: Photo from calibration a)

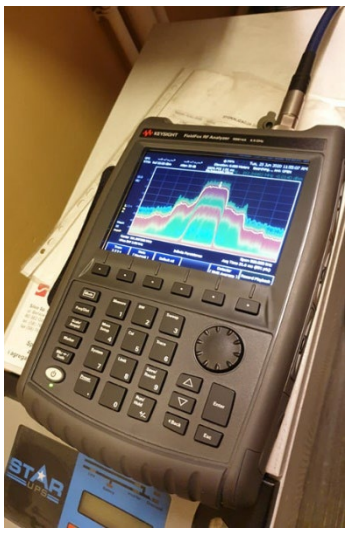

Figure 6-3: Photo from calibration b)

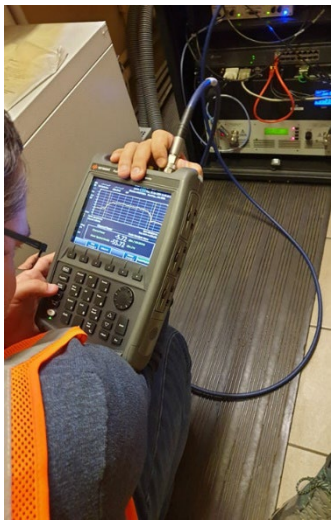

Figure 6-4: Photo from calibration c)

Figure 6-5: Photo from calibration d)

Figure 6-6: Photo from calibration e)

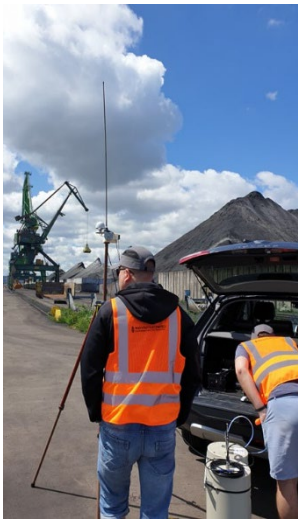

Figure 6-7: Photo from calibration f)

In the pictures below, we can see the signals recorded during calibration measurements in the NIT building. The recorded samples of I and Q are shown in Figure 6-8. The next screenshot shows a calibration measurement scenario for receiving signals from the NIT building. The preview picture shows a map with the marked place of sending and receiving samples. We can also preview the recorded signal and show the signal correlation application that determined the distance based on the recorded signal (Figure 6-9).

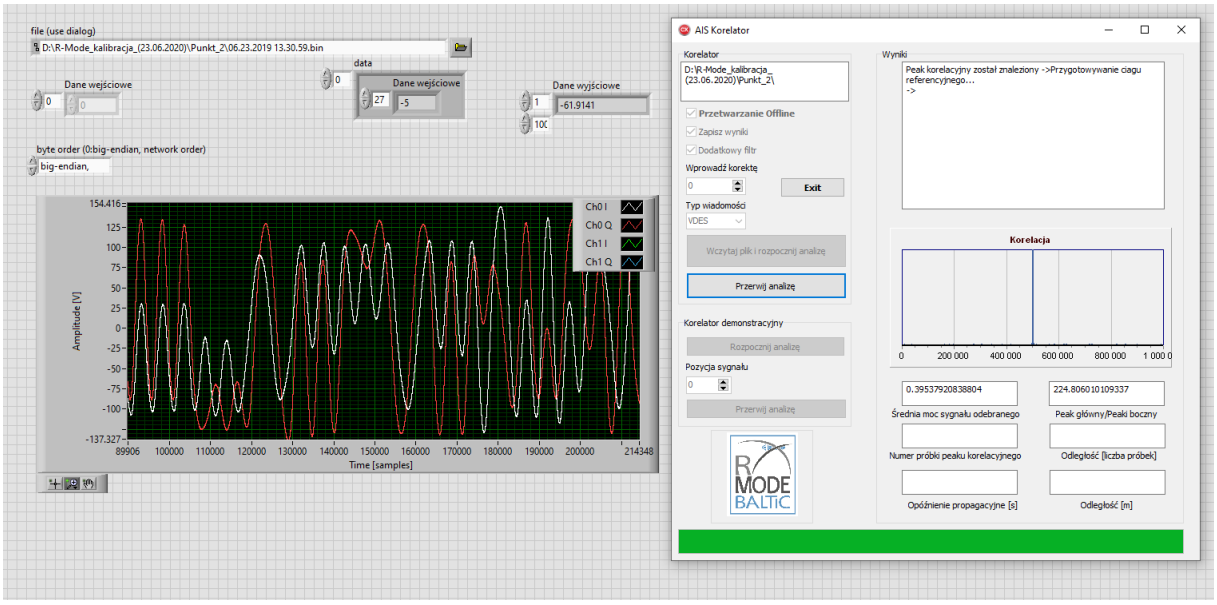

Figure 6-8: Application with recorded samples I and Q

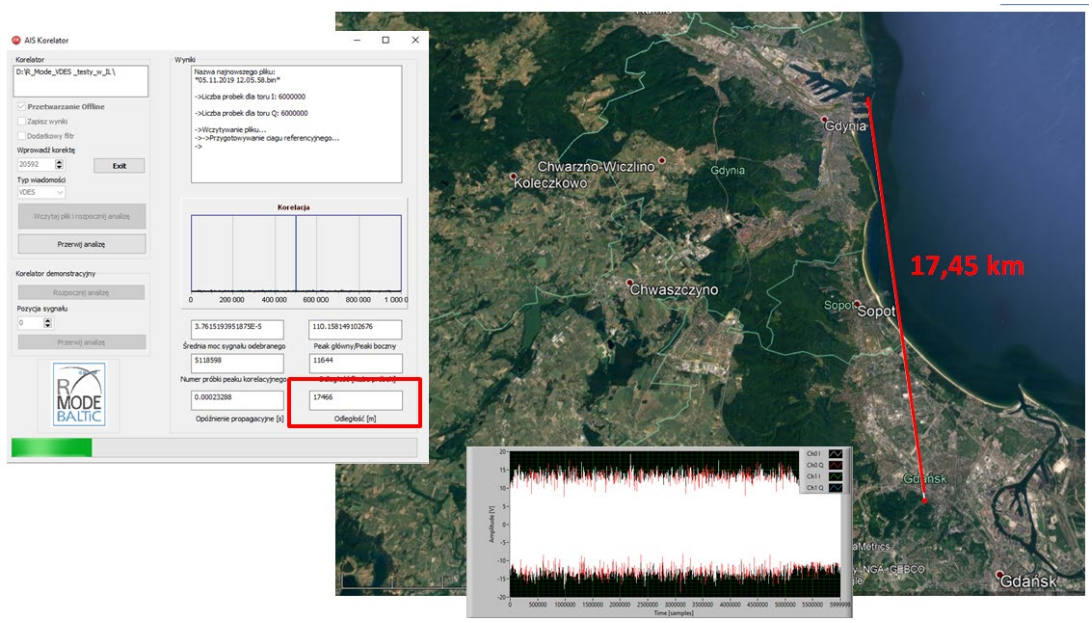

Figure 6-9: Application for the correlation of signals

6.1.2 Analysis of results from the VDES measurement campaign

The measurements took place on 29-30 June 2020. The Table 6-2 below shows the number and size of the files which have been processed by the application for signal correlation.

Table 6-2: Number and size of processed files for VDES

Route	Number of files	File size
Gdynia – Karlskrona	20830	494 GB
Karlskrona - Gdynia	20700	470 GB

The Table 6-3 gives the exact start and end times of the measurements.

Table 6-3: Time of processed files for VDES

Route	Start time	End time
Gdynia – Karlskrona	02:04:44	06:04:17
Karlskrona - Gdynia	16:16:32	22:10:33

Compared to the previous measurement campaigns, many more measurements records were collected during this campaign [VRPSD21]. The reason for that was the expected increase in the range of the received signal caused, among others, by removing the Hann window from the transmitted signal and by removing the VHF filter on the transmitting side.

Pictures from the measurement campaign are presented below (Figure 6-10 to Figure 6-13):

Figure 6-10: Photo from measurements a)

Figure 6-11: Photo from measurements b)

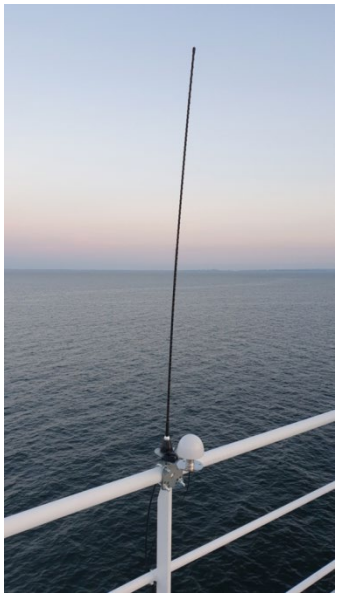

Figure 6-12: Photo from measurements c)

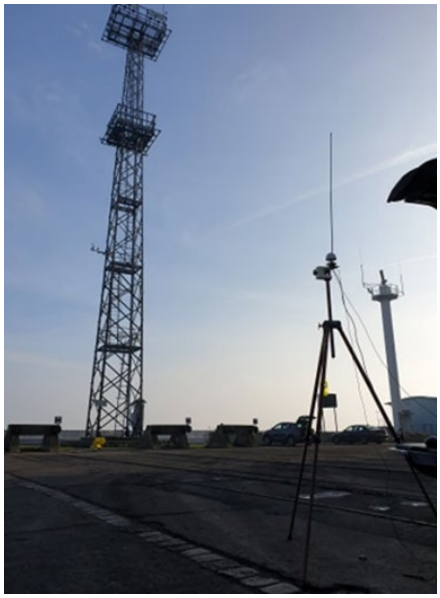

Figure 6-13: Photo from measurements d)

ANALYSIS ON THE KARLSKRONA – GDYNIA ROUTE

Below, two graphs present the distance depending on the number of the recorded file containing samples. The first graph (Figure 6-14) shows the results that have been calculated by the signal correlation application. It was possible to obtain the correct correlation up to about 150 km. This range is twice as large compared to the value obtained in the 2019 measurement campaign [AAVR20]. The second graph (Figure 6-15) shows the results recorded by the GNSS receiver.

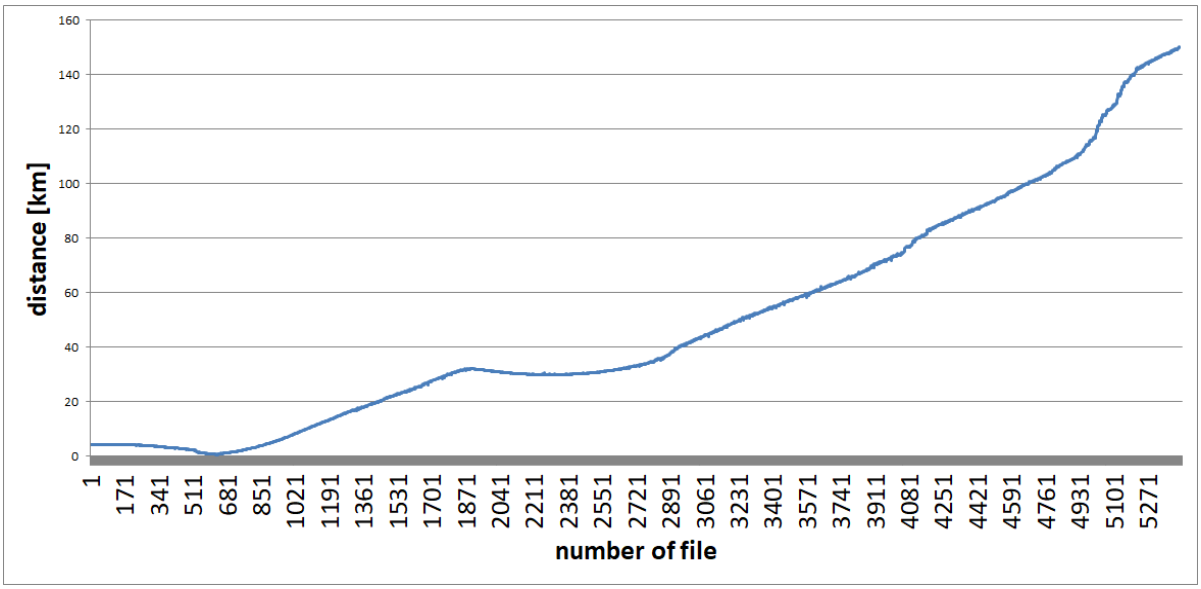

Figure 6-14: Distance measurements from the application for the correlation of signals on the Gdynia-Karlskrona route

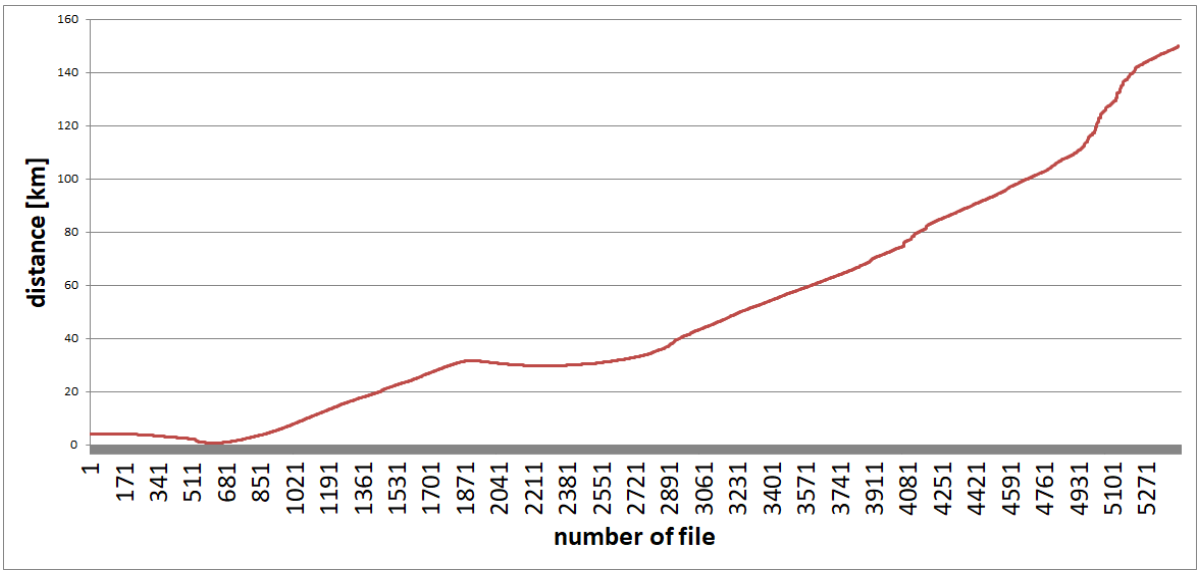

Figure 6-15: Distance measurements from the GNSS + EGNOS receiver on the Gdynia-Karlskrona route

On the basis of the results presented above, in the next steps it was possible to calculate the error of the determined distances and at the same time to calculate the RMS depending on the signal strength. By visually superimposing the results obtained from the correlator and the GNSS receiver for this campaign (Figure 6-16) and comparing these results with the AIS campaign (Figure 6-17) that took place in 2019, we can see a huge difference in the distance indicated. It is noticeable from the 20 km mark. This analysis is more for illustrative purposes. More detailed cases will be discussed in the following sections.

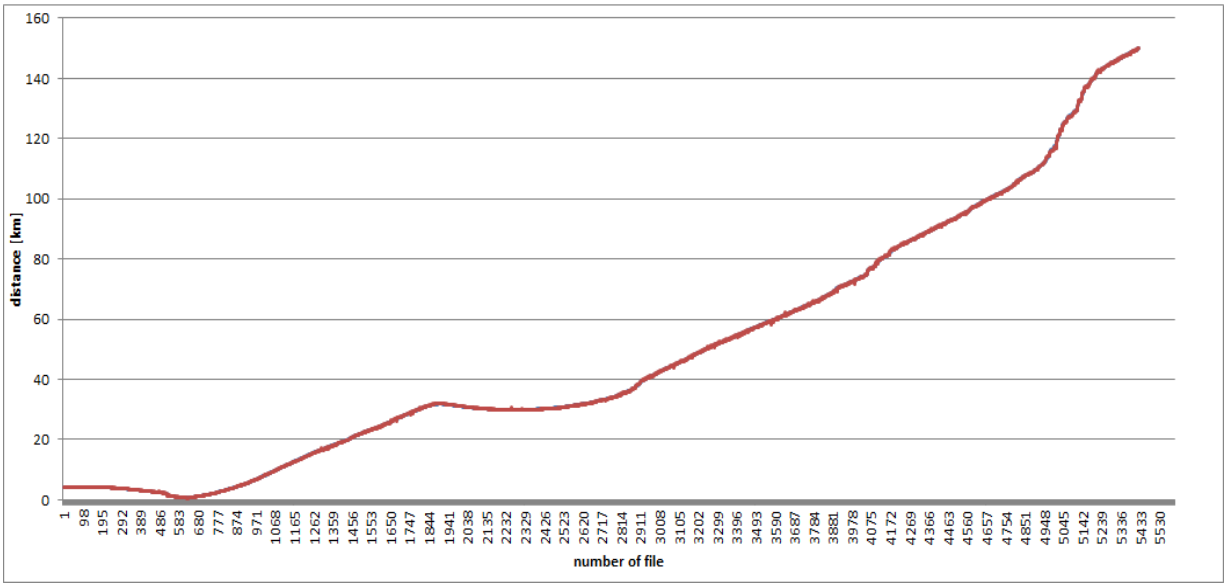

Figure 6-16: Superimposed results from the correlator and GNSS + EGNOS receiver for the VDES measurement campaign on the Gdynia-Karlskrona route

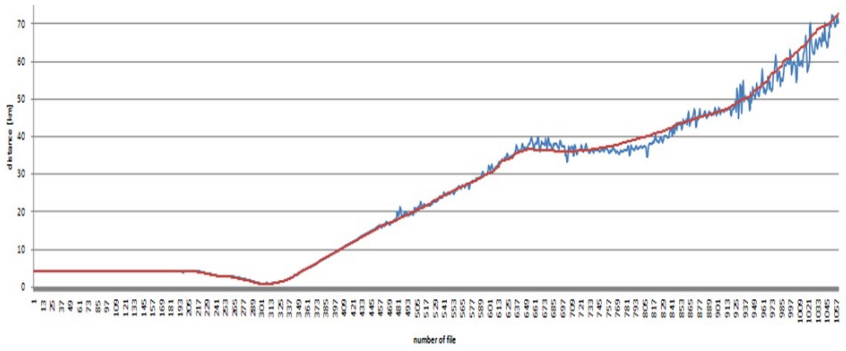

Figure 6-17: Superimposed results from the correlator and GNSS + EGNOS receiver for the AIS measurement campaign on the Gdynia-Karlskrona route

The next step presents the SNR values obtained on the Gdynia-Karlskrona route (Figure 6-18). This graph shows how the ratio of signal power to noise power was changing throughout the entire route. In the first part up to the file number 900, we can see that the survey vessel was in and in the vicinity of the port. The signal strength in this case is very high. As we got closer to the Hel Peninsula, the signal strength decreased proportionally. The next part of the chart shows the SNR value increases above the file number 1900. This is due to the fact that the ship in this section was parallel to the Hel Peninsula and the distance between the transmitting and receiving antennas was smaller than in the area where the ship had to circumnavigate Hel. By using a filter on the receiving side, it was possible to increase the signal power to noise power ratio.

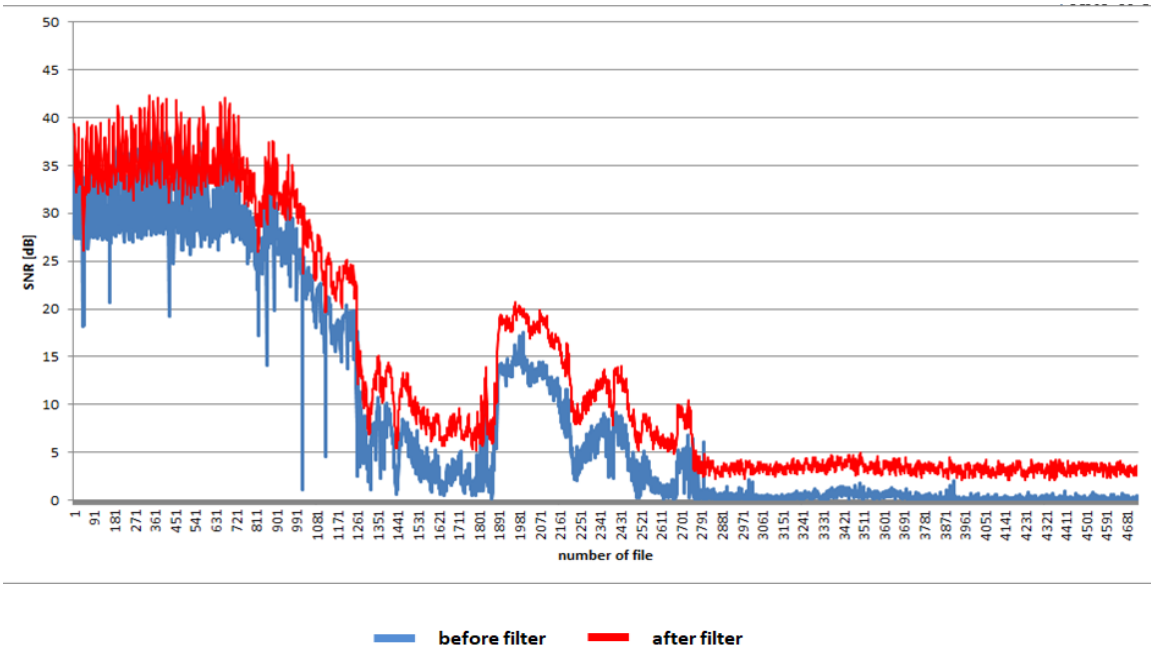

Figure 6-18: Measured SNR on the Gdynia-Karlskrona route

A plot of the correlation peak to adjacent peaks is shown below. This plot (Figure 6-19) allows us to find out at which times the correlation was the most effective. This factor is important because when its value is high, a better accuracy of the calculated distances can be observed. This means that the mean value of the main peak is much greater than the mean value of the adjacent peaks. It indicates very good correlation properties of the signal.

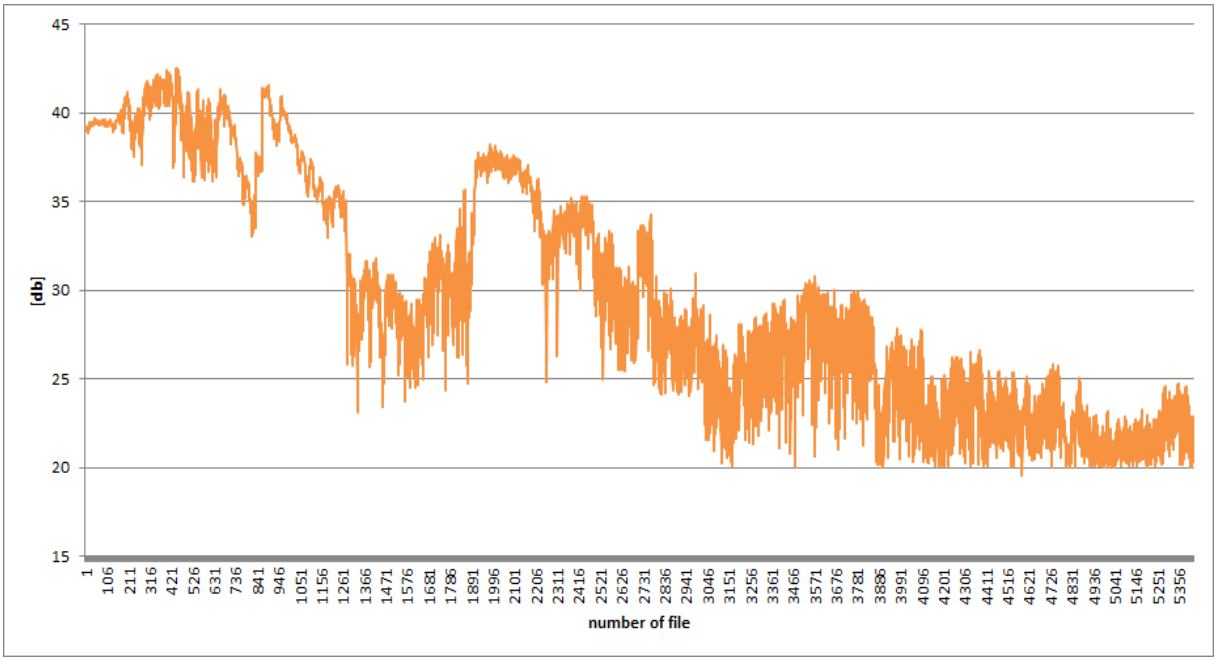

Figure 6-19: Measurements of the 'highest peak/ side peaks' ratio at the Gdynia – Karlskrona route

On the basis of many studies on the received samples and their processing in the correlation application, it was possible to establish correlation value thresholds. By using such a solution, the R-Mode positioning system is protected against false results from the correlation

application. This applies to files where it is difficult to distinguish the useful signal from noise with low SNR. On the basis of many studies, it is possible to estimate the threshold of the correlation value, below which we can assume that a given signal was noise, and not a useful signal. As a result, the correlation result for the uncorrelated data file is not saved and is not passed on to the next application, which is used to compute the position. This way we can avoid false position results.

In Figure 6-20 to Figure 6-22, there are three graphs that show the efficiencies obtained by the correlators. During the processing of measurement files, the signal correlation application recorded the calculated distance accuracy for several types of correlators in order to later analyze their effectiveness in real conditions. In the graphs below, the samples indicate by how many meters the determination of the accuracy of the distance per sample was improved = 1.5 meters (for the sampling frequency of 200 MHz). The efficiency of a given correlator means its ability to better optimize the determined distance errors.

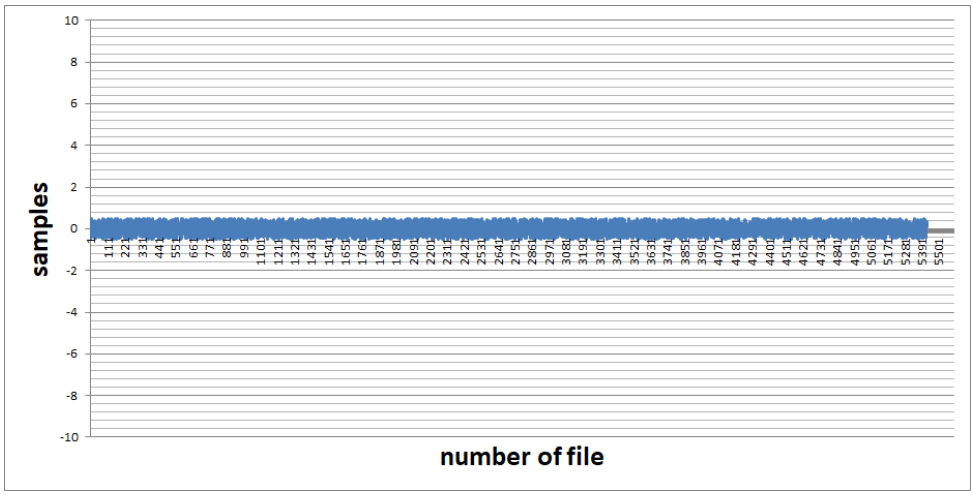

Figure 6-20: Effectiveness of using multicorrelation - Extended correlator d1=d2=1

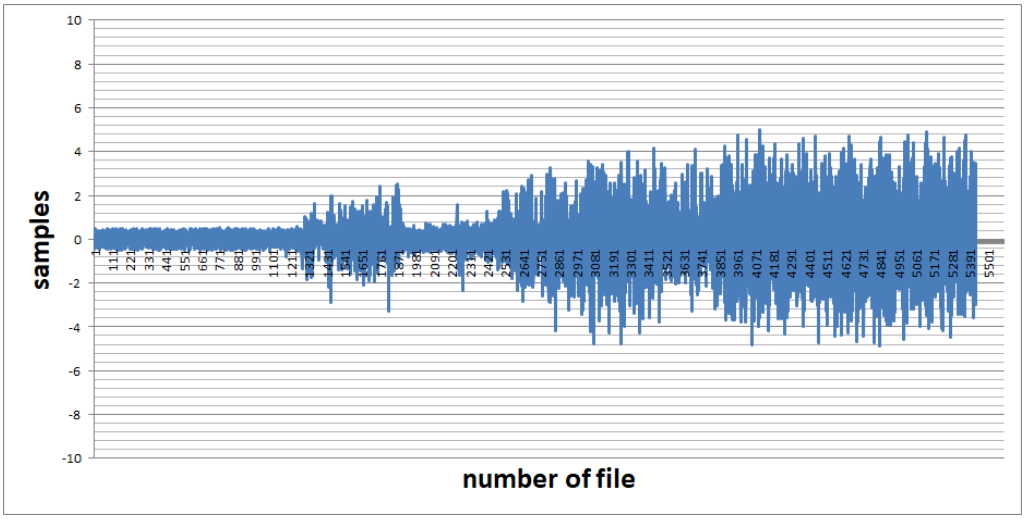

Figure 6-21: Effectiveness of using multicorrelation – Double-delta correlator d1=d2=10

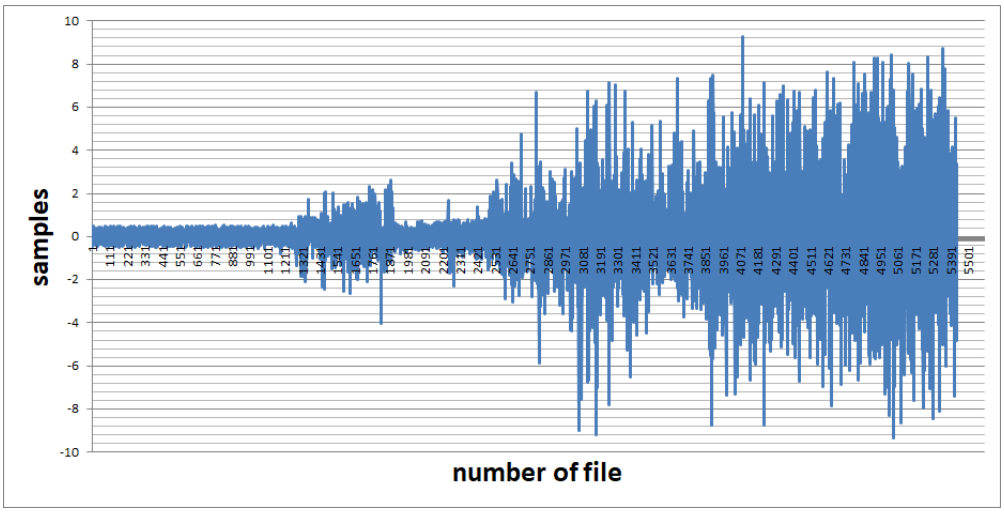

Figure 6-22: Effectiveness of using multicorrelation - Double-delta correlator d1=d2=20

The above graphs show the efficiency of the applied correlator depending on the width of the sample spacing of the second pair of this correlator. Three cases of this sample spacing have been studied in particular. In the first case, it was an extended correlator, where the analysis was focused between the peak with the maximum value and a pair of samples around this main peak. This solution only improves the determination of the accuracy of the distance by approx. one sample, which translates into a maximum improvement of 1.5 m in this case, where the sampling frequency on the receiving side is 200 MHz. In the next case, the spacing of the second pair of samples is 10 samples between the main peak and the sample coming from the second pair of correlators. Such a configuration already improves the determination of the distance accuracy by 5 samples, which in practice amounts to 7.5 meters. In the third case, with a sample spacing of 20, we have an improvement in the determination of the distance by about 13 meters. This is the best result obtained. It seems that if the next time the sample spacing in the correlator was increased, we would have obtained a better result. But this is not the case as we can see in the chart below (Figure 6-23):

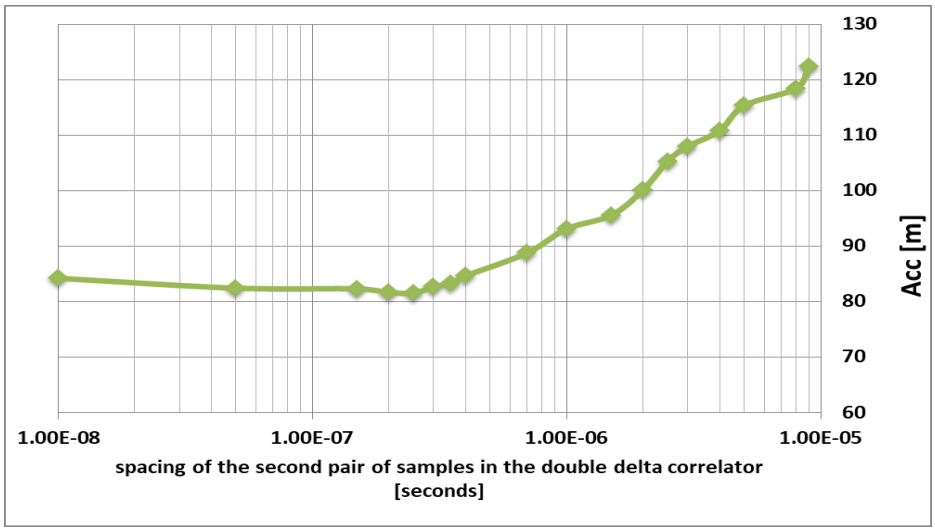

Figure 6-23: The accuracy of the distance as a function of the spacing of the pair of samples in the correlator

Figure 6-23 shows a chart with tests of the selection of the samples spacing in the correlator for determining the distance. These tests were performed on files obtained from calibration in the port of Gdynia. On this basis, a simulation was performed to apply different sample pair delays. With the selection exceeding 20 samples, the determination of the accuracy starts to deteriorate more and more. It needs to be added that VDES measurement campaign was carried out with the sampling frequency on the receiving side equal to 200 MHz. To see the best efficiency of a multicorrelator – we have to work with signals of lower frequencies. Such research will be presented in the next chapter.

For illustrative purposes, a graph (Figure 6-24) with the calculated distances by a signal correlation application superimposed on a graph of the efficiency of the correlator for the optimal sample spacing of the second pair (i.e. 20) is shown.

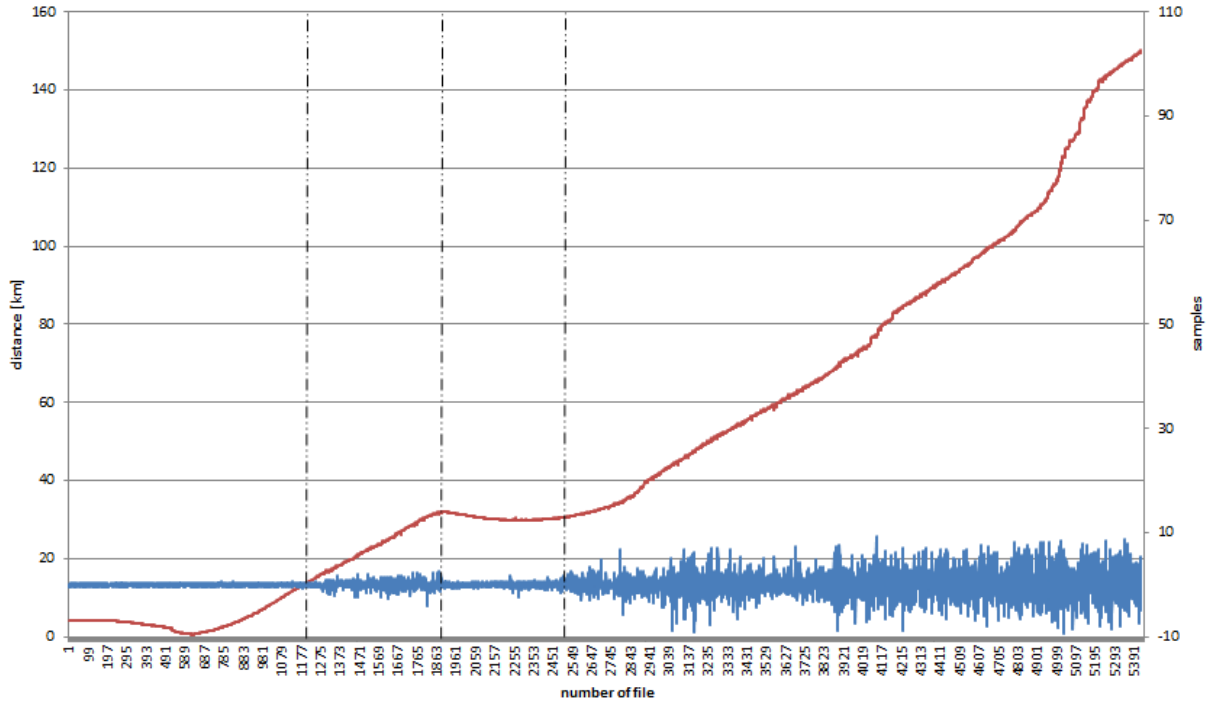

Figure 6-24: Ranges where the multicorrelator d2 = 20 operated most effectively

The red curve indicates the distance determined by the signal correlation application, while the blue one indicates how many samples have improved the determination of the distance due to the double delta correlator utilization.

The accuracies obtained at the calculated distances for selected places are presented below (Figure 6-25). These accuracies are much better than in the previous measurement campaign. For the short distances from the transmitting antenna, it can be seen that the distances from the GNSS receiver almost coincide with the results that were calculated by the signal correlation application. Such results allow for their subsequent transfer to the positioning application and the calculation of the exact position of the receiving station. This is very important, especially in the port where accurate navigation is critical. For long distances over a distance of 66 km, this error is 180 meters. This is a very good result compared to previous measurement campaigns. It should also be added that at a distance of about 120 km, these accuracies were in the order of 300 meters, which is still a satisfactory result.

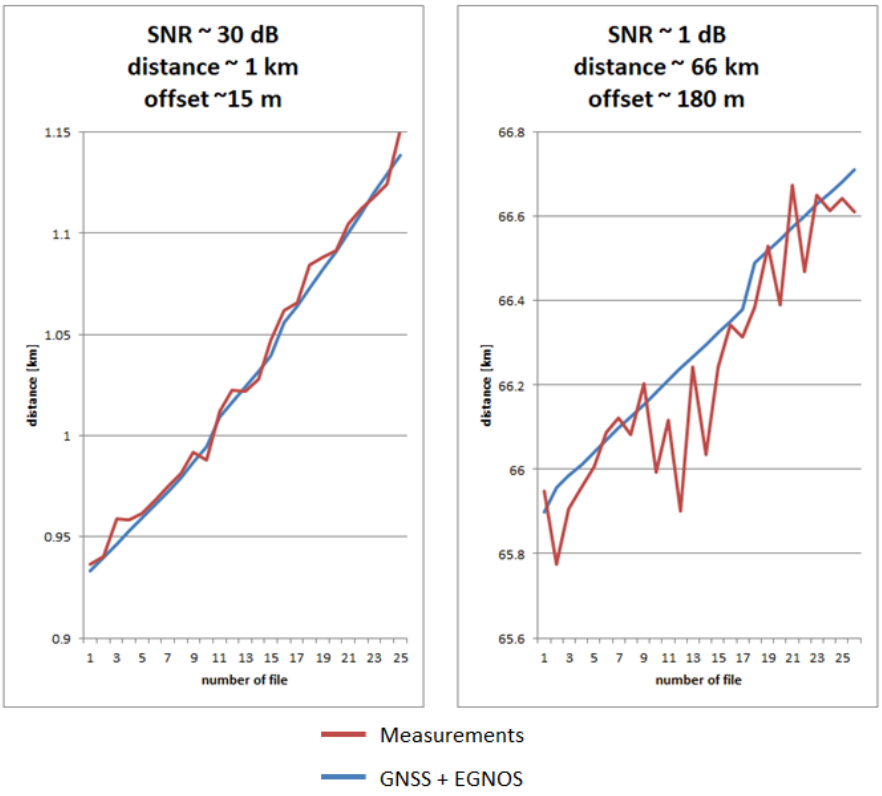

Figure 6-25: Accuracy obtained on measurements at the Gdynia – Karlskrona route

The characteristics of the error in determining the distance depending on the file number is presented below (Figure 6-26). It can be noticed that along the entire route, the errors here reach about 400 meters at the edge of the correlation. A more detailed discussion of this graph can be found in the next section when we will compare it with the errors obtained in the previous campaign.

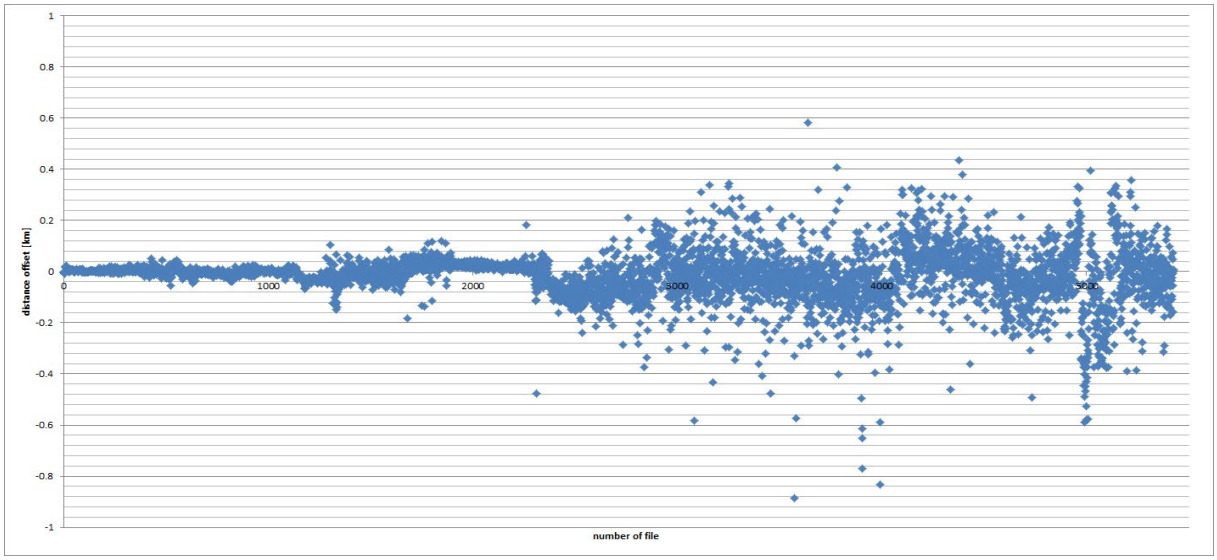

Figure 6-26: Distance error accuracy at the Gdynia – Karlskrona route

ANALYSIS ON THE KARLSKRONA – GDYNIA ROUTE

Unfortunately, some problems on the Karlskrona-Gdynia route occurred. At a distance of 50 km from the transmitting antenna, the oscillator became unsynchronized. The consequence of that was that the previously calculated correction value was no longer valid at that moment. During the desynchronization of the oscillator, there was a jump by 1000 samples, which in practice translates into 1.5 km. With each subsequent measurement, the delay value of one sample was added to the sample file. The next big fault occurred near the port of Gdynia. There, the value of 8,000 samples was added.

After analyzing the problems that occurred, correction values for fault points were applied manually, and additional delays were added in the form of one sample with each subsequent measurement.

Of course, for further analysis of the effectiveness of the positioning system, its RMS calculations and accuracy, only the route from Gdynia to Karlskrona – where no such problems occurred – were taken into account. For the experimental purposes, on the Karlskrona-Gdynia route, a manual delay correction was added and the accuracy of the distance after this correction was also analyzed, which is included in this subsection. Below is the graph before the correction (Figure 6-27):

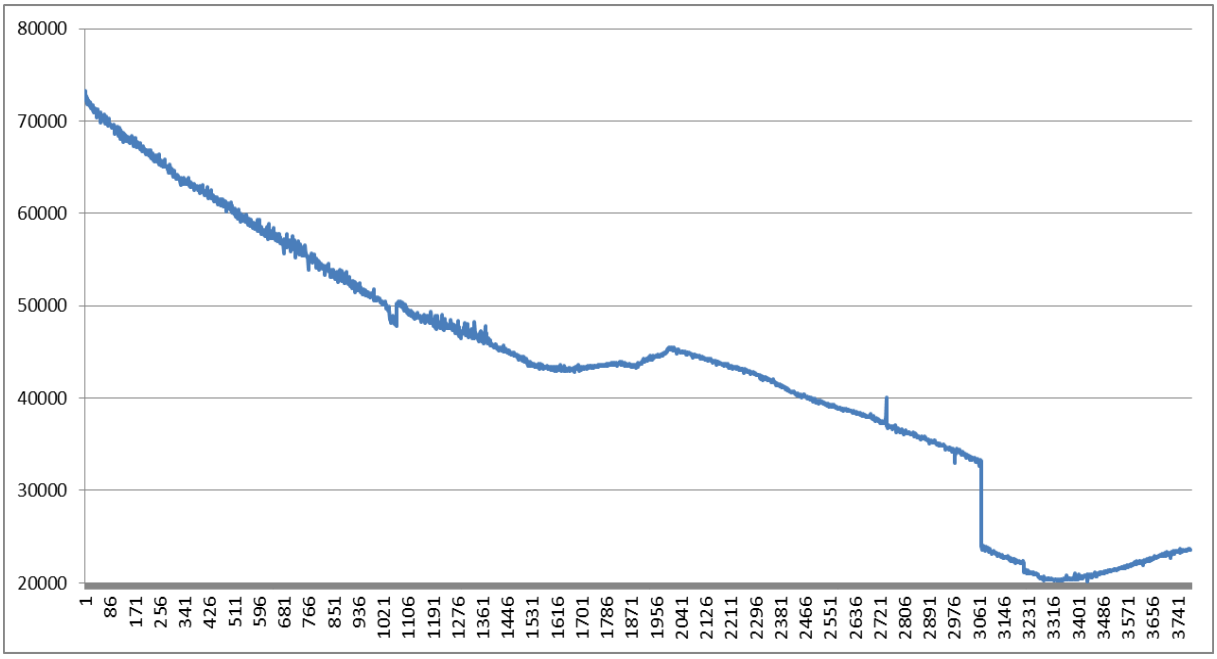

Figure 6-27: Karlskrona - Gdynia route with problems during measurements

Below are two graphs showing the distance depending on the number of the recorded file with samples. The first graph (Figure 6-28) shows the results that have been calculated by the signal correlation application. It was possible to obtain the correct correlation up to about 80 km. The second graph (Figure 6-29) shows the results recorded by the GNSS receiver.

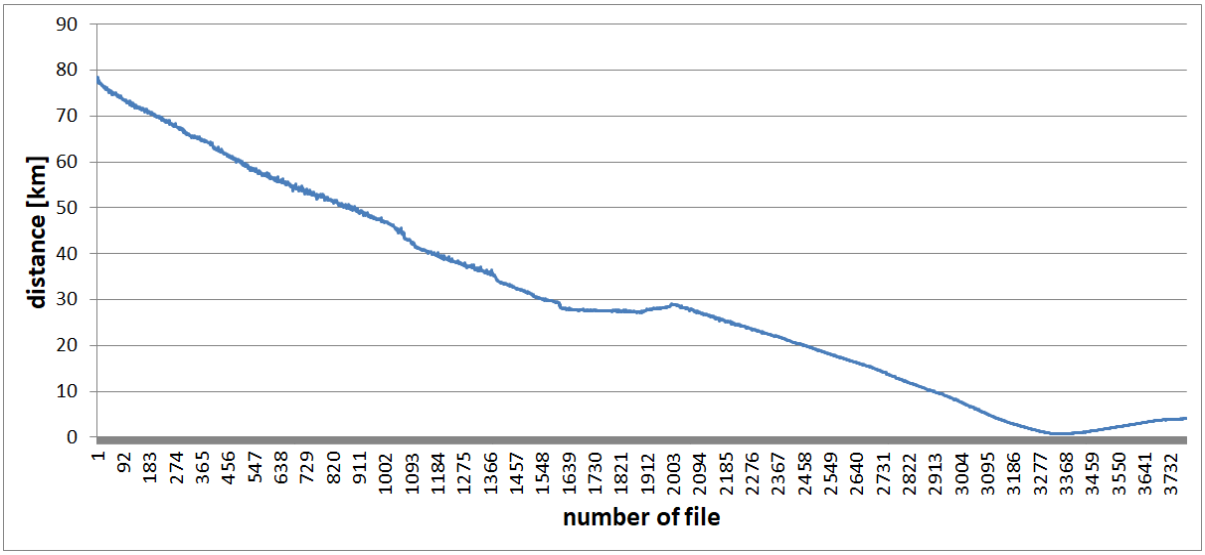

Figure 6-28: Distance measurements from the application for the correlation of signals on the Karlskrona-Gdynia route

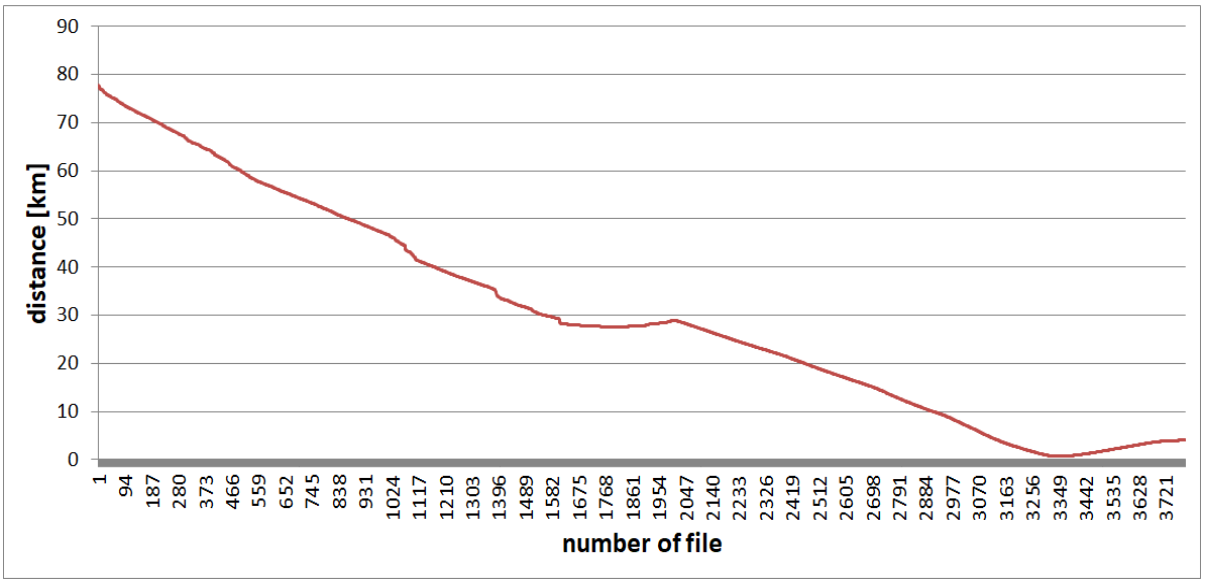

Figure 6-29: Distance measurements from the GNSS + EGNOS receiver on the Karlskrona-Gdynia route.

Thanks to the results obtained above, in the next steps it was possible to calculate the error of the determined distances and at the same time to calculate the RMS as a function of the signal strength. By visually superimposing (Figure 6-30) the results obtained from the correlator and the GNSS receiver for this campaign and comparing these results with the AIS campaign (Figure 6-31) that took place in 2019 [AAVR20], we can see a huge difference in the distance indicated. It is noticeable from 16 km. This analysis is more for illustrative purposes. More detailed cases will be shown in the following sections.

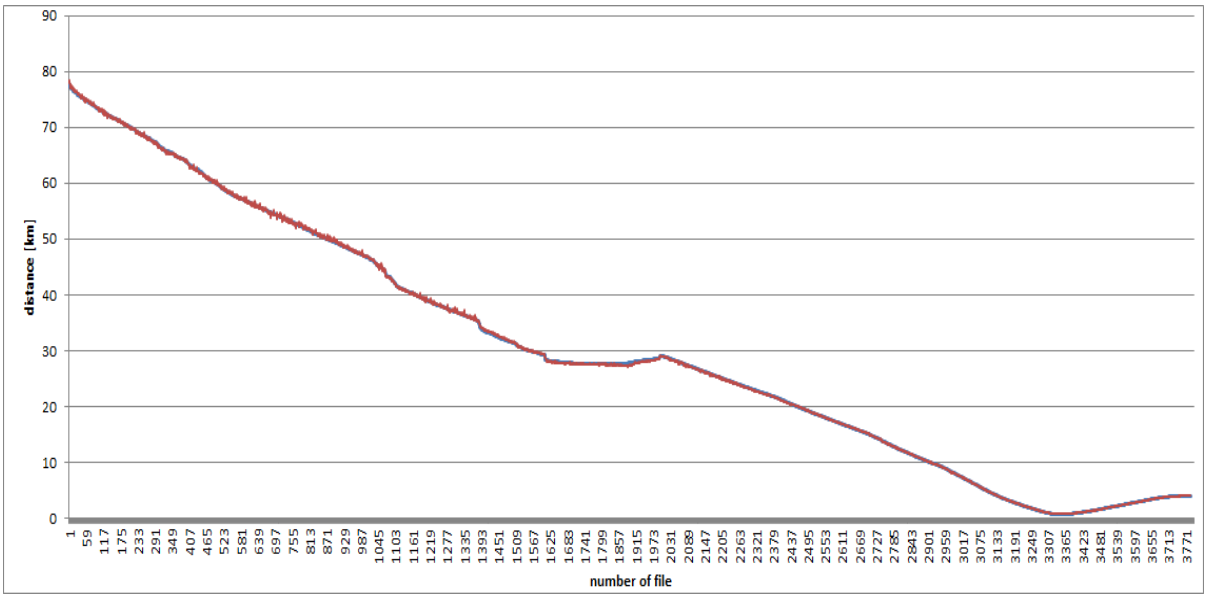

Figure 6-30: Superimposed results from the correlator and GNSS + EGNOS receiver for the VDES measurement campaign on the Karlskrona-Gdynia route

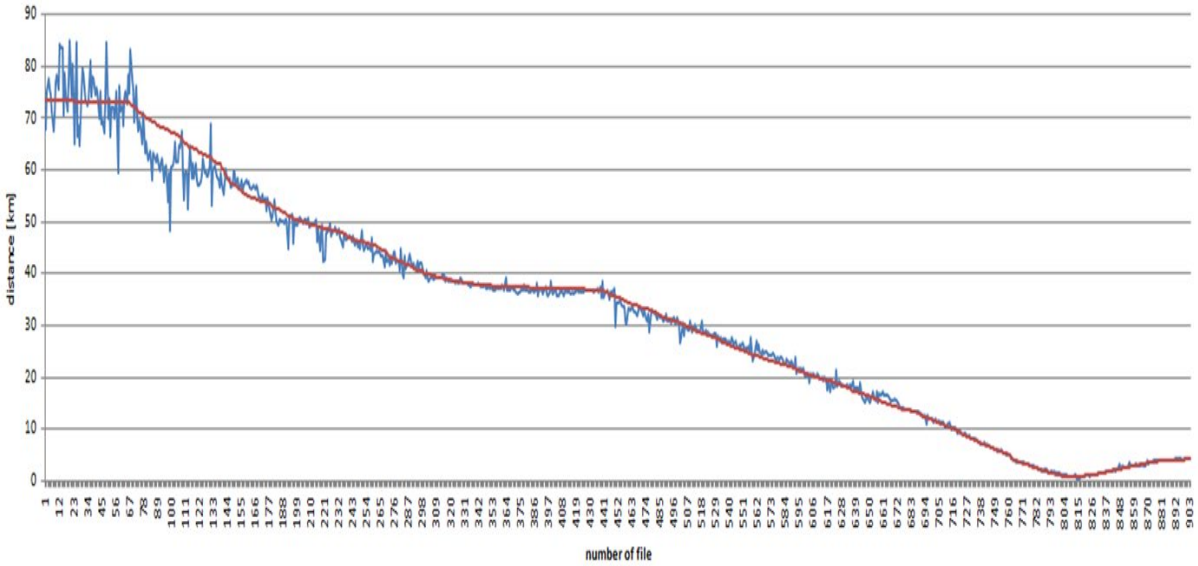

Figure 6-31: Distance measurements from the GNSS + EGNOS receiver on the AIS measurement campaign on the Gdynia-Karlskrona route

The next step presents the obtained SNR values on the Karlskrona-Gdynia route. Below is a graph of this relation (Figure 6-32). The graph shows how the ratio of signal power to noise power has changed throughout the entire route. In the first part, the files up to the number 1700 represent the low SNR case; they were recorded beyond the Hel Peninsula. Files from number 1700 to 2300 represent the period when the ship began to sail along the peninsula. Starting from the file number 2300, the ship begins to sail around the tip of the Hel Peninsula and from that moment on, the SNR starts to increase significantly until the end of the chart, i.e. until reaching the port in Gdynia.

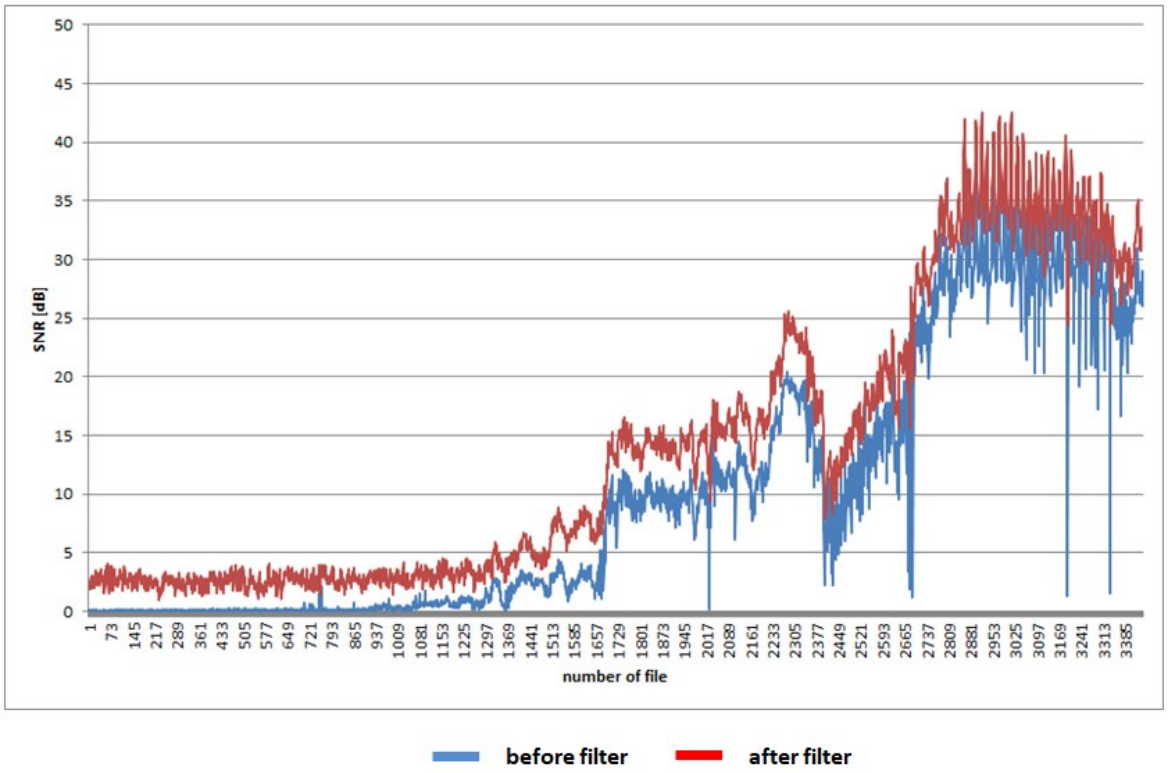

Figure 6-32: Measured SNR on the Karlskrona-Gdynia route

A plot of the correlation peak to adjacent peaks is shown below (Figure 6-33). This plot allows us to see at which times the correlation was the most effective.

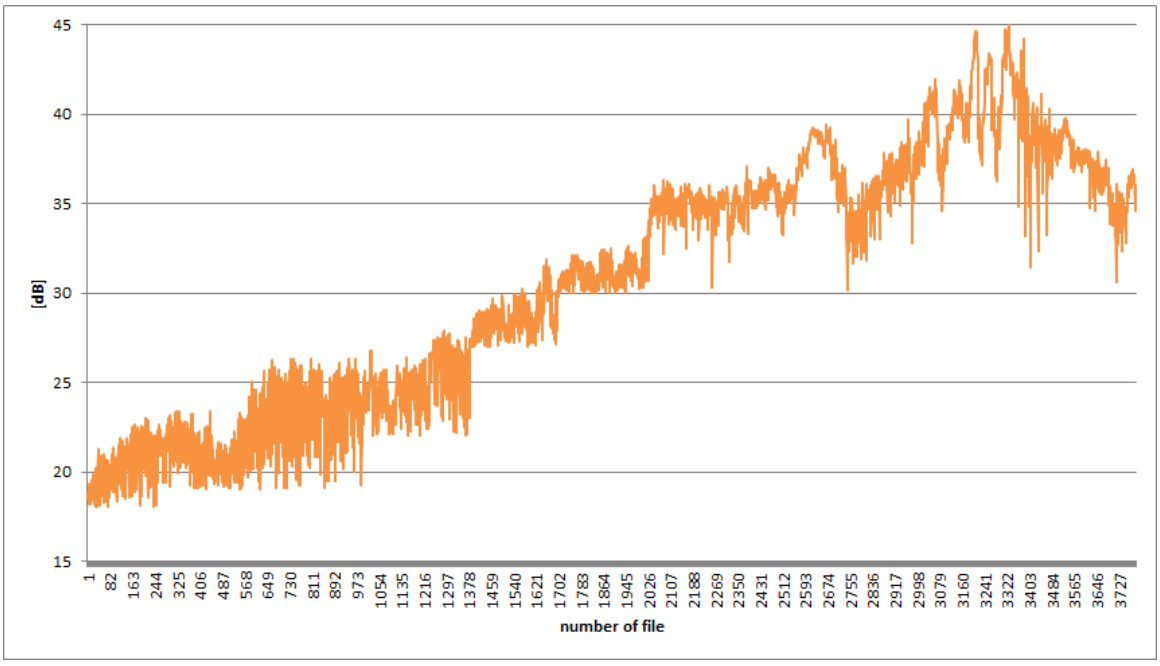

Figure 6-33: Measurements of the 'highest peak/ side peaks' ratio on the Karlskrona-Gdynia route

On the basis of many studies on the received samples and their processing in the correlation application, it was possible to establish correlation value thresholds. By using such a solution, the R-Mode positioning system is protected against false results obtained from the correlation application. This applies to files where it is difficult to distinguish the useful signal from noise with low SNR. On the basis of many studies, it is possible to estimate the threshold of the correlation value, below which we can assume that a given signal was noise, and not a useful signal. As a result, the correlation result for the uncorrelated data file is not saved and is not passed on to the next application, which is used to compute the position. This way we can avoid a false position result.

In Figure 6-34 to Figure 6-36, there are three graphs showing the efficiencies achieved by the correlators. During the processing of the measurement files, the signal correlation application recorded the calculated distance accuracy for several types of correlators in order to later analyze their effectiveness in real conditions.

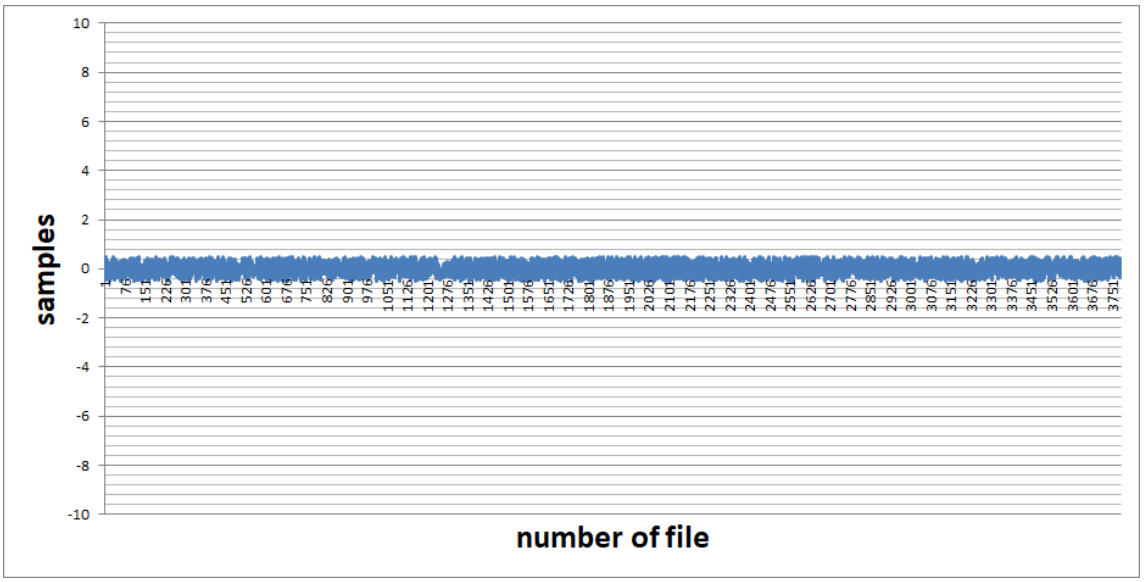

Figure 6-34: Effectiveness of using multicorrelation - Extended correlator d1=d2=1

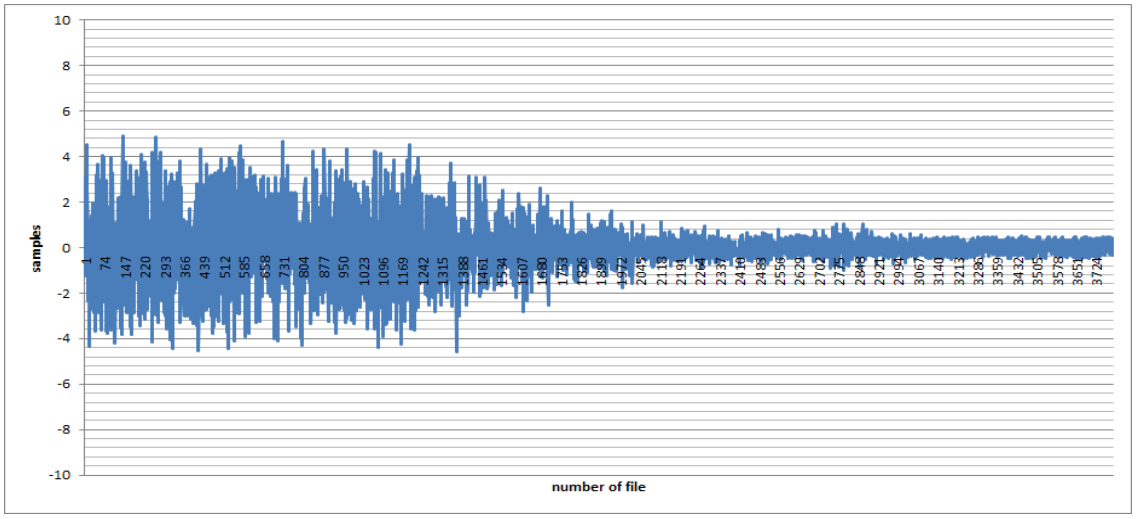

Figure 6-35: Effectiveness of using multicorrelation - Double-delta d1=d2=10

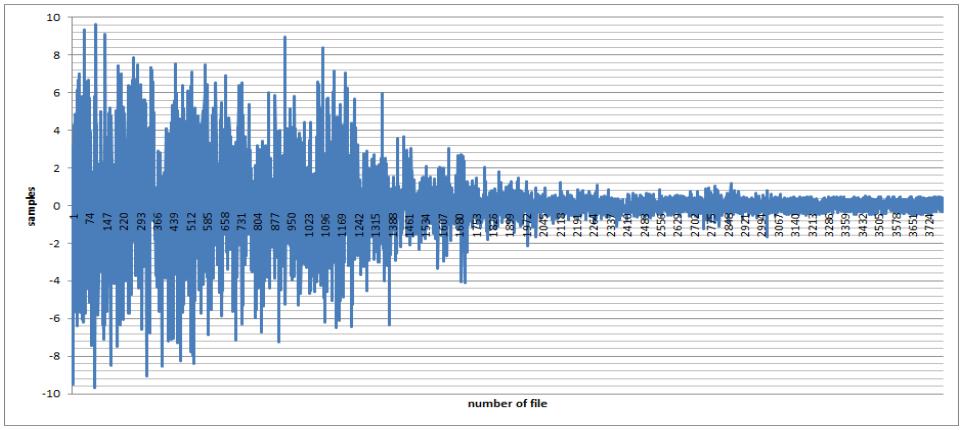

Figure 6-36: Effectiveness of using multicorrelation - Double-delta d1=d2=20

The above graphs show the efficiency of the applied correlator depending on the width of the sample spacing of the second pair of this correlator. Three cases of this sample spacing have been studied in particular. In the first case, it was an extended correlator, where the analysis was focused between the peak with the maximum value and a pair of samples around this main peak. This solution only improves the determination of the accuracy of the distance by approx. one sample, which translates into a maximum improvement of 1.5 m in this case, where the sampling frequency on the receiving side is 200 MHz. In the next case, the spacing of the second pair of samples is already 10 samples between the main peak and the sample coming from the second pair of correlators. Such a configuration already improves the determination of the distance accuracy by 5 samples, which in practice amounts to 7.5 meters. In the third case, with a sample spacing of 20, we have an improvement in the determination of the distance by about 13 meters. This is the best result obtained. For illustrative purposes, a graph (Figure 6-37) we can see the distances calculated by a signal correlation application superimposed on a graph of the correlator's efficiency for the best sample spacing of the second pair (i.e. 20).

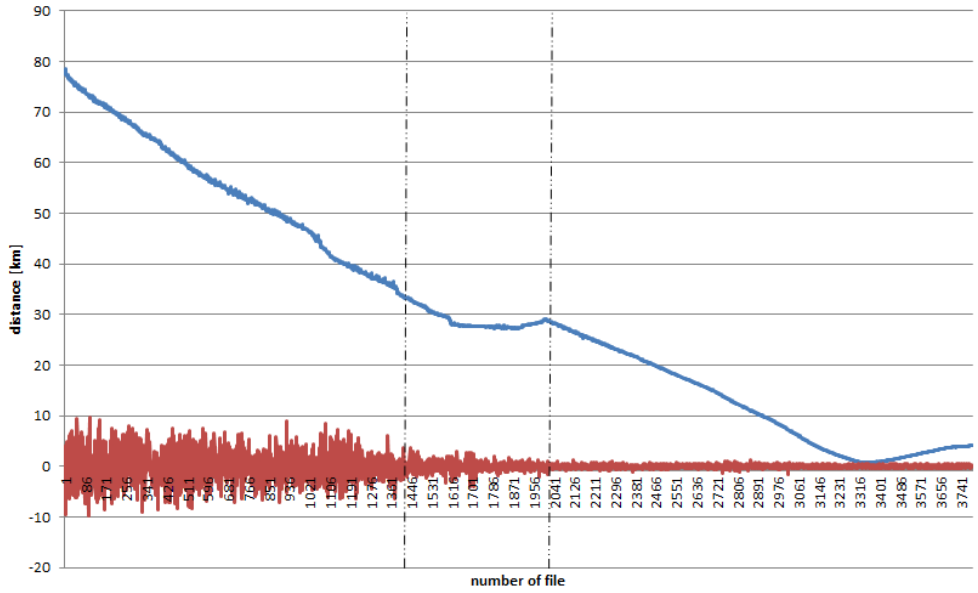

Figure 6-37: Ranges where the multicorrelator d2 = 20 operated most effectively

The blue curve indicates the distance determined by the signal correlation application, while the red one indicates how many samples have improved the distance determination due to the double delta correlator utilization.

Figure 6-38 depicts the error in determining the distance depending on the file number. It can be noticed that along the entire route, the errors here reach up to 500 meters at the edge of the correlation. A more detailed discussion of this graph will be in the next section when we will compare it with the errors obtained in the previous campaign.

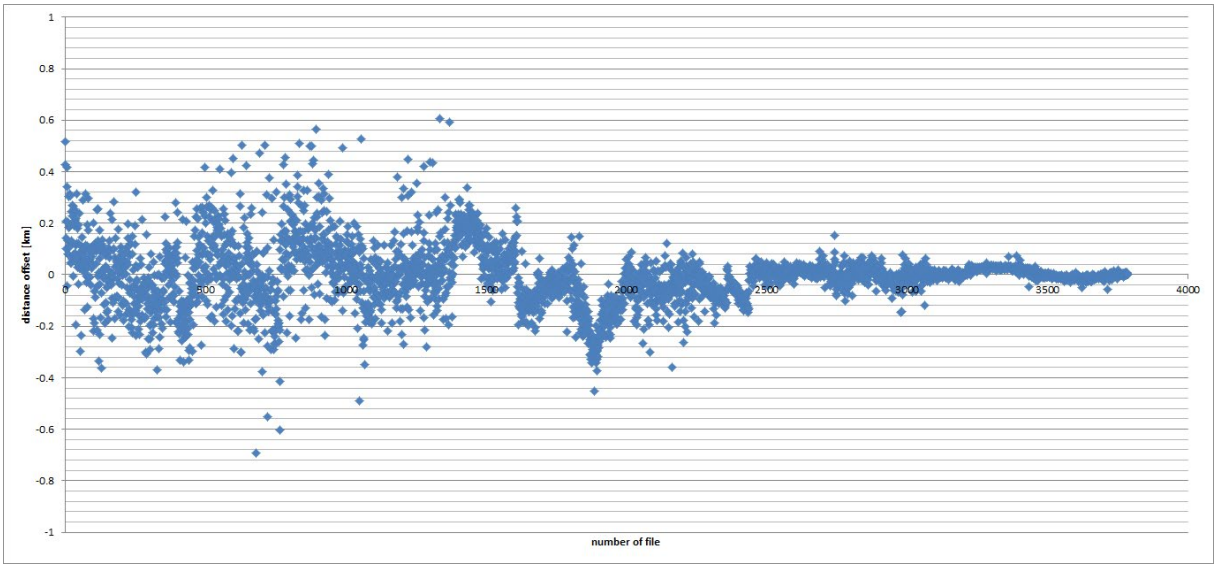

Figure 6-38: Distance error accuracy on the Gdynia – Karlskrona route

6.1.3 The obtained results of the accuracy of the measured distances from two VDES campaigns

In this section, graphs will be shown that illustrate the difference in measurement errors between the 2019 VDES measurement campaign and the VDES campaign that took place in 2020. In addition, the results will also be shown where the correlation sequence used to determine the distance is not the Gold sequence but a training sequence normally used to synchronize the signal in the receiver. For illustrative purposes, a graph with the influence of the Hel Peninsula on the determination of the distance accuracy is also presented.

The 2020 VDES measurement campaign also uses the same sampling frequency on the receiving end so the results can be reliably compared. After calculating the difference between the indications of the GNSS receiver and the signal correlation application, it was possible to generate the RMS plot. It clearly shows the ratio of the distance accuracy error to the SNR. Thanks to this data, it was possible to compare the results obtained for all measurement campaigns in a meaningful way.

Some changes were made in the 2020 measurement campaign in relation to the 2019 campaign:

- in order to improve the power of the transmitted signal, changes were made to the filtration of the transmitted signal: Hann windows were turned off and the physical VHF filter was removed,
- the transmitted sequence has been modified in accordance with the IALA Guideline VDES guidelines,
- application on the receiving side of the physical VHF PROCOM BPF 2 / 2-250 filter with a narrower passband (previously installed on the transmitting side),
- in order to eliminate the need to use an attenuator at the USRP input, a low-noise amplifier with lower gain than before was used,
- in order to maximize the number of used GPS and Galileo satellites, the reference GNSS receiver was reconfigured.

With the second VDES 2020 campaign, the ERP power was increased to 14.8 dBW

The chart (Figure 6-39) shows the distance accuracy of the results obtained in both measurement campaigns. The next graph (Figure 6-40) shows the determined distances for the correlation of the training sequence compared against the results obtained using the Gold sequence correlation. Then on the next graph (Figure 6-41), it is possible to see the obtained RMS results and finally, in Figure 6-42, the errors obtained in the presence of the Hel Peninsula are shown.

1st measurement campaign: 15-16 November 2019

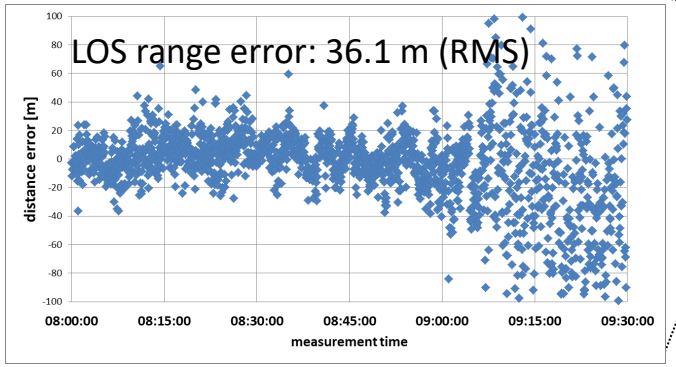

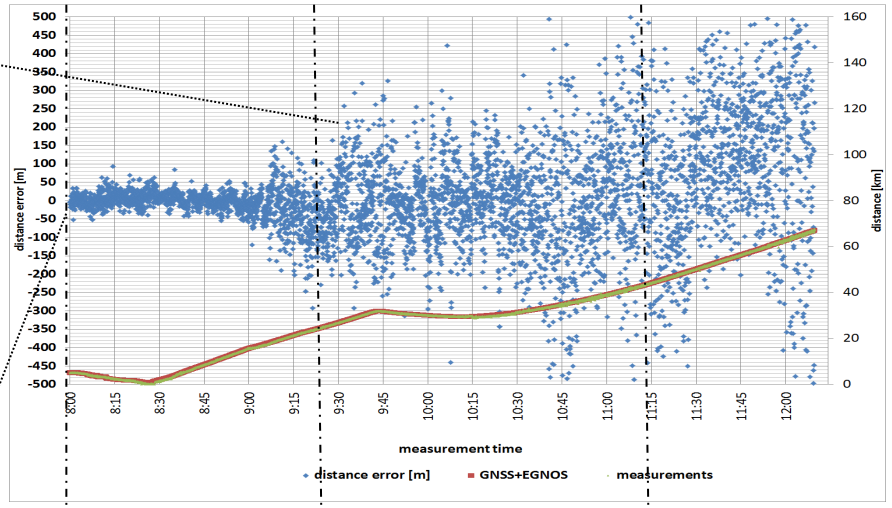

<-- Range up to 65 km

Range much greater than 150 km !!

2nd measurement campaign: 29-30 June 2020.

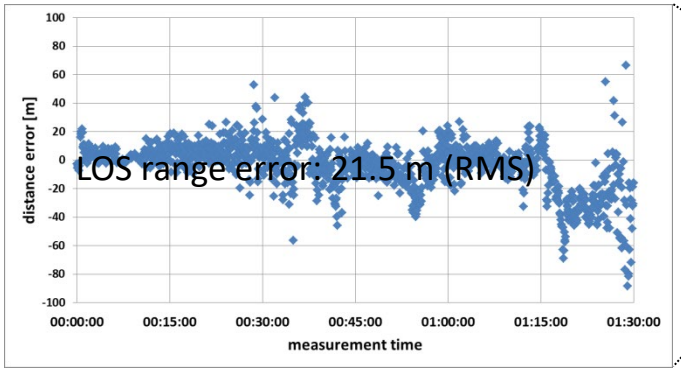

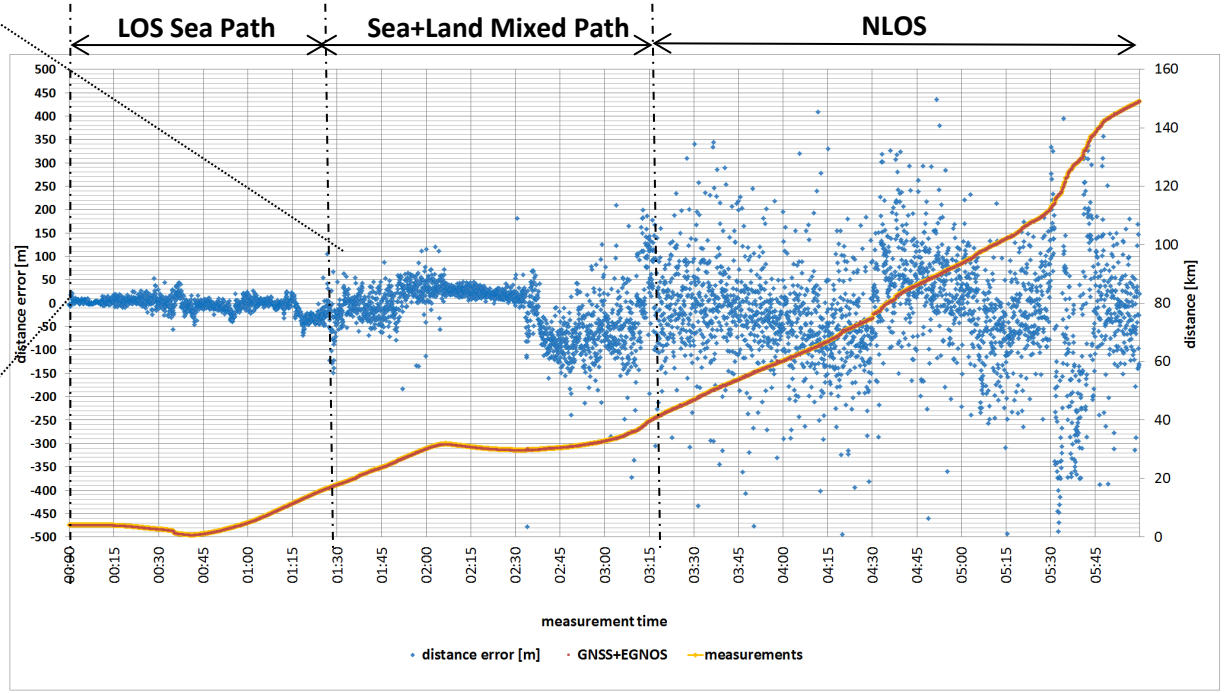

Figure 6-39: Obtained measurement results – ranging accuracy

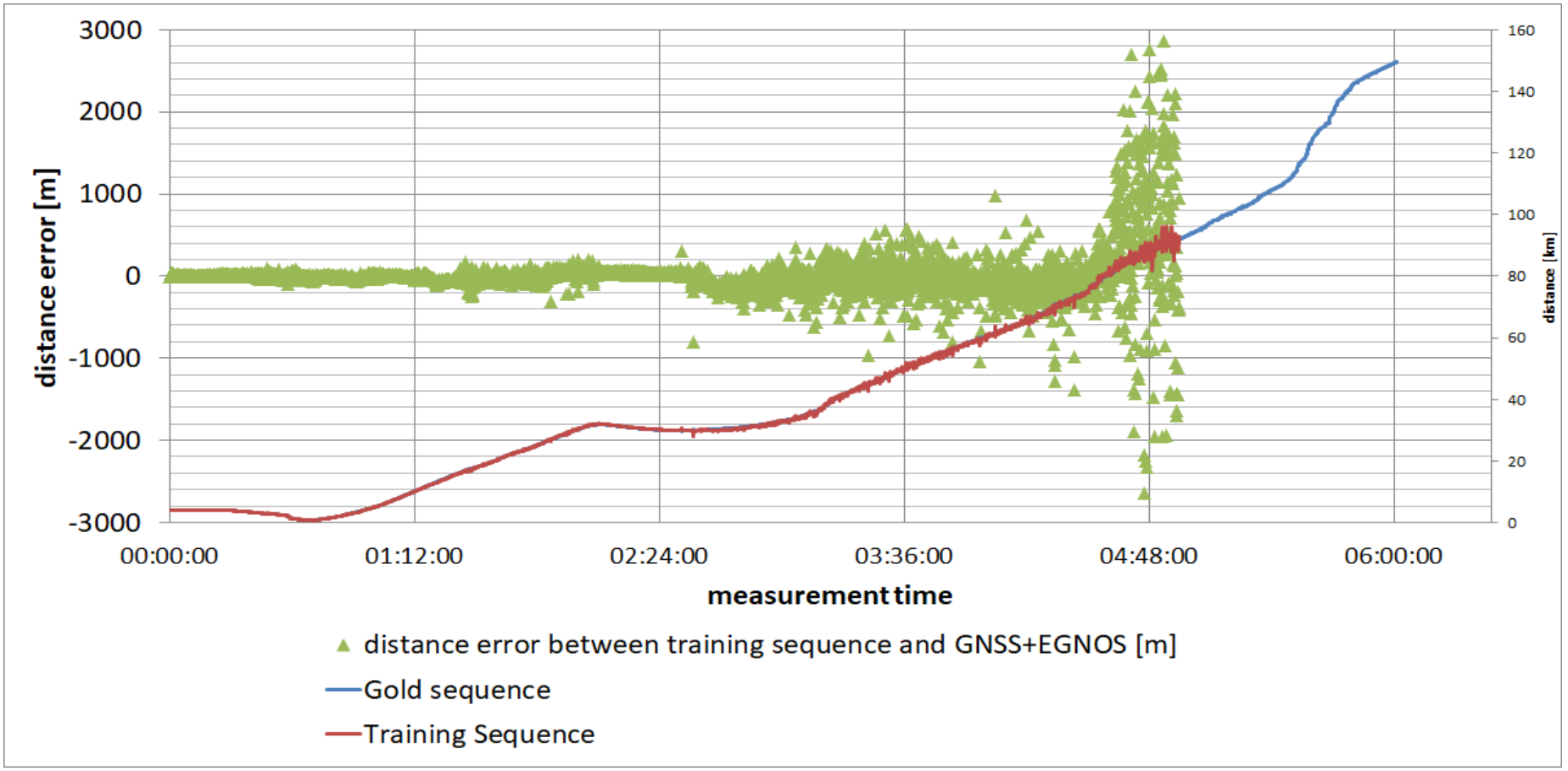

Figure 6-40: Comparison of the correlation effectiveness for the training and Gold sequences

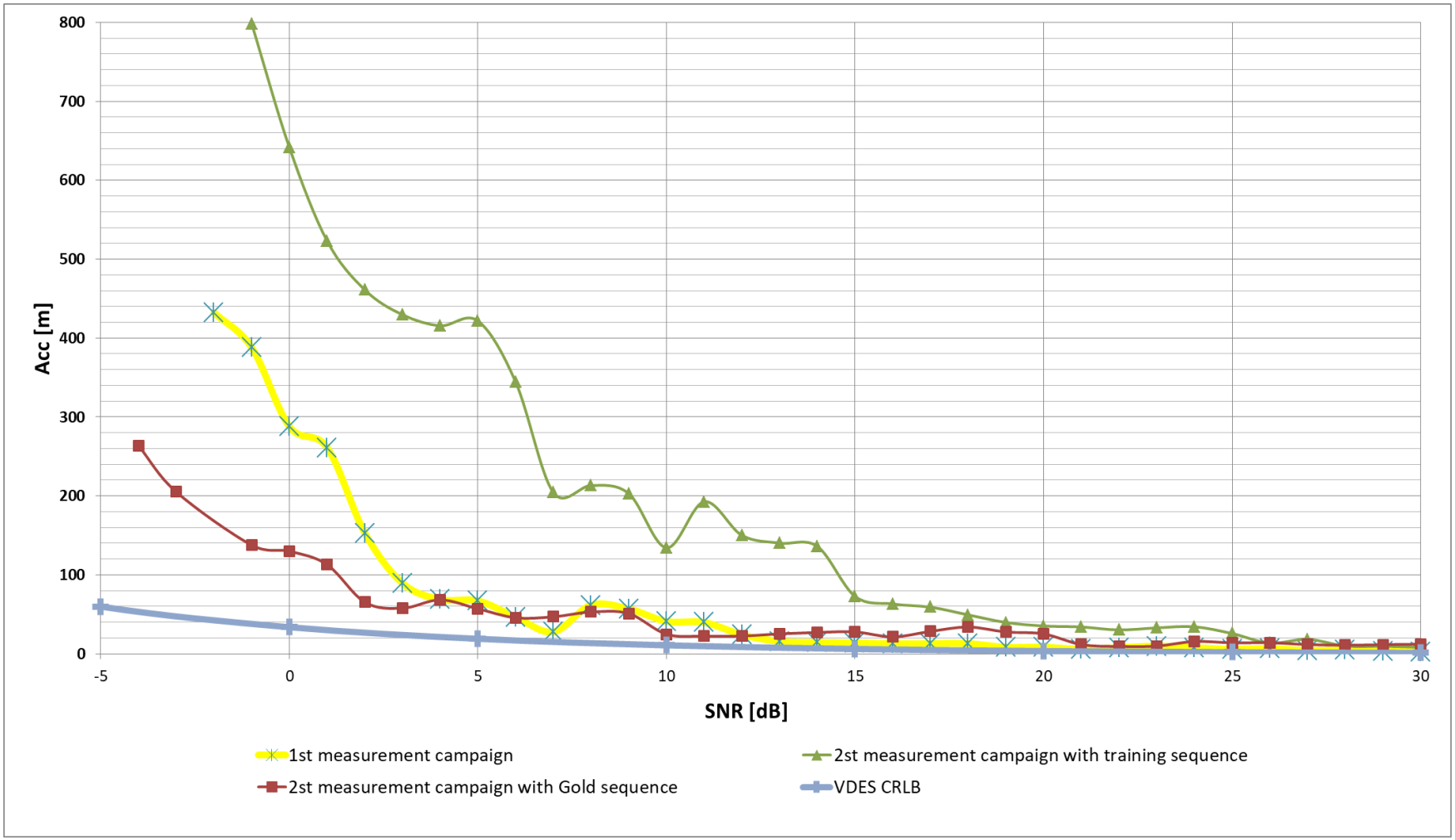

Figure 6-41: Accuracy obtained – as a function of SNR

The results of the first measurement campaign on the Stena Line ferry showed that the configuration changes made both on the transmitter and receiver sides of the system allowed, first of all, to significantly extend the operating range of the system - from approx. 70 km obtained as part of the measurement campaign carried out in 2019 to approx. 150 km obtained in the June 2020 campaign (Figure 6-39).

The results presented in Figure 6-39 show that due to the introduced changes and optimization of transmitting and receiving stations, not only was it possible to more than double the range of the R-Mode VDES system, but also the accuracy of the determined distance was improved. In the frame structure of the VDES system, in addition to the Gold sequence sent as part of the data packet, there is also a training sequence (Figure 6-40) that is used to synchronize the receiver. As part of the analyzes, the possibility of using this sequence to determine the distance from the base station was also compared. Figure 6-41 shows the accuracy of the determined distance based on data from the 2019 measurement campaign and on the basis of the Gold sequence and training sequence obtained as part of the measurement campaign of June 2020. This comparison shows that although the training sequence of the VDES frame can be used for ranging, the accuracy obtained in this case does not meet the assumptions of the R-Mode system even for high SNR values. The comparison also shows an increase in the accuracy of the determined position due to the applied modifications.

The results obtained in the measurement campaigns were compared with theoretical curves calculated on the basis of the Cramer-Rao Lower Bound (CRLB) method. As can be seen in fig. Figure 6-41, for very low SNR values the discrepancy between the theory and the measurements was initially very significant but it was going down as the SNR increased. The fact that for lower SNR values the accuracy of the determined distance was not satisfactory for both analyzed systems, confirms the well-known limitation of the Cramer-Rao method that it is more suitable for high SNR scenarios. On the other hand, the results obtained for high SNR values almost coincided with the theoretical curves generated for the AIS and VDES systems, with the exception of the nearly constant, about 10 m difference of the RMS error. On the basis of the results, it can be stated that much better accuracy of the determined distance was obtained for the VDES system. In the second measurement campaign for the VDES system, for low SNR values, a clear improvement in the determination of the distance accuracy can be seen.

Other possible sources of errors resulting in a behavior observed in Figure 6-41 which caused some deviation between theory and measurements, have been identified and are listed in Table 6-4. It should be noted that some of these errors only apply to the low-SNR region, while others are valid for the entire SNR range in Figure 6-41.

Below in the table, the '+' sign indicates problems that may have occurred on the measurement route and affected the measurement results. Problems which in the given case did not occur and did not have any influence on the problems were marked with the '-' sign.

Table 6-4: Source of error

Source of error	low SNR region	high SNR region
Possible impact of residual clock errors	+	+
Errors caused by the presence of the Hel Peninsula	+	-
Errors that can be caused by lack of EGNOS and/or high HDOP	+	+
Ship's speed too high	+	+
Weather conditions	+	+
Error resulting from passing the line of sight distance (beyond the 42.4 km mark)	+	-
Sampling rate	+	+

The chart below (Figure 6-42) shows the influence of the Hel Peninsula terrain on the determined distance accuracy during the measurement campaign.

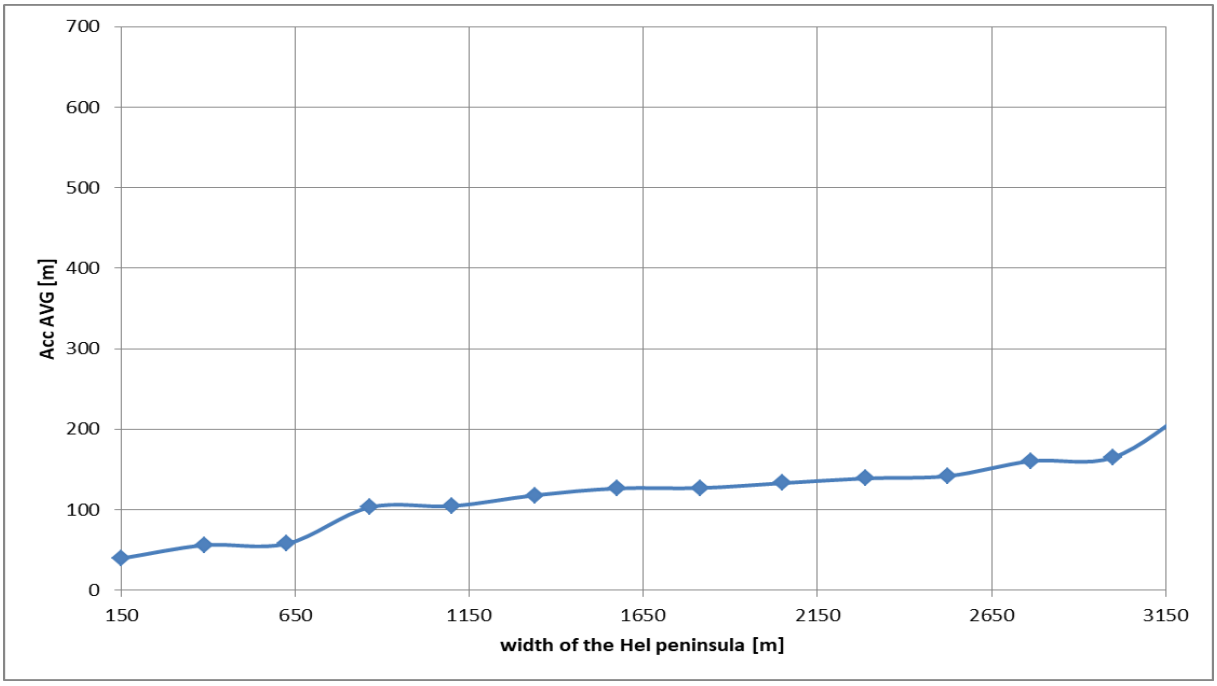

Figure 6-42: Hel peninsula influence for VDES

It can be clearly seen that in places where the width of the land on the Hel Peninsula was greater, the accuracy of the distance determination deteriorated. It was also related to the existing forest areas.

Below is a map from the second measurement campaign on the Gdynia-Karlskrona route, where the magnitude of the errors was marked (Figure 6-43).

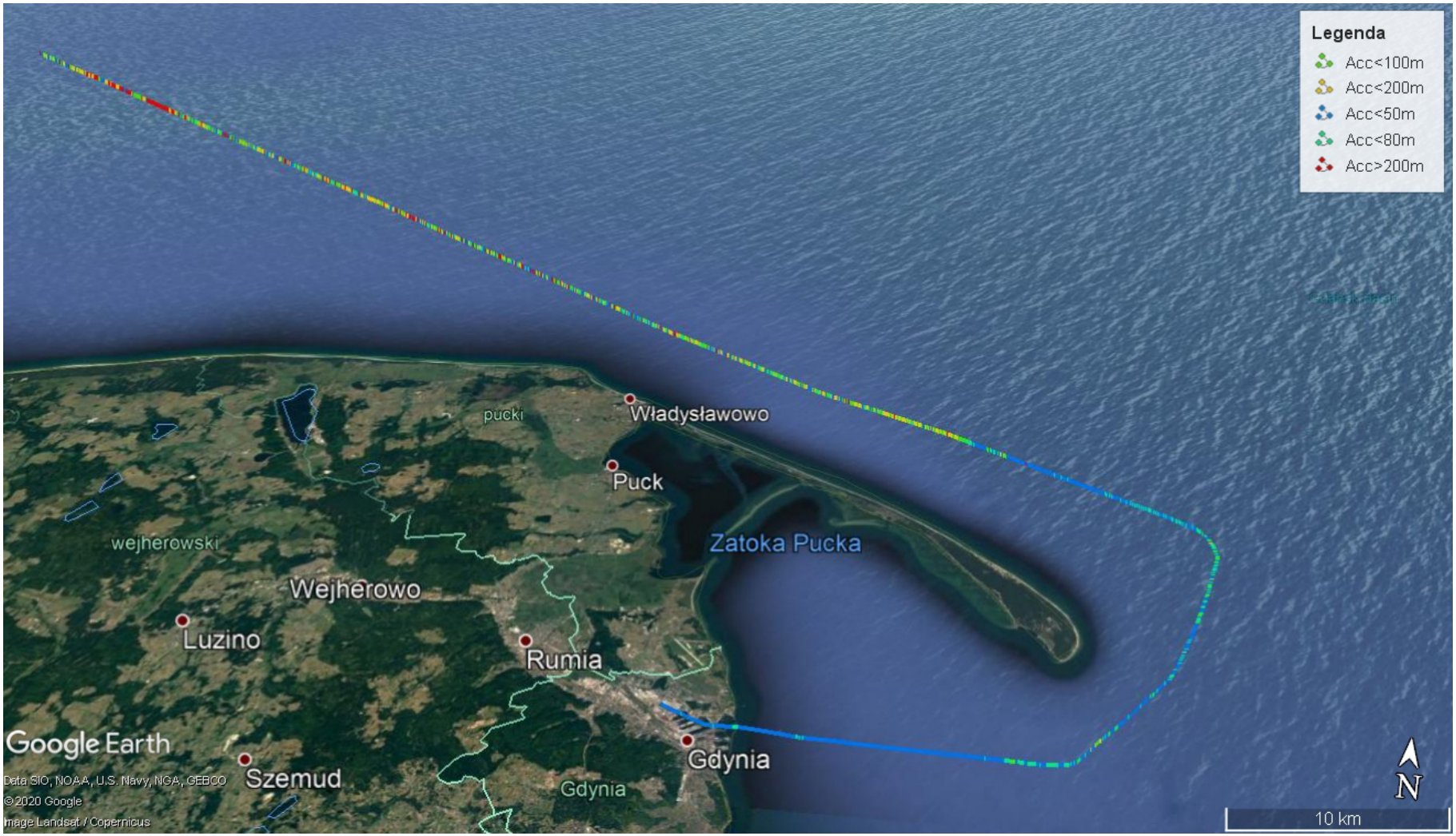

Figure 6-43: Measurement route and accuracy – 2nd campaign

Below are brief conclusions from the measurement campaigns:

- Lack of line-of-sight (LoS) and potentially high noise at the Rx are the main accuracy limiting factors,
- Theoretical analysis fits quite well with measurements for high SNRs,
- Mixed paths introducing additional (almost constant) range error / delay,
- System is still usable in deep non-line-of-sight (NLoS) conditions (for rough position estimation) – even much below communication sensitivity level / range,
- VDES training sequence has limited applications only,
- Quite sophisticated filters and LNA used at the Rx – minimizing noise needed.

6.2 Ranging Accuracy Tests based on the Reception of a Multi-Slot Message (Emulation of the Multiple R-Mode Stations - Based on One Physical Station in Gdynia)

This chapter presents the results of the research that was carried out in the NIT building. The receiving part was located in Gdańsk (NIT premises), and the transmitting part was located in the port of Gdynia, 17.4 km from the receiver antenna in Gdańsk. The following subsections present the results obtained for the application of different sampling frequencies on the receiving end. Using the calculated RMS, it was possible to objectively compare all the obtained results. Various measurement scenarios were also used in the research. By introducing an additional delay, the presence of up to four transmitting stations was simulated. For the simulated different distances of the transmitting stations, the powers of the transmitted signals were also simulated: they were proportionally changed depending on the artificially introduced delay in a given slot. This solution allowed to conduct the research for one-slot, two-slot and 4-slot messages. All these studies helped to optimally select the sampling frequency on the receiving side and the appropriate correlation sequence, which gave the best results (i.e. the highest accuracy of the calculated distance).

6.2.1 Performing tests to calculate the accuracy of the distance based on the change of the sampling frequency of the received signal

As part of further activities carried out under the R-Mode Baltic project, the correlators operating on the receiving side were modified, which, on the one hand, would allow to increase the accuracy of the determined distance, and on the other hand, would make it possible to reduce the sampling frequency of the received signal. The latter aspect is particularly important due to the possibility of building the R-Mode VDES target receiver in the programmable radio technology using commercially available electronic components (as opposed to the expensive laboratory equipment that was used during system tests). As part of subsequent measurement campaigns carried out in the point-to-point relation, i.e. the VDES R-Mode base station in the port of Gdynia - the premises of the NIT in Gdansk, a number of solutions were tested. The results of the conducted analyzes allowed for a significant reduction of the sampling frequency from the initially used 200 MS/s, down to 2 MS/s, with a simultaneous reduction of the error level, as shown in Figure 6-44.

The reduction of the sampling frequency had yet another colossal significance - the computational complexity of the algorithms used decreased, as did the amount of the

measurement data processed in real time. It is worth mentioning here that, so far, all measurement data was first recorded and then analyzed in post-processing.

A series of measurements was made for the following frequencies:

- 200 MHz,
- 100 MHz,
- 50 MHz,
- 10 MHz,
- 5 MHz,
- 2 MHz,
- 1 MHz.

For each series of measurements for different frequencies, 100 files were recorded. This was a sufficient number for which reliable results could be calculated.

Until now, all measurements in the measurement campaign were conducted the receiving frequency of 200 MHz. This resulted in a large size of the files with the recorded samples. Thanks to tests with lower frequencies and testing the effectiveness of multi-correlators, it will be possible to select a lower frequency that will allow to reduce the size of the recorded files with samples.

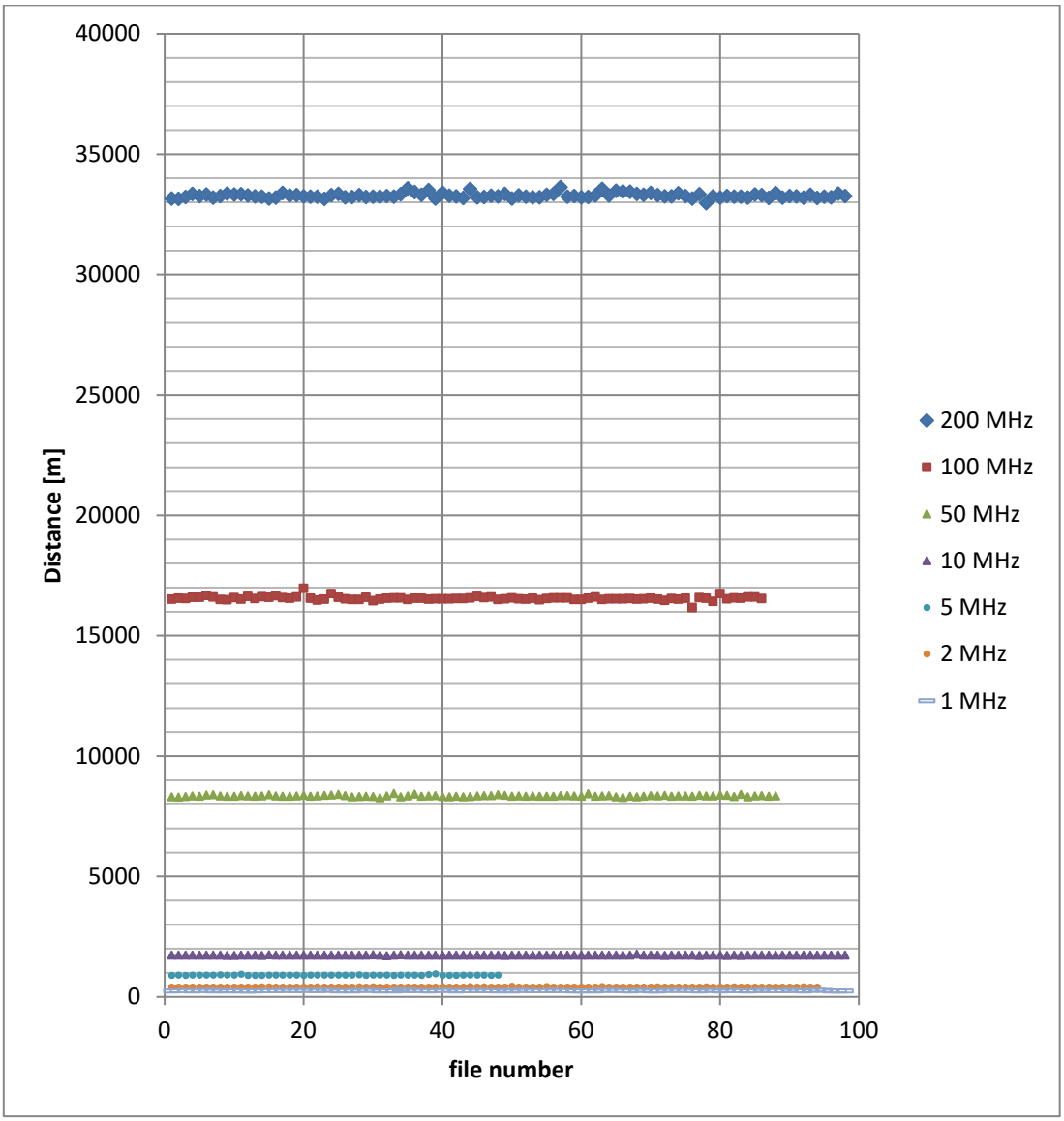

Figure 6-44: Analysis of the calculated distance accuracy depending on the sampling frequency

Figure 6-45 to Figure 6-51 below show the exact results for each of the tested sampling frequencies on the receiving side.

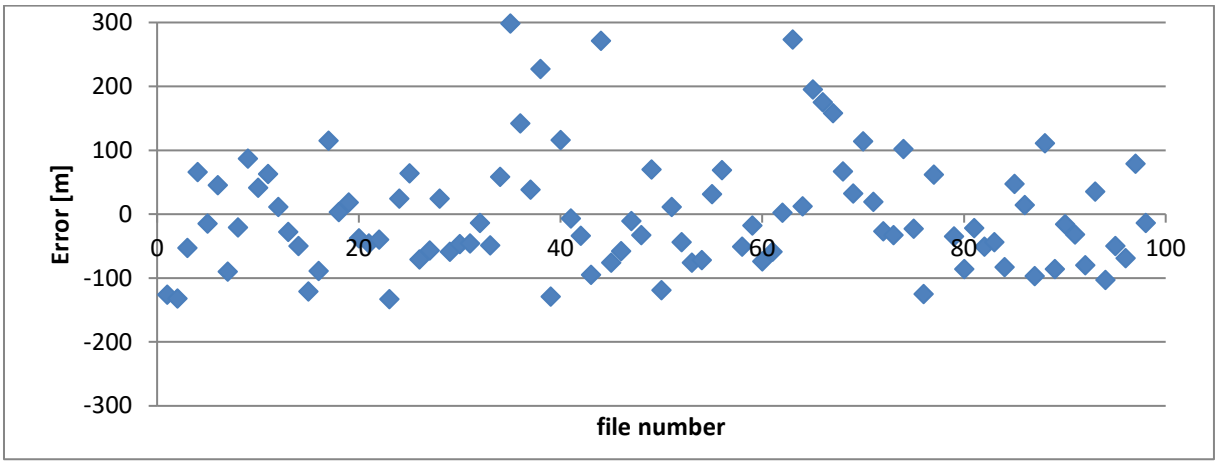

Figure 6-45: Measurement results for 200 MHz sampling frequency

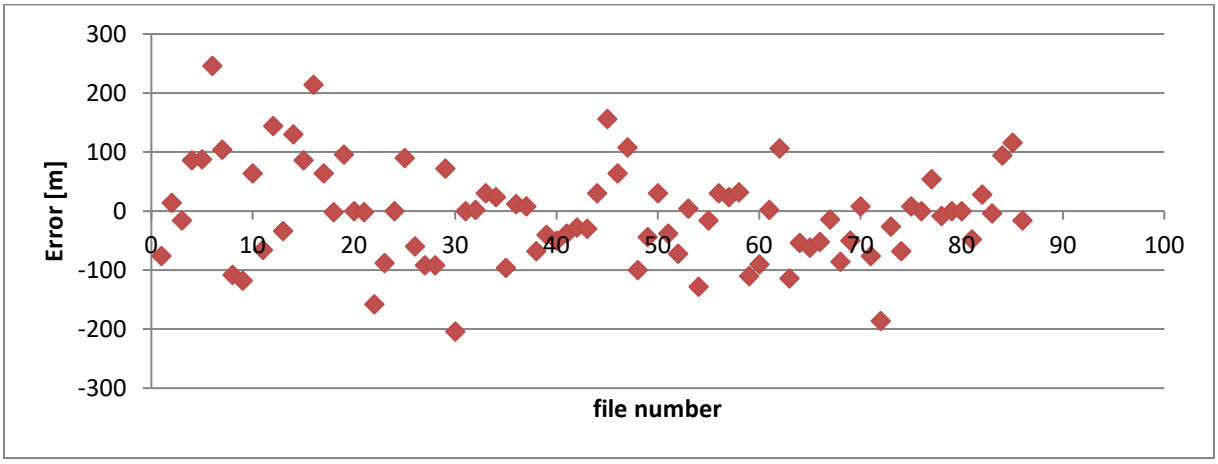

Figure 6-46: Measurement results for 100 MHz sampling frequency

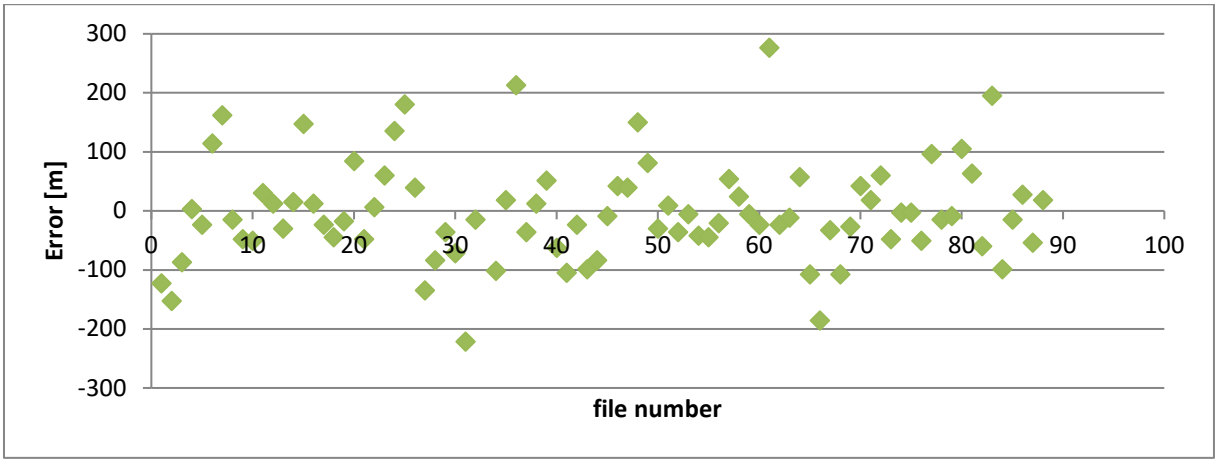

Figure 6-47: Measurement results for 50 MHz sampling frequency

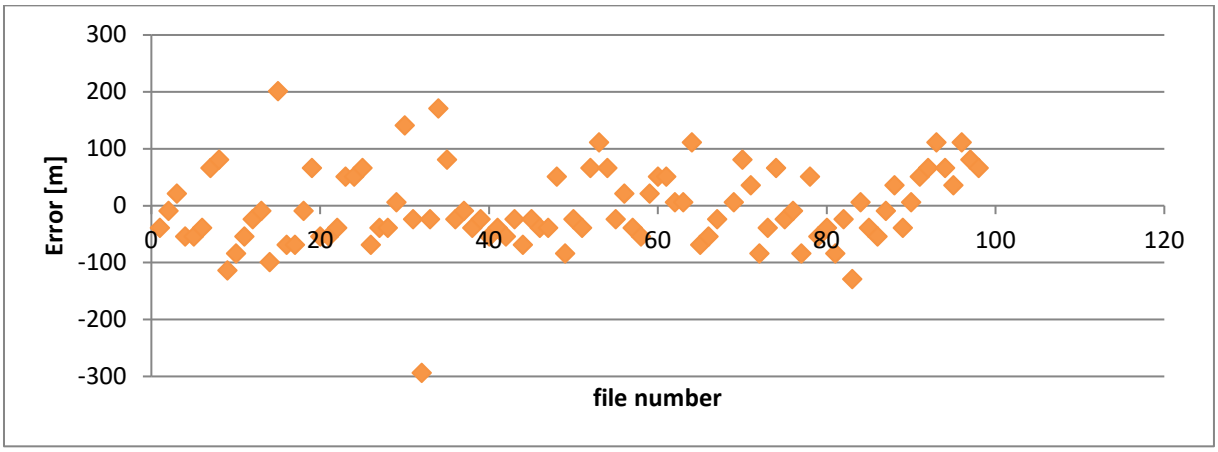

Figure 6-48: Measurement results for 10 MHz sampling frequency

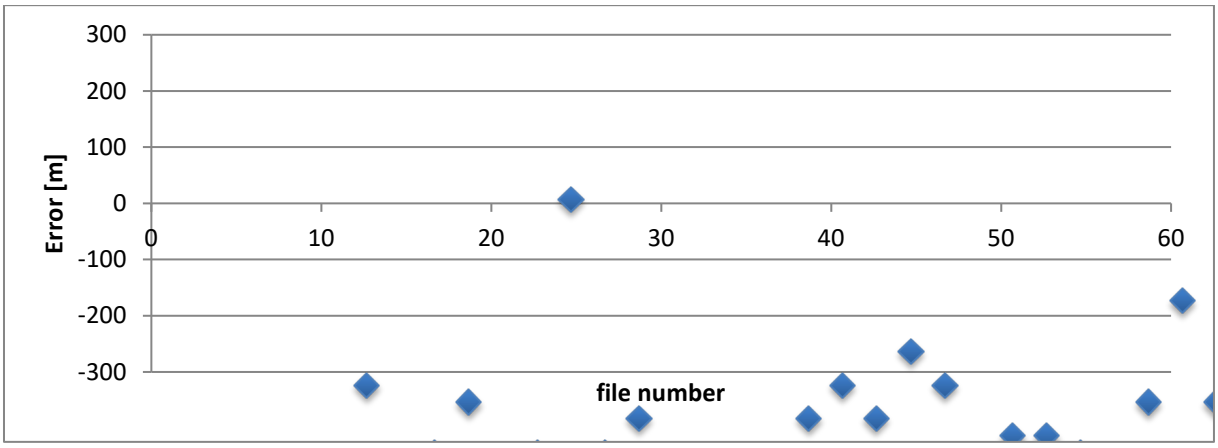

Figure 6-49: Measurement results for 5 MHz sampling frequency

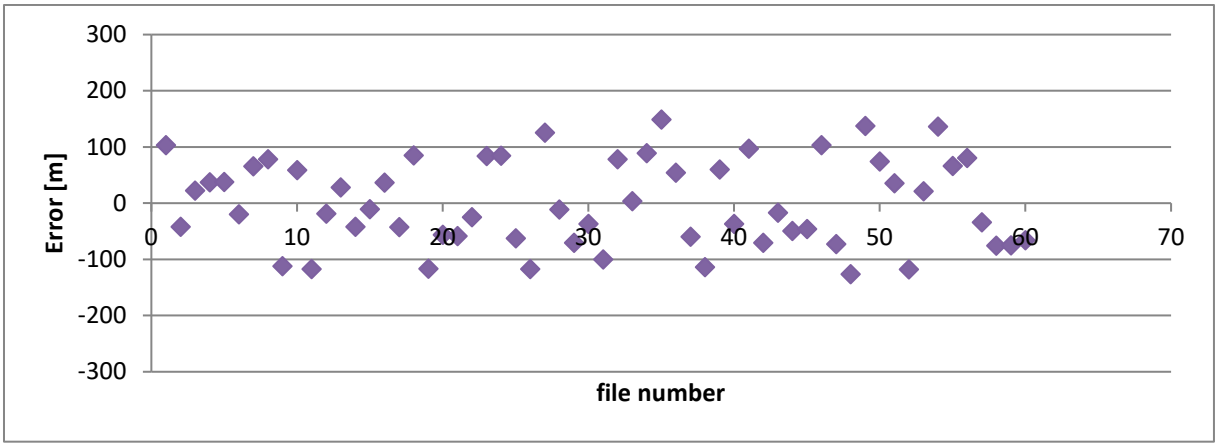

Figure 6-50: Measurement results for 2 MHz sampling frequency

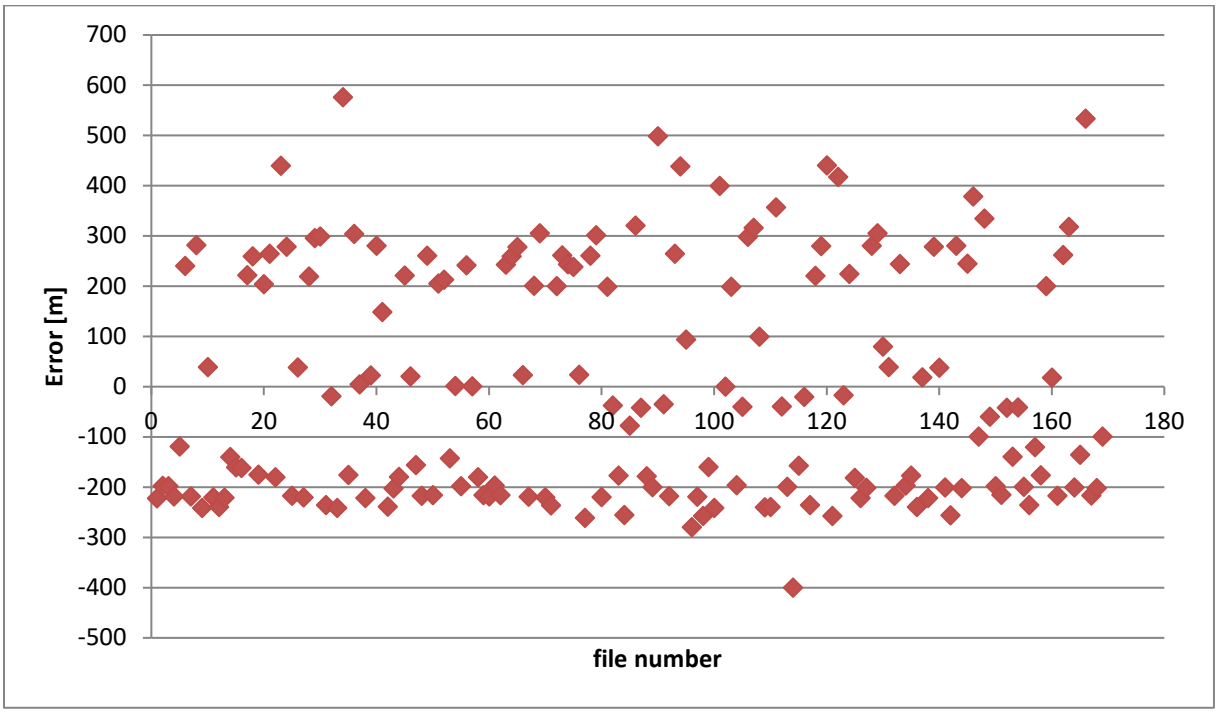

Figure 6-51: Measurement results for 1 MHz sampling frequency

Table 6-5 below shows all the RMS results that were computed in the signal correlation application.

Table 6-5: Correlation of the signal received at the NIT location in Gdańsk at different sampling frequencies

Sampling frequency [MHz]	RMS for the extended correlator [m]	RMS for the double delta correlator [m]
200	97.31	97.22
100	88.81	88.19
50	91.12	91.54
10	82.25	82.41
5	92.3	90.8
2	98.2	96.65

For selected frequencies, the results for a set containing more than 1000 files are presented below (Figure 6-52, Figure 6-53).

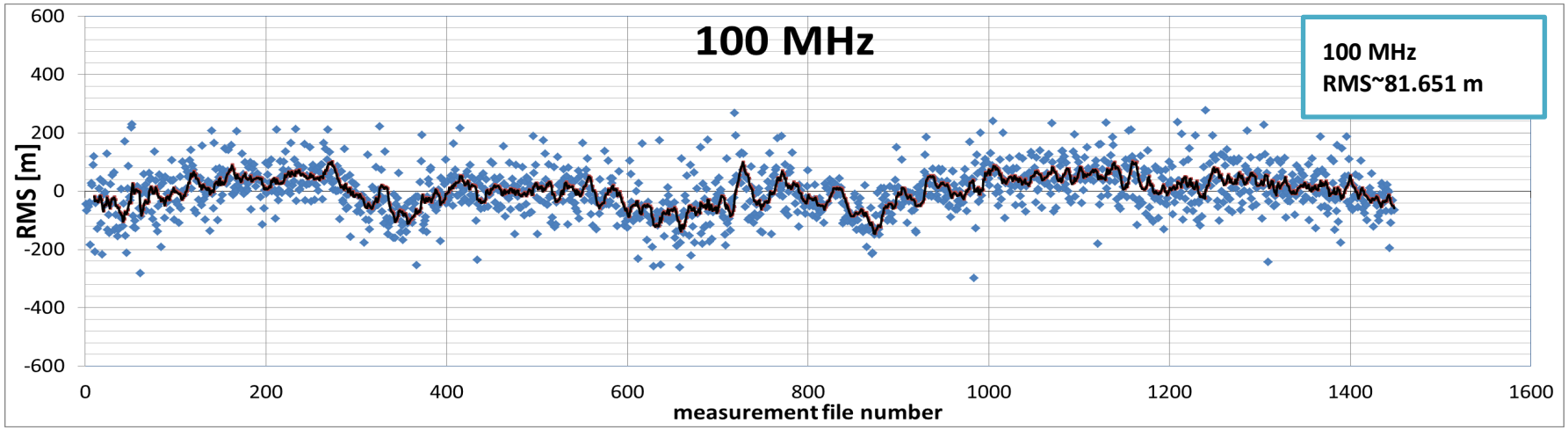

Figure 6-52: Results for a sampling frequency of 100 MHz

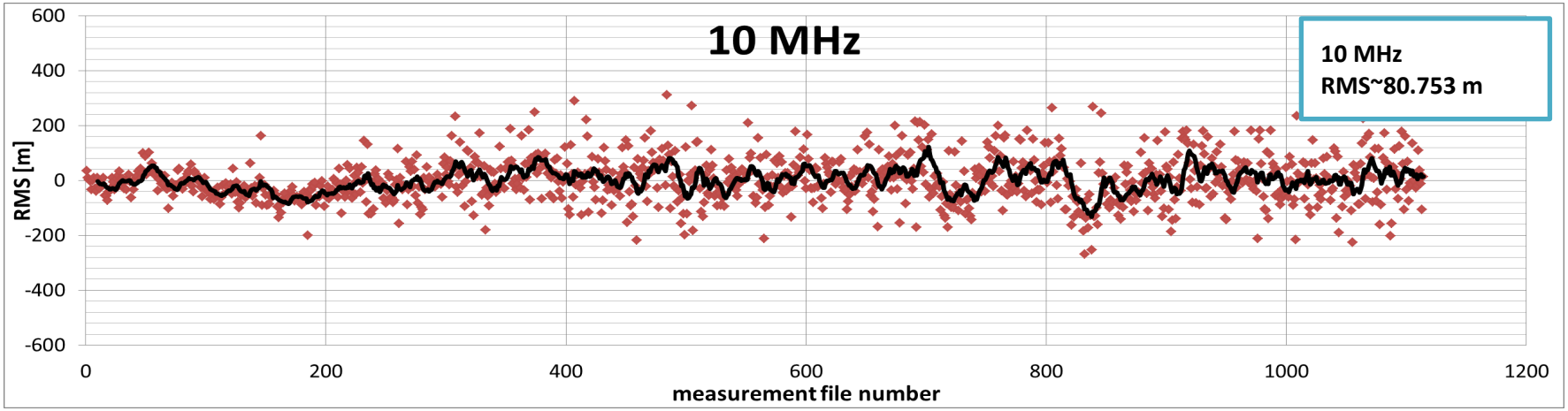

Figure 6-53: Results for a sampling frequency of 10 MHz

A series of graphs showing the results of the research conducted in NIT are presented above. First, a series of tests was performed for different sampling rates on the receiving end. Based on these studies, the frequencies of 100 MHz and 10 MHz were selected for further measurements due to their better stability over time. After conducting research on a large sample of files, it was decided to use the 10 MHz frequency for further measurements, which gave the best and most stable results.

The average RMS obtained here is about 80 meters. It should also be emphasized that this was a study for a signal using 1877 Gold sequence symbols, used for correlation and determination of distance accuracy.

6.2.2 Two-slot message composed of a Gold sequence and an alternating sequence.

In this case, the signal was broadcast in two time slots. The first slot broadcasts a stream containing Gold's sequence consisting of 1877 symbols (Figure 6-54) [VDES15].

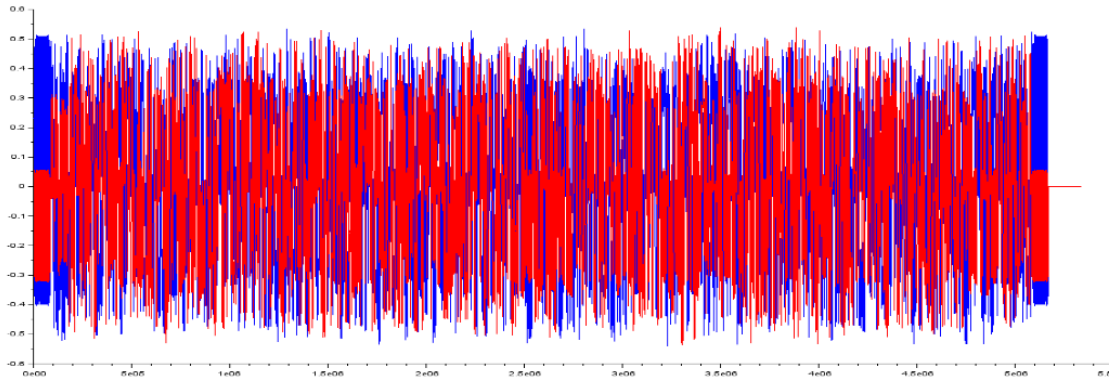

Figure 6-54: VDES signal transmitted with Gold sequence

For the second slot, a new correlation sequence was transmitted - containing an alternating sequence (Figure 6-55). The alternating sequence – as the name suggests – contains an alternating stream of „0”s and „1”s; it provides more correlation peaks than the Gold code-based sequences. The station transmitting such a signal has already been established. The measurements will allow to compare the performance of these types of ranging sequences in real maritime environment.

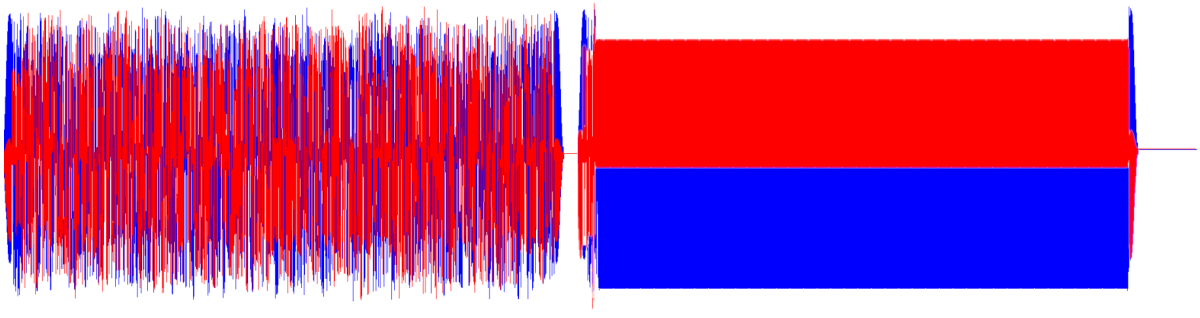

Figure 6-55: VDES signal transmitted in two time slots. In the first slot, the Gold sequence is transmitted, in the second slot the alternating sequence is transmitted.

The shape of the correlation function for the alternating sequence is shown below (Figure 6-56). At a first glance, it can be seen that it contains a large number of correlation peaks compared to the Gold correlated sequence.

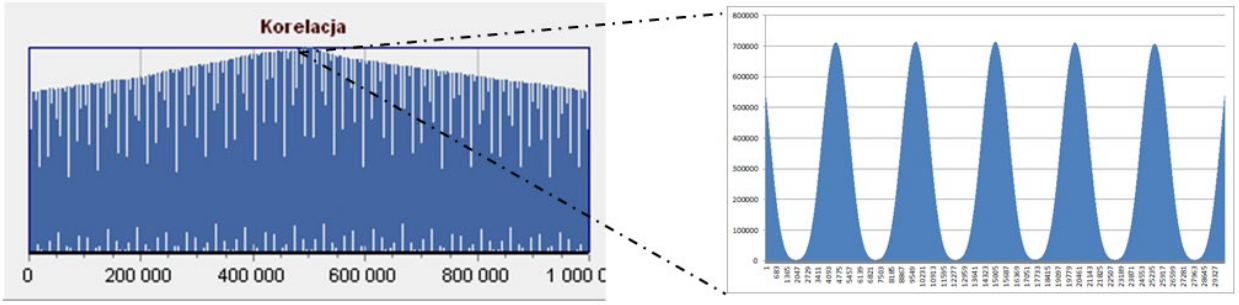

Figure 6-56: New shape of the correlation peak for analysis – alternating sequence

Studies by the NIT were performed for both sequences. Assuming that the two-slot sequence will be transmitted continuously, where the correlation will be performed first for the Gold sequence - the exact position of the correlation peak for the alternating sequence can be determined. By determining the correlation peak for the Gold sequence, knowing the sizes of the slots and signals - we can calculate where the correlation peak for the alternating sequence should be. Why did we choose this approach? It was due to the fact that for the SNR with smaller values, if we correlated the message only for the alternating sequence - we would get correlation peaks with unequal heights. It would be difficult to estimate which of the correlation peaks is the peak from which the distance has to be determined. Sending an alternating sequence would make more sense if the SNR is high.

6.2.3 Four-slot message - emulation of four base stations - for the Gold sequence

In the next research measurements, the signal was sent in four slots. This was to simulate the presence of four transmitting stations and prepare the system for measurements in a real environment with the presence of several base stations. The four-slot message was created by combining four signals with a Gold sequence with a frequency of 10 MHz. In order to simulate different distances of the transmitting stations from the receiver, additional delays were added and the powers were proportionally adjusted.

The research was carried out on a group of 1500 offline files. Each of the slots simulated a separate broadcasting station. The transmitted signal is presented below (Figure 6-57):

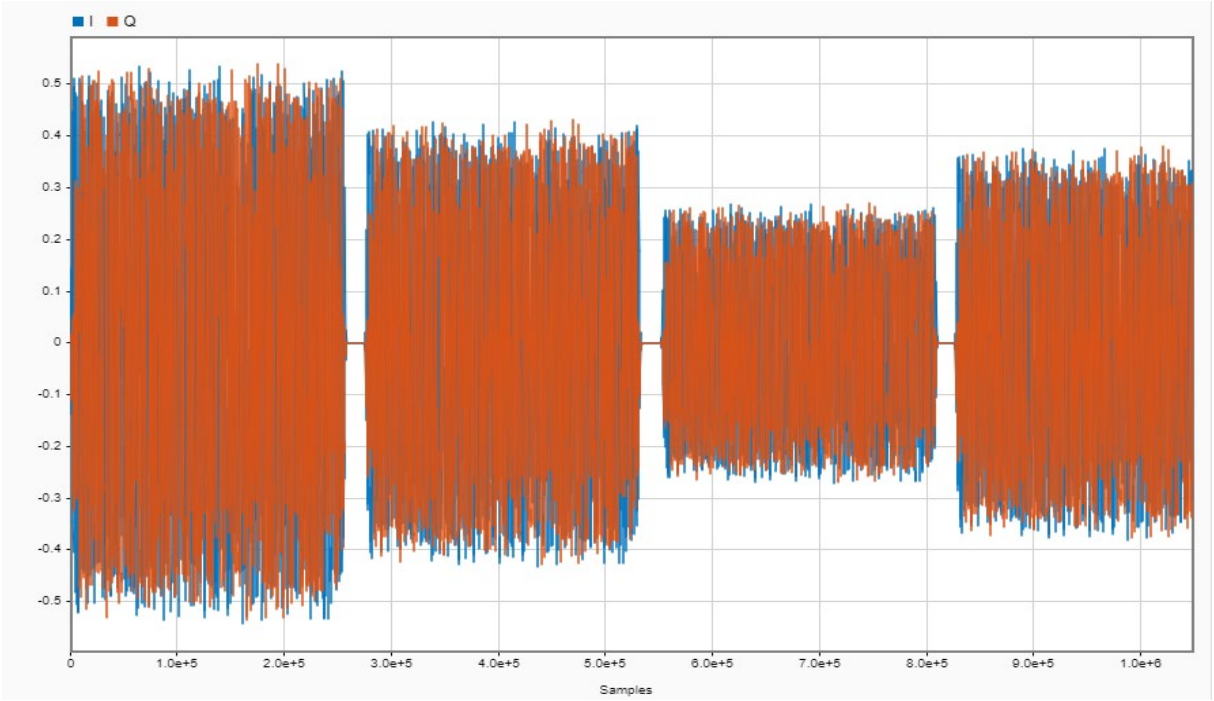

Figure 6-57:A four-slot message

Shown below are graphs showing the frequency domain (Figure 6-58) and time domain characteristics (Figure 6-59) of the received signal.

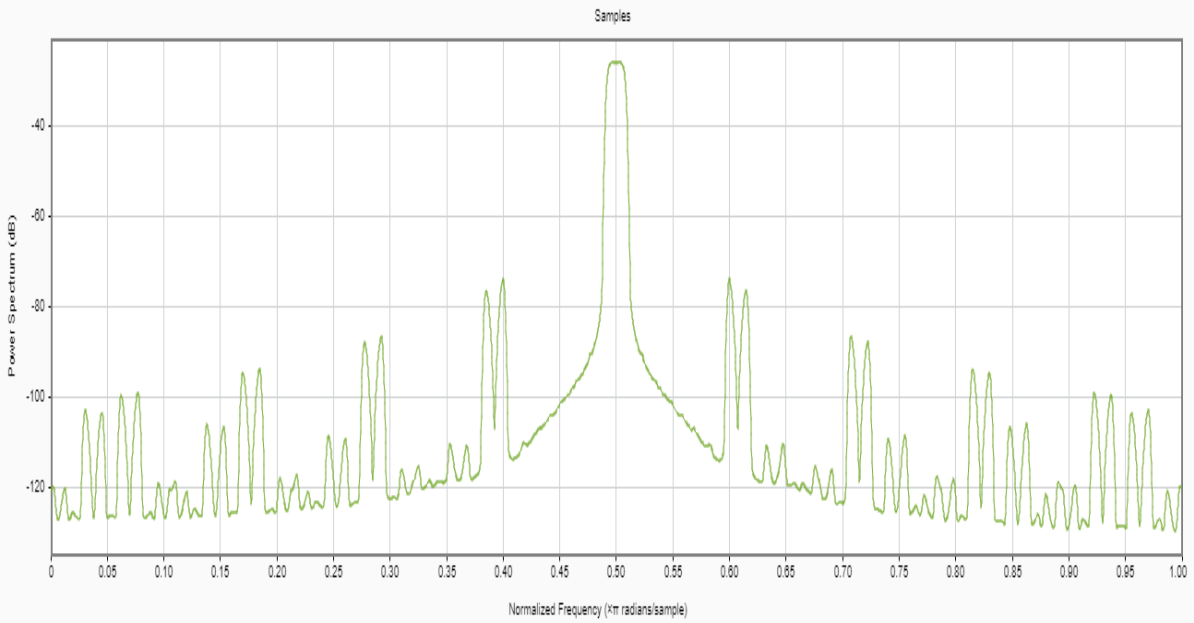

Figure 6-58: Frequency domain signal

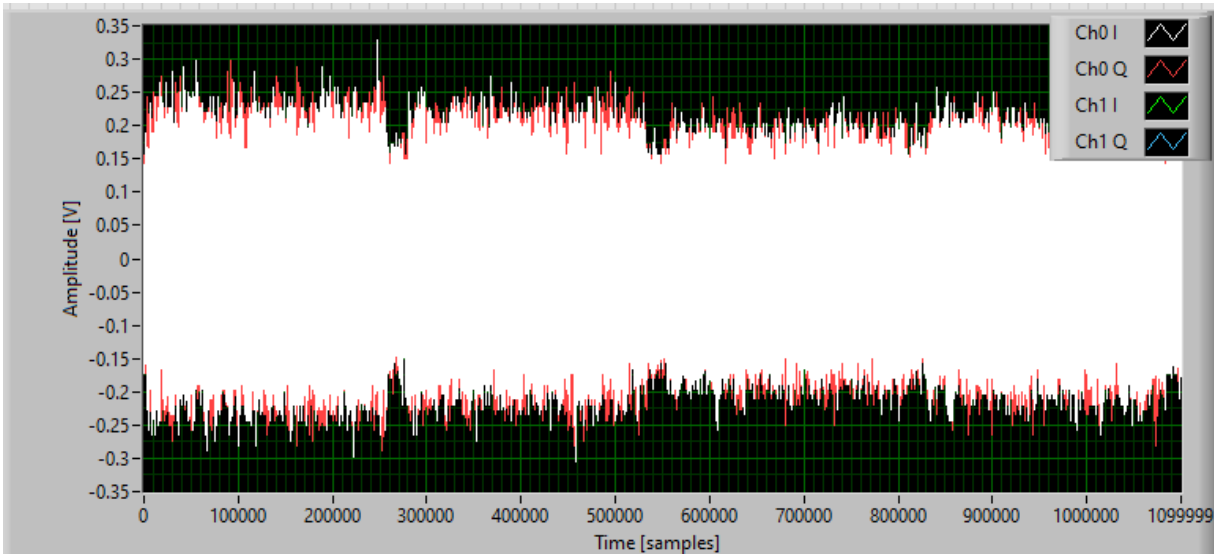

Figure 6-59: Time domain signal

Figure 6-60 below shows the results obtained from the signal correlation application. It is clear from the graph that the distances for the four stations at different distances have been calculated.

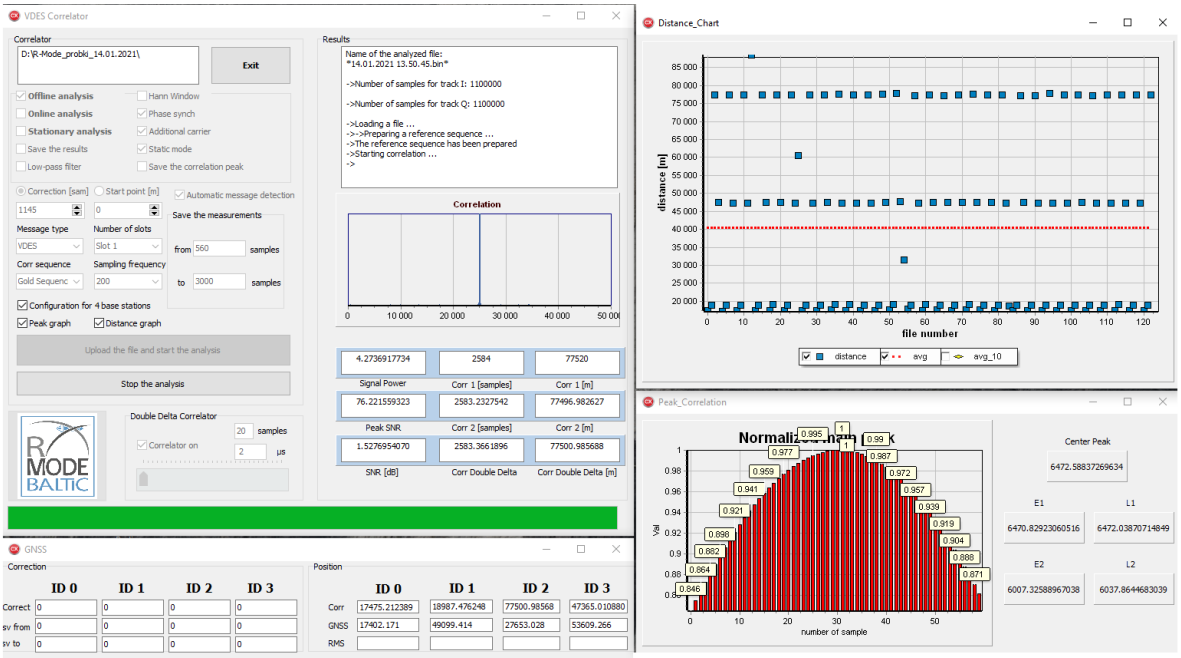

Figure 6-60: Signal correlation application - scenario for four stations

Above is a screenshot of some of the processed data. All the results were saved to a csv file and then detailed distance accuracy results for each of the four stations were generated. On the basis of the results, we can conclude that for the transmitting station at the distance of 17.4 km, ranging accuracy with respect to the GNSS receiver was around 20 m. We may assume that for shorter distance between the transmitter and receiver, the accuracy will significantly improve – to just a few meters.

The determined distances for each of the slots that represent the base station are shown below (Figure 6-61).

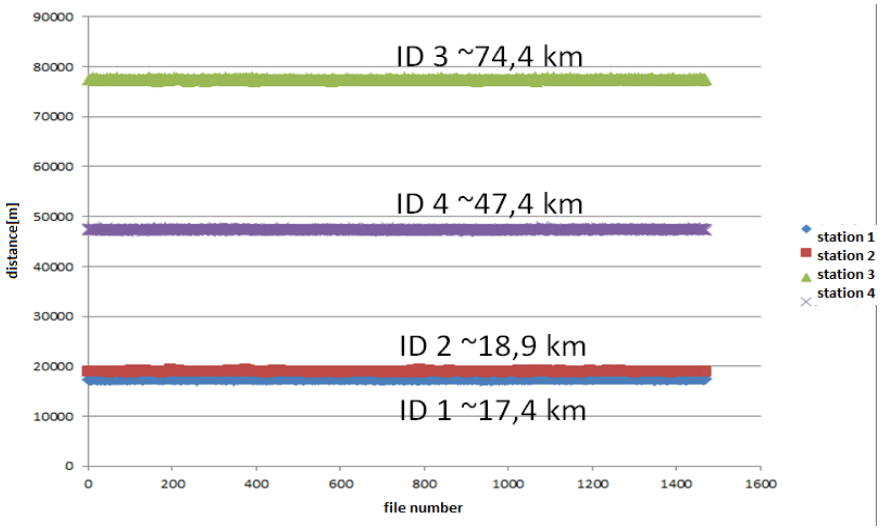

Figure 6-61: Designated distances for four base stations

The values of the correlation peaks depending on the signal strength and the distance from the receiver are presented below (Figure 6-62):

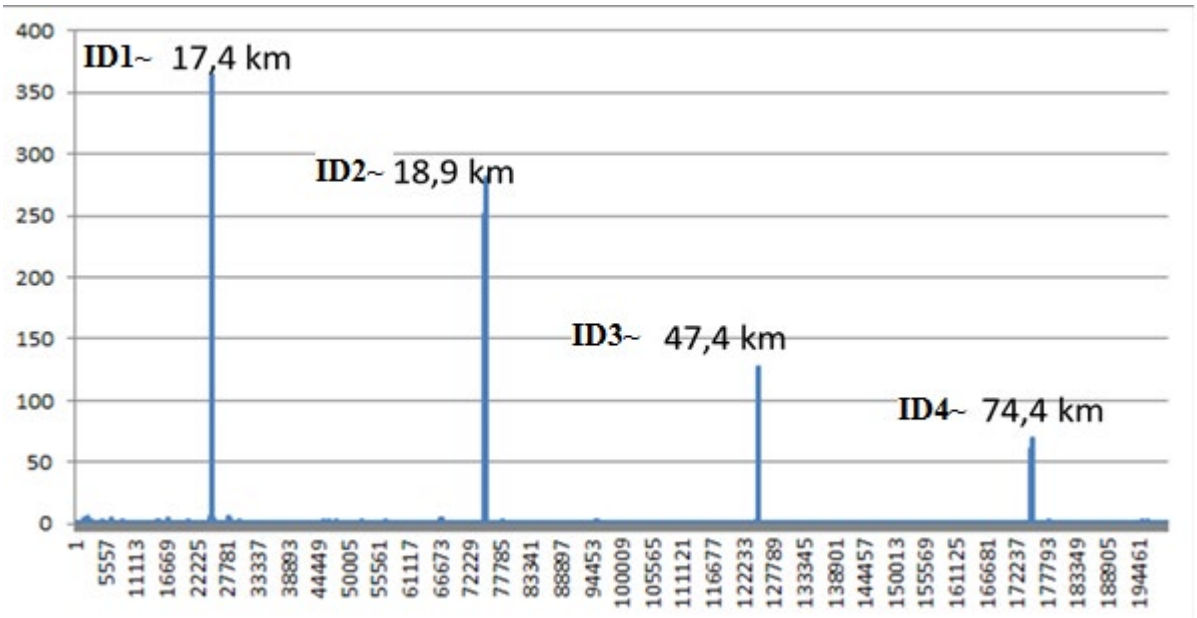

Figure 6-62: Correlation peaks for each of the slots

During the reception, the signals from other transmitters were received simultaneously, which caused the calculated SNR of the target signal to be false. The calculated SNR for each slot is listed below. By manually changing the value of the transmitted signal depending on its simulated distance, it was possible to obtain different SNR values (Figure 6-63)

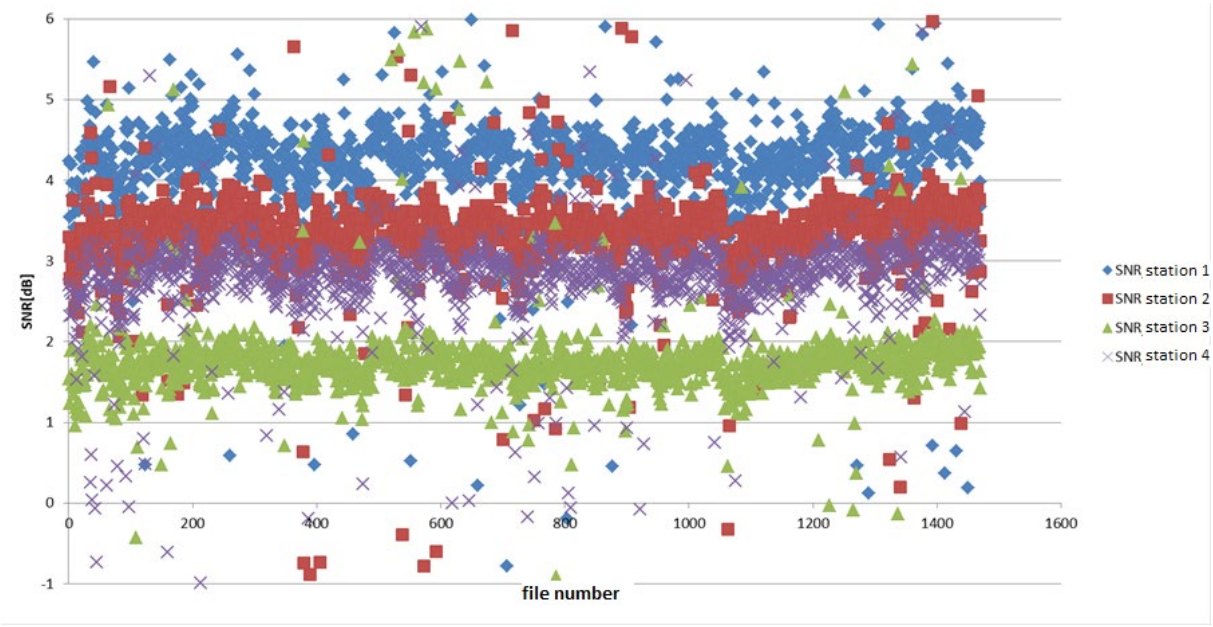

Figure 6-63: Calculated SNR for all slots

SNR values do not exceed 5 dB due to the fact that the transmitting station was actually about 17 km from the NIT building. The other simulated signals had even lower powers, which, as we can see, reached a minimum of 1 dB.

The exact results for the first station are presented below (Figure 6-64). The chart shows the calculated distance accuracy and the Table 6-6 shows the calculated RMS.

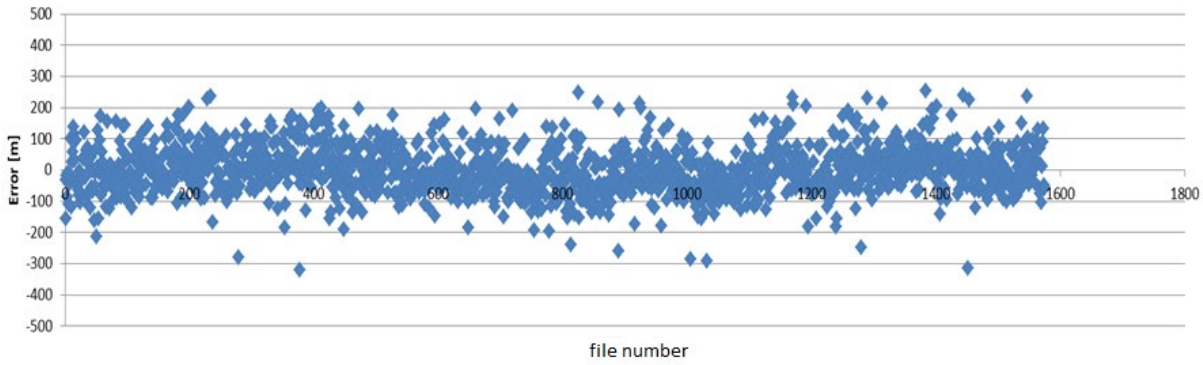

Figure 6-64: Calculated distance accuracy for the first station

Table 6-6: Calculated distance accuracy for the first station

Station number	Average distance from transmitter	Sampling frequency [MHz]	RMS for the double delta correlator [m]
1	17437 m	10	75.314 m

The calculated accuracies for the second station are presented below (Figure 6-65). Table 6-7 shows the calculated RMS.

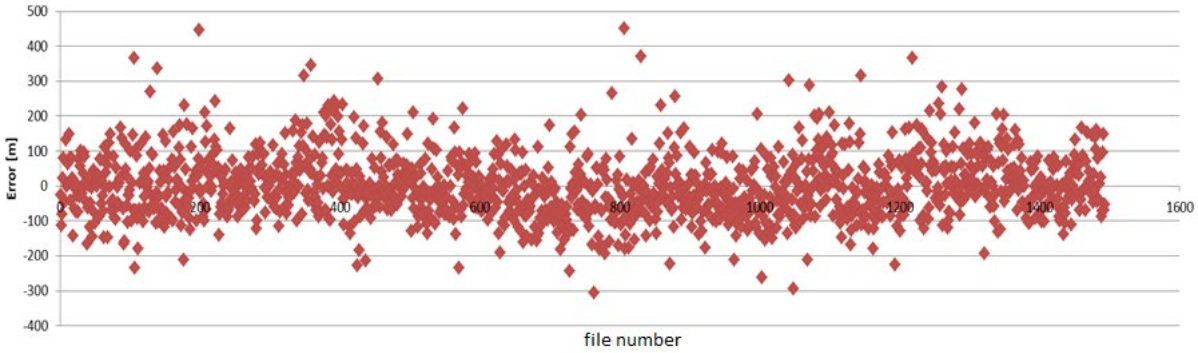

Figure 6-65: Calculated accuracy for the second station

It can be seen that the results for the second station are already worse than for the first station. This station was 1500 meters farther away from the first station. The power of the signal transmitted for the second slot was also reduced proportionally, which can be seen from the value of the correlation peak. These conditions translated into the calculated RMS, which, as we can see, is about 15 meters worse than for the first slot.

Table 6-7: Calculated distance accuracy for the second station

Station number	Average distance from transmitter	Sampling frequency [MHz]	RMS for the double delta correlator [m]
2	18931 m	10	89.549 m

The distance accuracy graph for the third slot is shown below (Figure 6-66):

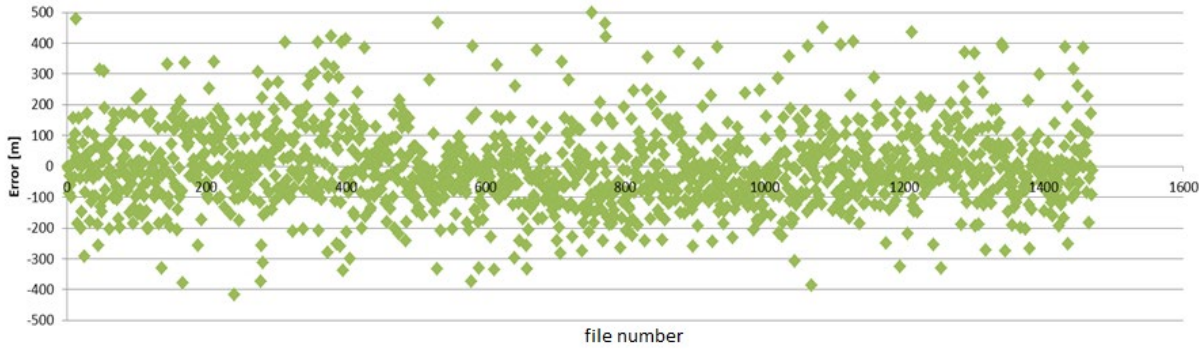

Figure 6-66: Calculated accuracy for the third station

Table 6-8 below shows the exact RMS results calculated for the third slot:

Table 6-8: Calculated distance accuracy for the third station

Station number	Average distance from transmitter	Sampling frequency [MHz]	RMS for the double delta correlator [m]
3	77427 m	10	135.263 m

The case for the third slot had the highest delay introduced and the lowest signal strength. This is especially seen in the calculated RMS, which is much greater than the rest. The error is at the level of 130 meters, which is significant.

The distance accuracy graph for the fourth slot is shown below (Figure 6-67):

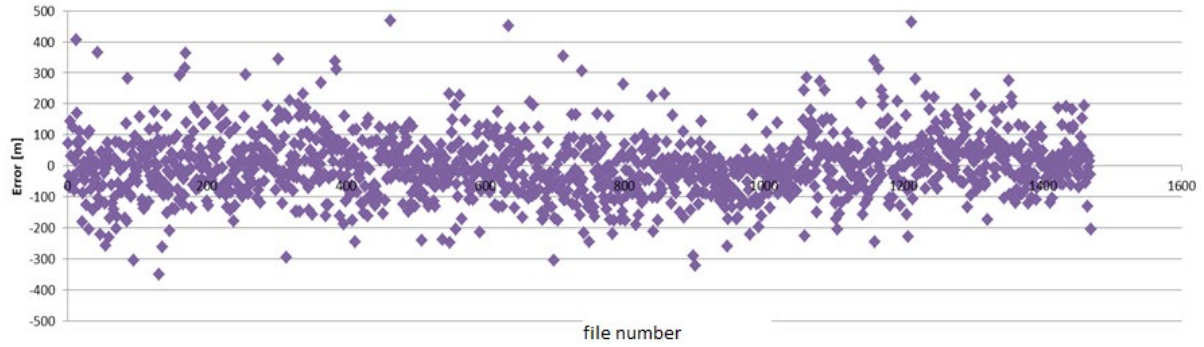

Figure 6-67: Calculated accuracy for the fourth station

Table 6-9 below shows the RMS obtained for the results for the fourth slot.

Table 6-9: Calculated distance accuracy for the fourth station

Station number	Average distance from transmitter	Sampling frequency [MHz]	RMS for the double delta correlator [m]
4	47388 m	10	98.499 m

Table 6-10shows a summary of all the results obtained for the four slots:

Table 6-10: A summary of all the results obtained for the four slots

Station number	Average distance from transmitter	RMS for the double delta correlator [m]
1	17437 m	75.314 m
2	18931 m	89.549 m
3	77427 m	135.263 m
4	47388 m	98.499 m

As we can see above, all the results obtained for the four slots have been compiled. Thanks to this, it was possible to check the correctness of the implementation of all modules in the system until the distance accuracy was determined. In the scenario for four base stations, their presence was simulated as separate time slots. In a signal correlation application, each slot has been correlated with a reference signal. After numerous mathematical operations, the calculated distance was obtained. The tests confirm the correctness of the implemented modules for determining the signal distance from the transmitting station based on the signal delay.

6.2.4 Measurement scenario with ranging accuracy studies for four slots with gamma = 0.7

In this research scenario, a signal consisting of a Gold sequence and an alternative sequence was used [R-MODE19].

The ranging sequence is known and it is a part of the data payload. Each shore station shall send out the ranging sequence once per second.

The ranging sequence is a combination of two sequences to customize the required performance based on the given scenarios. The scenarios are:

- Shorter distances between shore station and vessel

- Longer distances between shore station and vessel

The first sequence is based on the π/4-QPSK modulation alphabet and alternates its constellation points. The second part of the ranging sequence is a Gold code.

Both sequences are weighted and then added together. The alternating sequence is multiplied by a weighting factor $\gamma(short) = 0.7$ for short distances (higher SNR) and $\gamma(large) = 0.3$ for larger distances (lower SNR). The Gold code is multiplied by a weighting factor $1 - \gamma(short) = 0.3$ for short distances and $1 - \gamma(large) = 0.7$ for large distances.

The signal for γ= 0.7 is shown below (Figure 6-68)

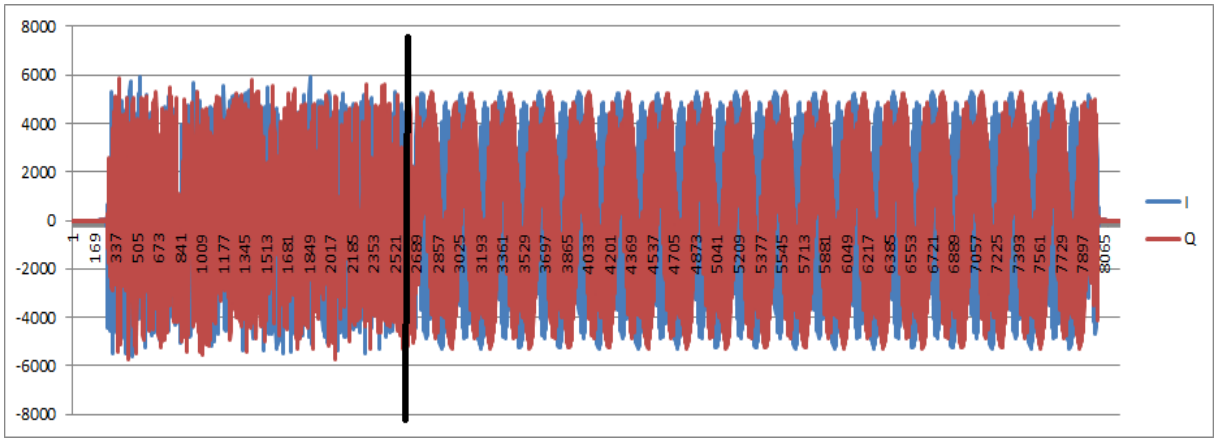

Figure 6-68: Signal for γ= 0.7

Correlation plots for this signal are shown below. The first graph shows the correlation for the part with the Gold signal (Figure 6-69). In the second plot (Figure 6-70), there is a correlation of the part with the alternating sequence. The last graph (Figure 6-71) shows what the autocorrelation function of this signal looks like.

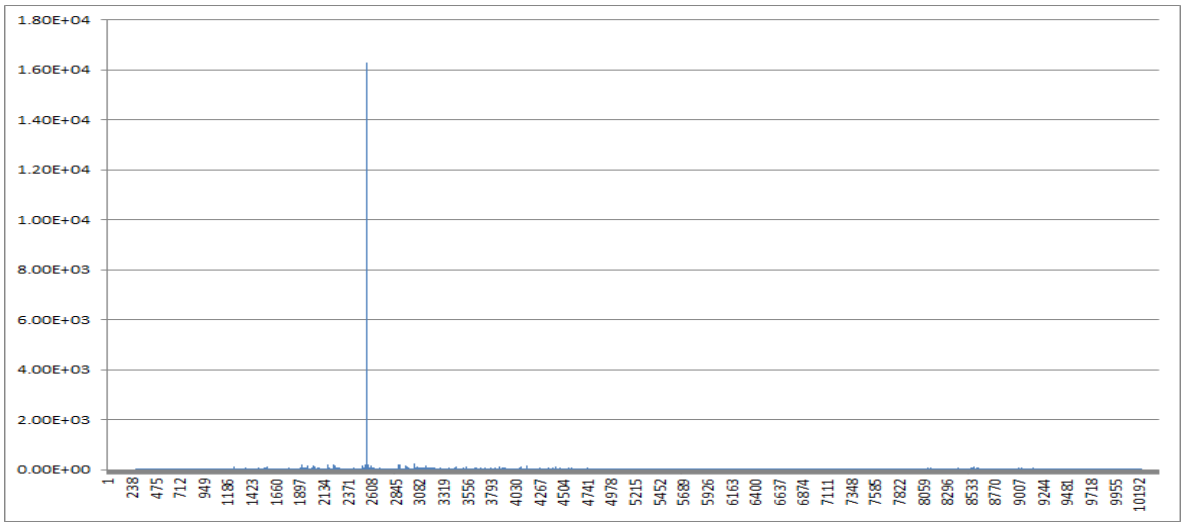

Figure 6-69: Correlation of parts of the Gold sequence

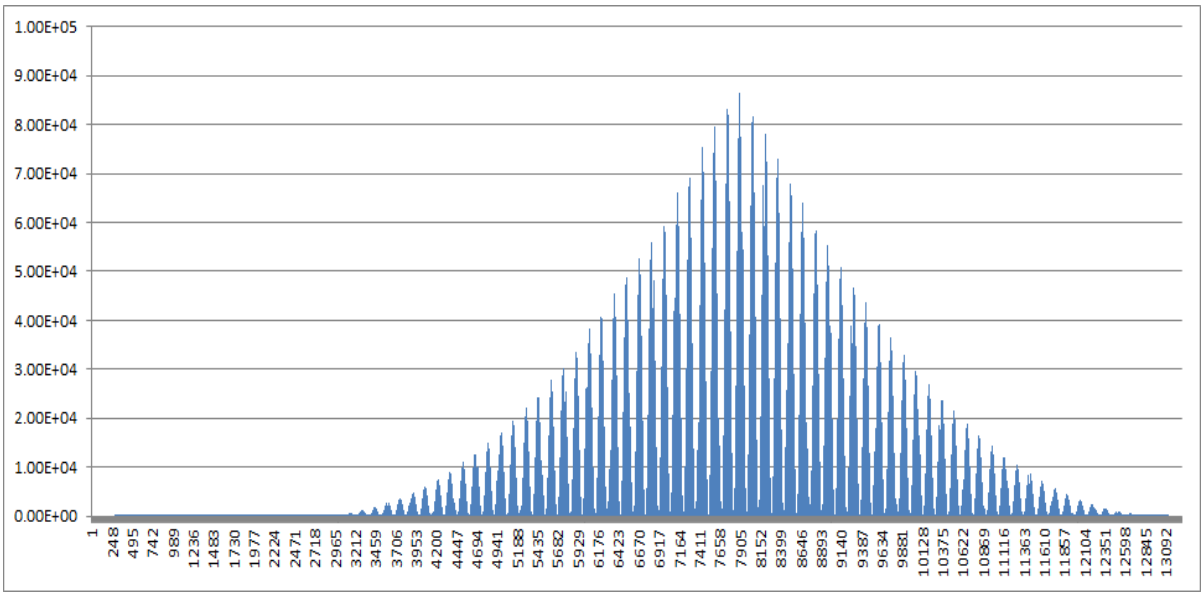

Figure 6-70: Correlation part of the string alternative sequence

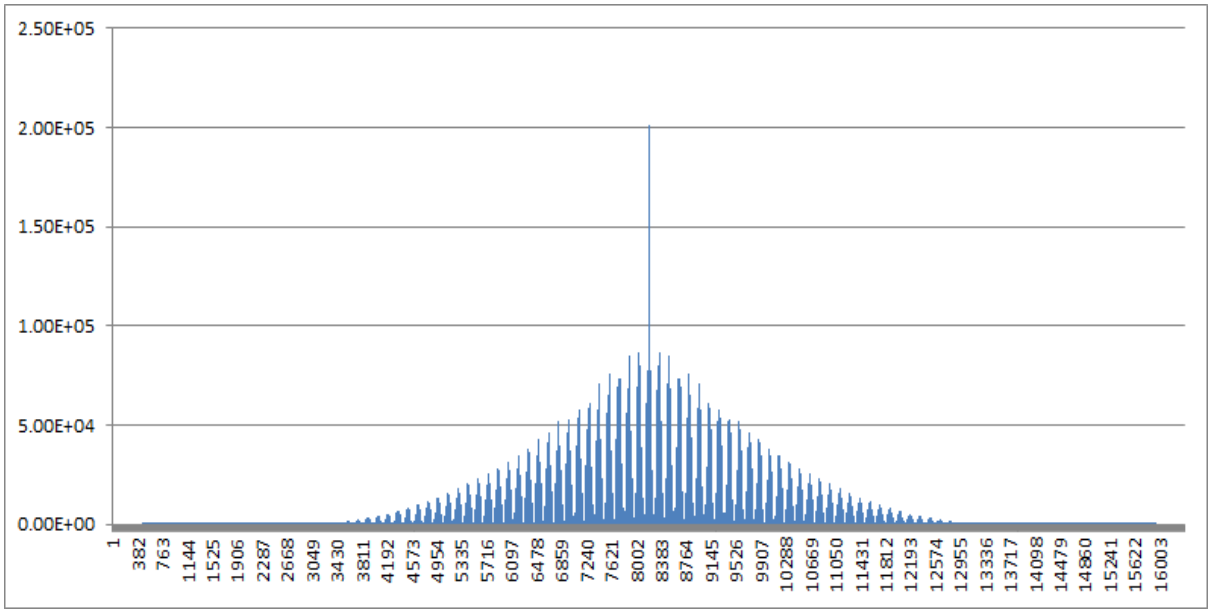

Figure 6-71: Autocorrelation for the entire signal

The above shows the correlations for this type of signals. Thanks to the combined sequence in the measurement tests, even better distance accuracy was obtained, which greatly influenced the obtained results. The screenshot below (Figure 6-72) shows a signal correlation application that processes recorded samples from a transmitting station located in Gdynia, 17 km from the receiving antenna. With the correlation of signals for the $\gamma = 0.7$, distance accuracy of an average of 20 meters was obtained.

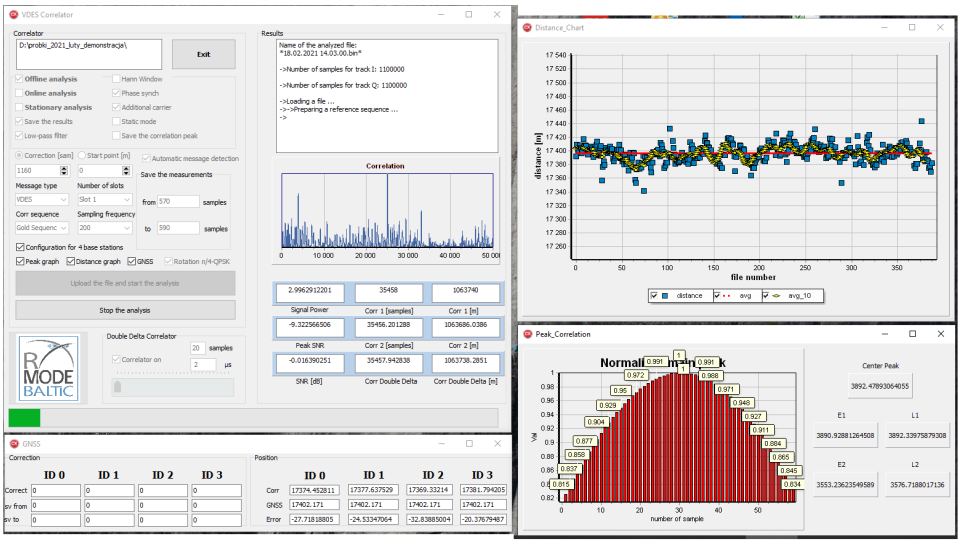

Figure 6-72: Processing samples with $\gamma = 0.7$

The screenshot also shows the signal correlation application, which determines the accuracy of distances up to 20 meters. In this case, the sample file was saved as a four-slot message, i.e. the presence of four base stations located at equal distances from the receiver was simulated. In addition, measurements were read from the GNSS module in order to calculate the accuracy of the determined distance in real time.

First, the correlation of the signal set to $\gamma = 0.7$ was dealt with. In the first analysis, it was correlated with the $\gamma = 0$ signal, i.e. the full Gold sequence, to compare it with the correlation for $\gamma = 0.7$ to see how the obtained distance accuracy changes.

With the correlation (Figure 6-73) of the $\gamma = 0.7$ signal with the $\gamma = 0$ signal, RMS = 44.68 m was obtained, which is still very accurate compared to the previous analyzes. However, for the same signal with $\gamma = 0.7$ (Figure 6-74), which was also correlated with the $\gamma = 0.7$ signal, the result was RMS = 17.58 m for about 5400 files, which is a really good result.

Below are graphs on the same scale for comparison:

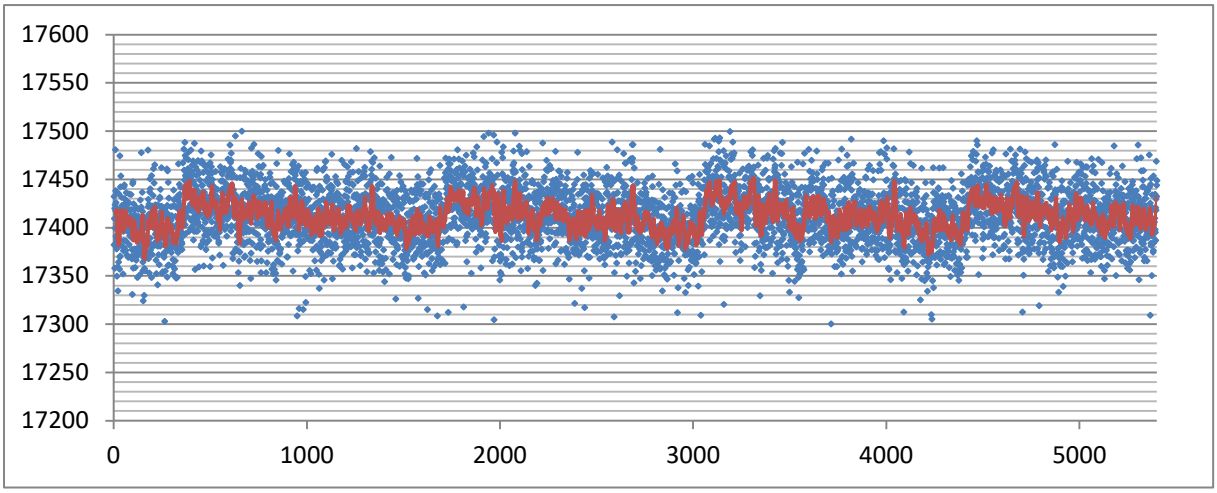

Figure 6-73: GAMMA (γ) signal = 0.7 correlated with GAMMA (γ) signal = 0

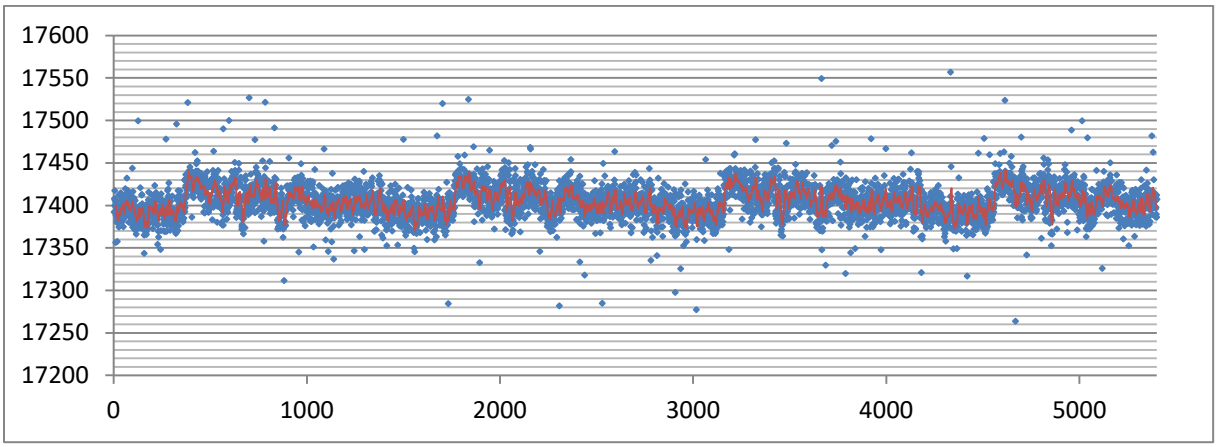

Figure 6-74: GAMMA (γ) signal = 0.7 correlated with GAMMA (γ) signal = 0.7

Almost the same results were observed for the transmitted signal γ = 0.3. Here, the RMS for that signal correlated with the γ = 0 signal Figure 6-75) is RMS = 44.52 m and the RMS for that signal correlated with the γ = 0.3 signal (Figure 6-76) is RMS = 20.54 m.

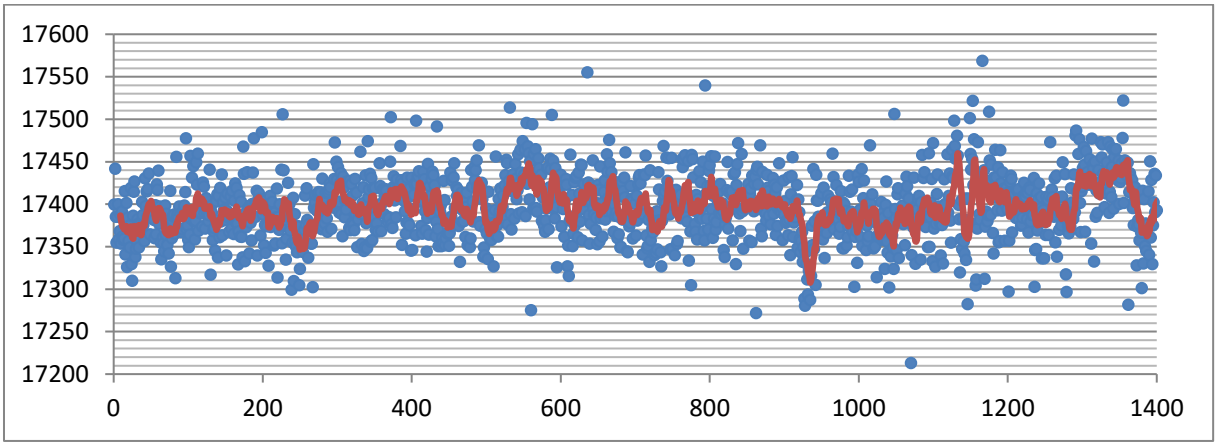

Figure 6-75: GAMMA (γ) signal = 0.3 correlated with GAMMA (γ) signal = 0

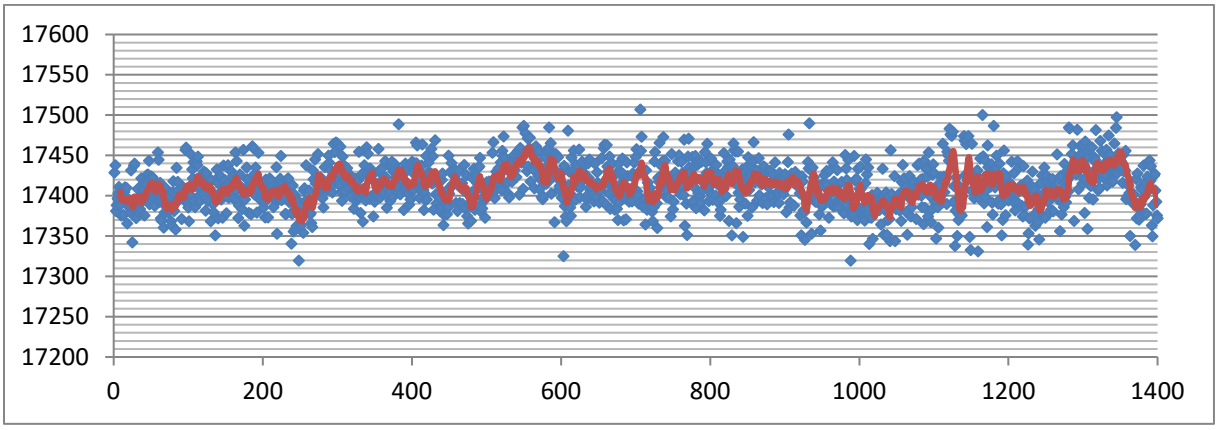

Figure 6-76: GAMMA (γ) signal = 0.3 correlated with GAMMA (γ) signal = 0.3

7 R-Mode Positioning Demonstration

In March 2021, the R-Mode system for real-time positioning was tested under laboratory conditions. The research consisted in integrating all hardware and software modules, thanks to which a demonstration stand of the R-Mode system was created.

In the first stage, the part in which the USRP and u-blox recorded all the necessary data was integrated, and then that data were transferred to the second module with the signal correlation application.

Our implemented solution consists of four cooperating modules - two hardware and two software modules.

They are presented in the diagram (Fig. 7-1) and their functions are as follows:

- RF module - periodically receives radio transmissions from the R-Mode stations and stores IQ samples,
- Signal correlation application - reads files with IQ samples, correlates them, and then, having information about the coordinates of the stations, determines the pseudoranges,
- GNSS receiver - records the UTC time, GNSS position, speed and track angle. The first two parameters are used for accuracy comparison purposes, while the other two are fed to the input of the Kalman filter,
- R-Mode real-time positioning application - determines the position based on the calculated pseudo-ranges to the R-Mode stations and additionally using the Kalman filtration. It also determines positioning errors with respect to GNSS position.

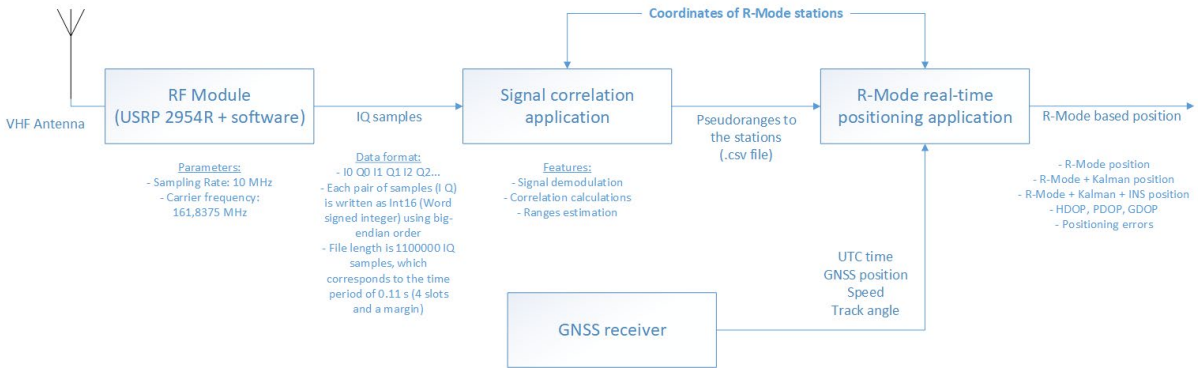

Figure 7-1: A diagram of the R-Mode system implementation

The integration was successful and its effects are presented below (Figure 7-2 to Figure 7-7).

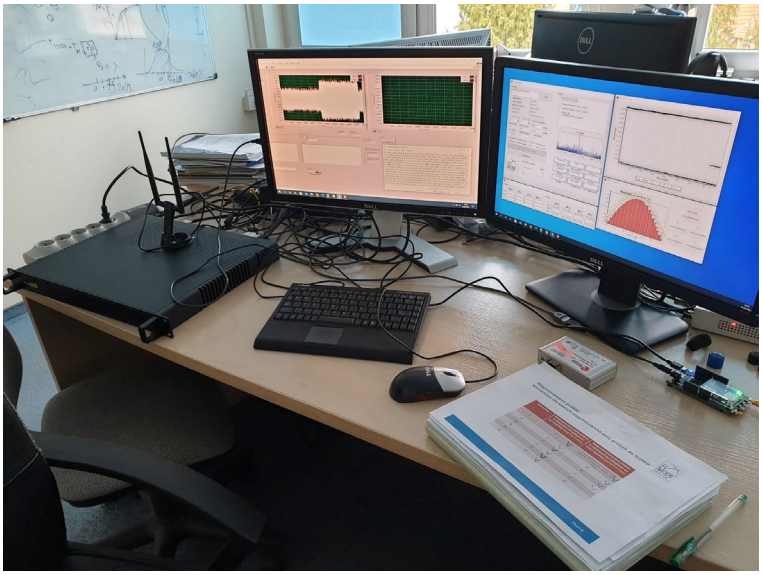

Figure 7-2: Integration of a sample recording module with a signal correlation module that determines pseudoranges a)

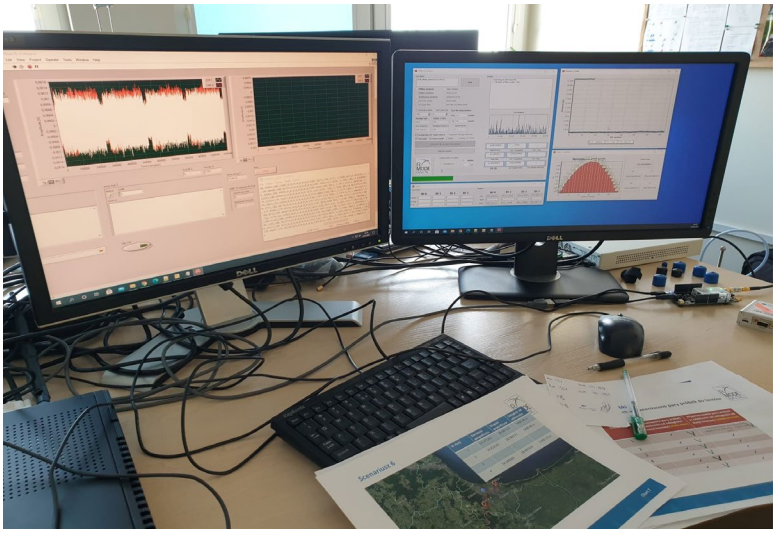

Figure 7-3: Integration of a sample recording module with a signal correlation module that determines pseudoranges b)

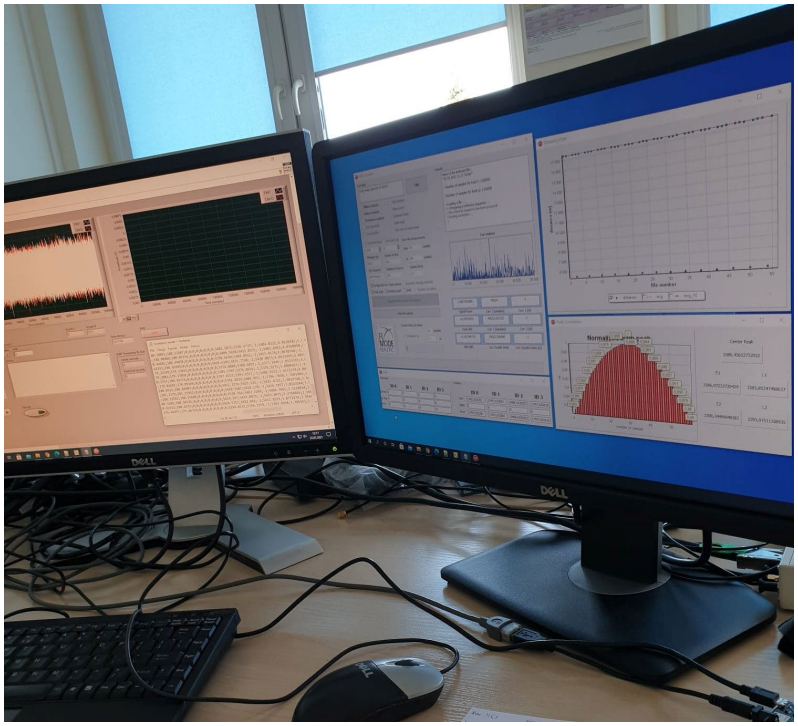

Figure 7-4: Integration of a sample recording module with a signal correlation module that determines pseudoranges c)

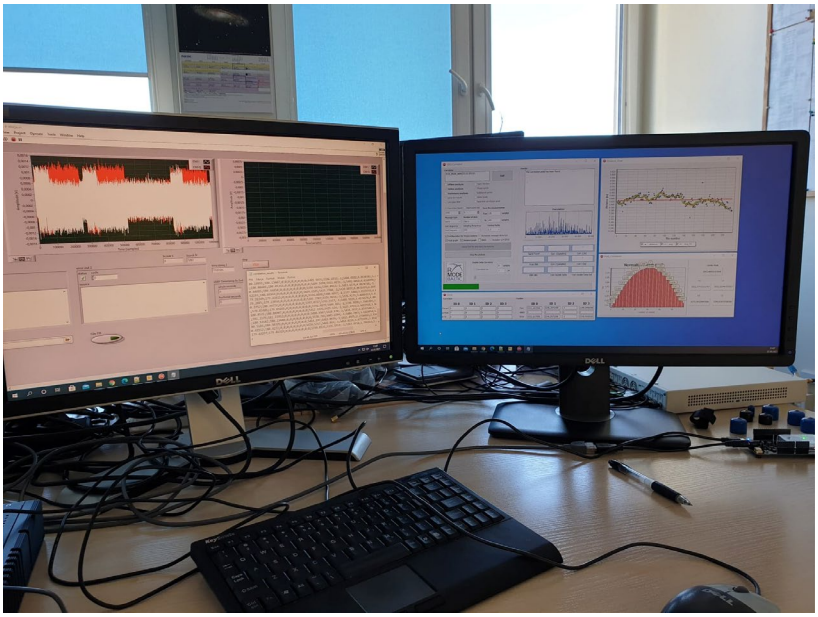

Figure 7-5: Integration of a sample recording module with a signal correlation module that determines pseudoranges d)

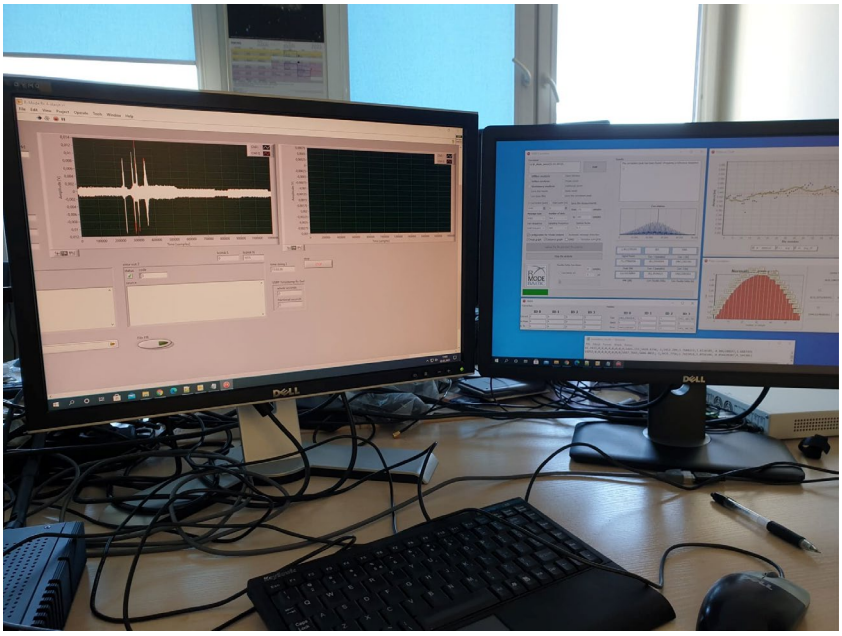

Figure 7-6: Integration of a sample recording module with a signal correlation module that determines pseudoranges e)

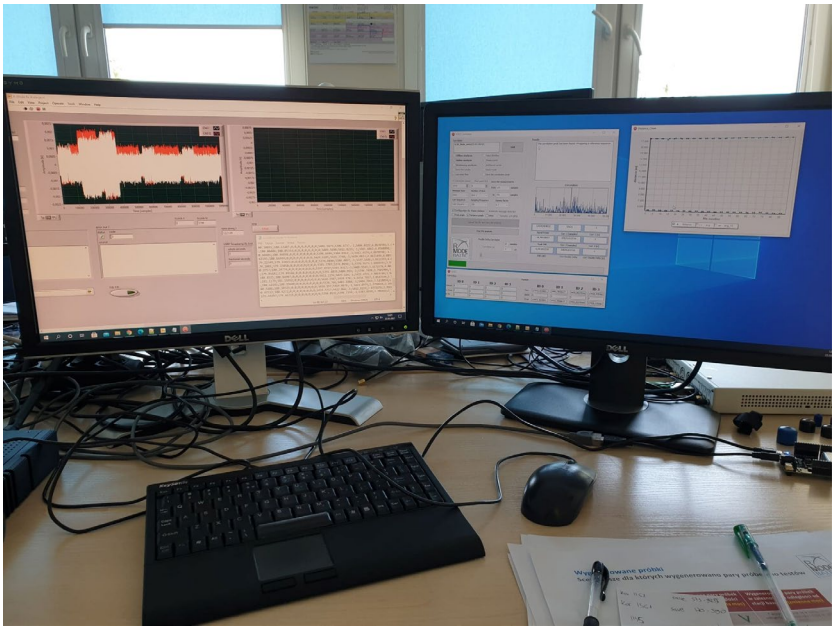

Figure 7-7: Integration of a sample recording module with a signal correlation module that determines pseudoranges f)

In the second stage, the integration of all modules was completed, i.e. the module with samples from USRP together with the module for correlation of signals were integrated with the application for determining the position based on the obtained pseudoranges.

As part of the tests, the influence of different positioning of the R-Mode base stations in relation to the receiver and the influence of various factors on the errors of the determined position was examined.

The 6 scenarios based on which all tests were performed are presented below (Figure 7-8 to Figure 7-13):

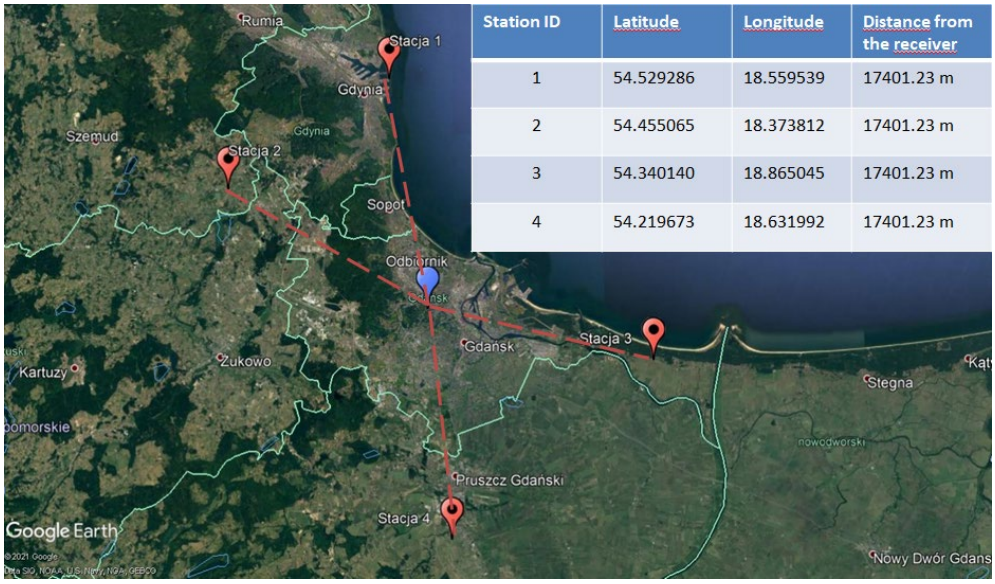

Station ID	Latitude	Longitude	Distance from the receiver
1	54.529286	18.559539	17401.23 m
2	54.455065	18.373812	17401.23 m
3	54.340140	18.865045	17401.23 m
4	54.219673	18.631992	17401.23 m

Figure 7-8: The first measurement scenario for testing the positioning R-Mode demonstrator in real time

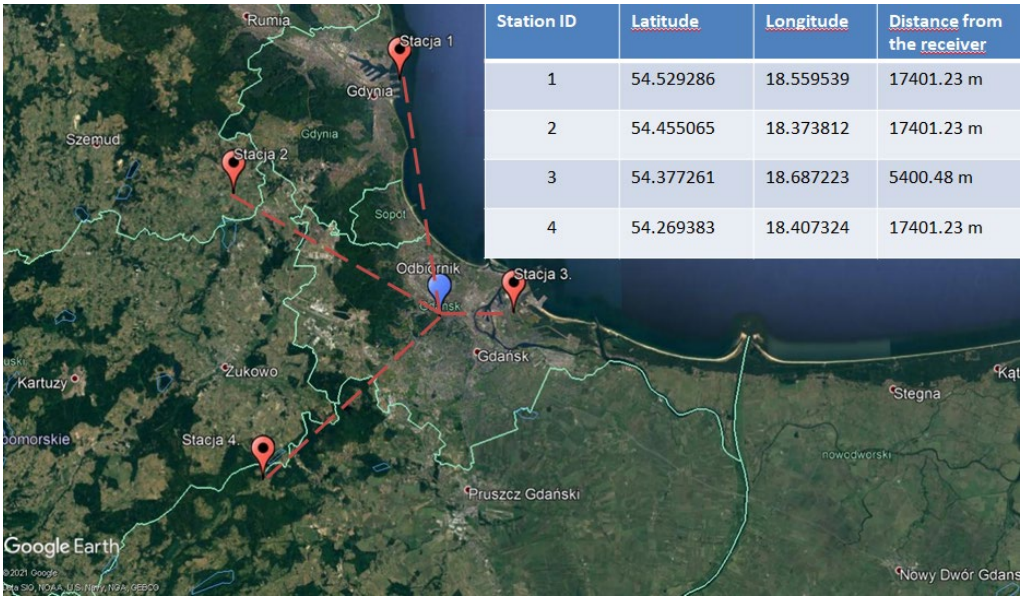

Station ID	Latitude	Longitude	Distance from the receiver
1	54.529286	18.559539	17401.23 m
2	54.455065	18.373812	17401.23 m
3	54.377261	18.687223	5400.48 m
4	54.269383	18.407324	17401.23 m

Figure 7-9: The second measurement scenario for testing the positioning R-Mode demonstrator in real time

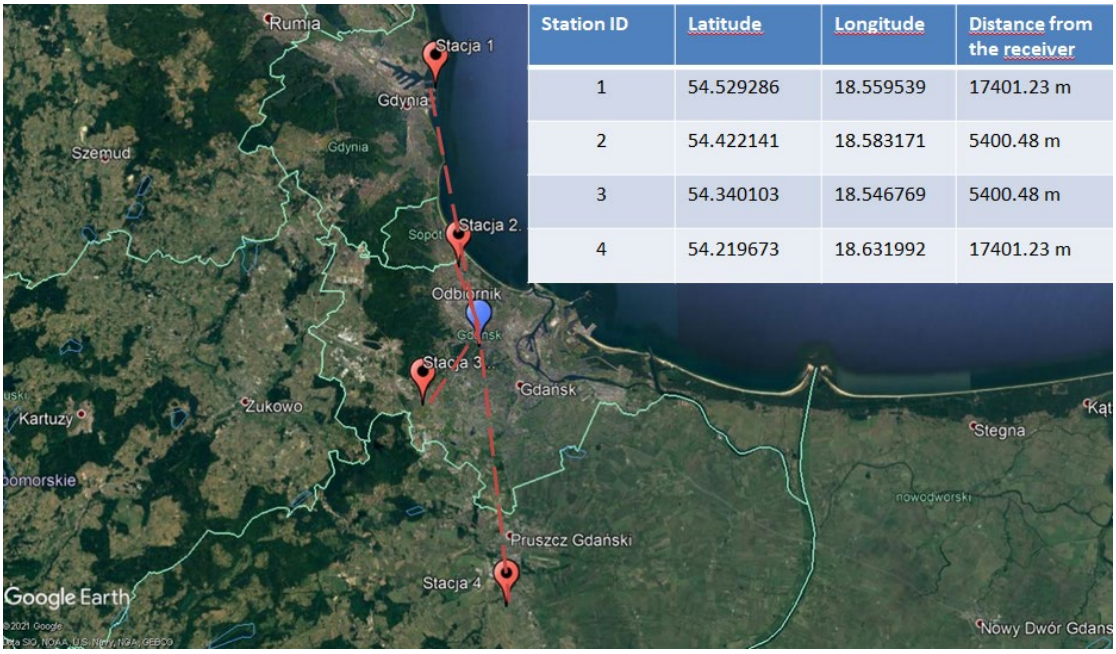

Station ID	Latitude	Longitude	Distance from the receiver
1	54.529286	18.559539	17401.23 m
2	54.422141	18.583171	5400.48 m
3	54.340103	18.546769	5400.48 m
4	54.219673	18.631992	17401.23 m

Figure 7-10: The third measurement scenario for testing the R-Mode positioning system demonstrator in real time

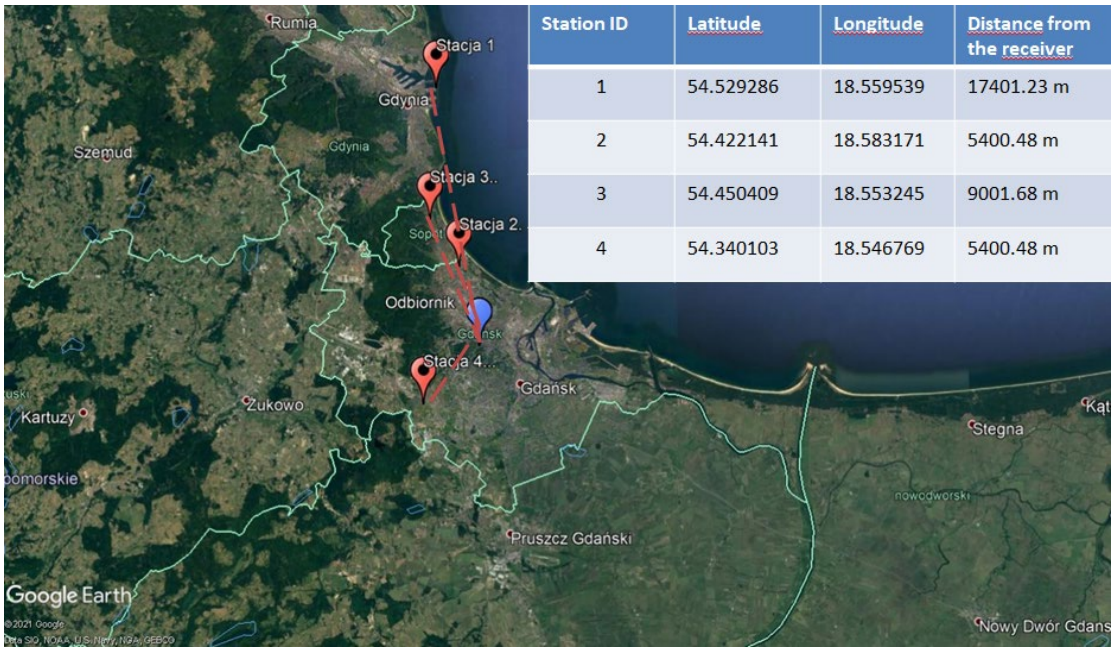

Station ID	Latitude	Longitude	Distance from the receiver
1	54.529286	18.559539	17401.23 m
2	54.422141	18.583171	5400.48 m
3	54.450409	18.553245	9001.68 m
4	54.340103	18.546769	5400.48 m

Figure 7-11: The fourth measurement scenario for testing the R-Mode system demonstrator that determines the position in real time

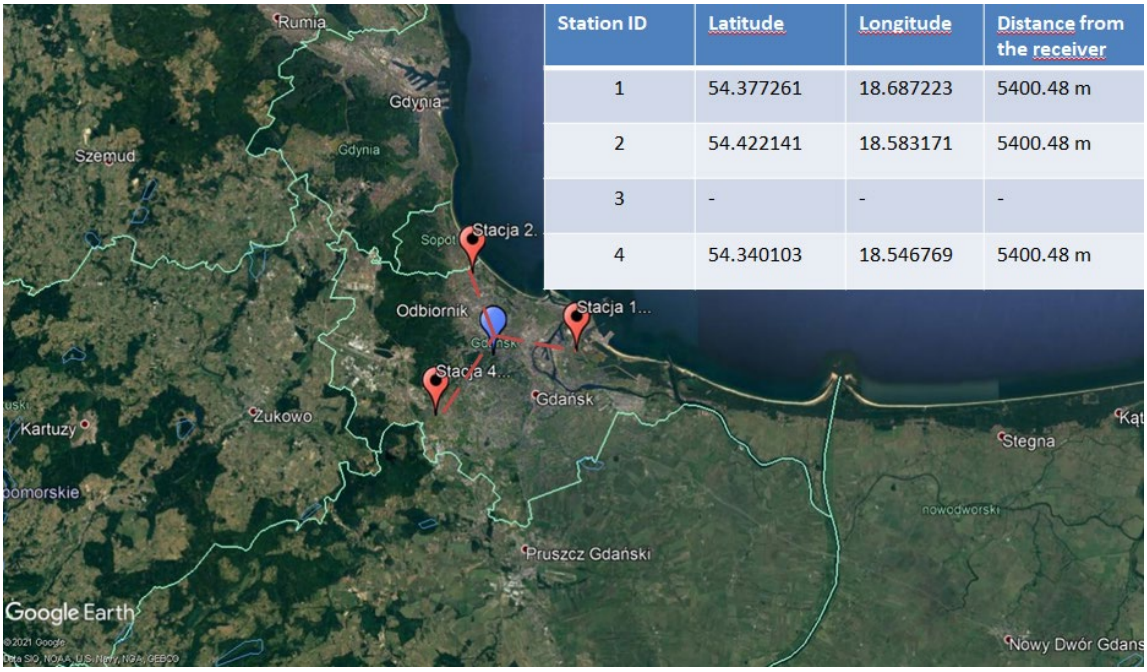

Station ID	Latitude	Longitude	Distance from the receiver
1	54.377261	18.687223	5400.48 m
2	54.422141	18.583171	5400.48 m
3	-	-	-
4	54.340103	18.546769	5400.48 m

Figure 7-12: The fifth measurement scenario for testing the R-Mode positioning system demonstrator in real time

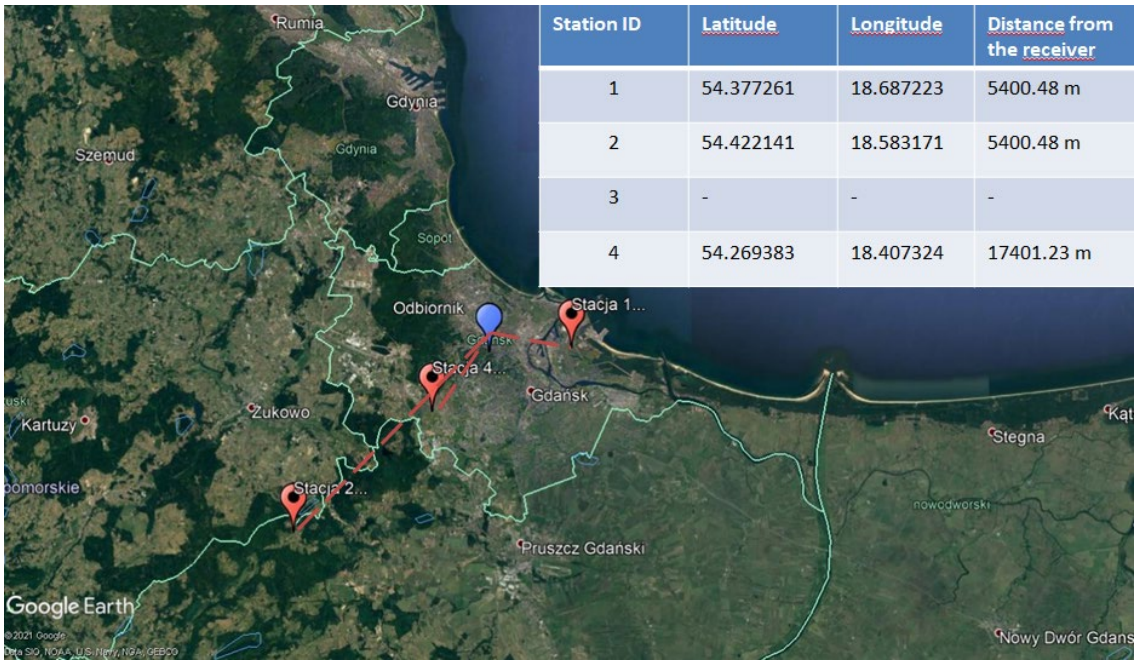

Station ID	Latitude	Longitude	Distance from the receiver
1	54.377261	18.687223	5400.48 m
2	54.422141	18.583171	5400.48 m
3	-	-	-
4	54.269383	18.407324	17401.23 m

Figure 7-13: The sixth measurement scenario for testing the R-Mode positioning system demonstrator in real time

Measurement studies were carried out for the above scenarios. Pictures from the R-Mode system demonstrator are shown below (Figure 7-13 to Figure 7-18).

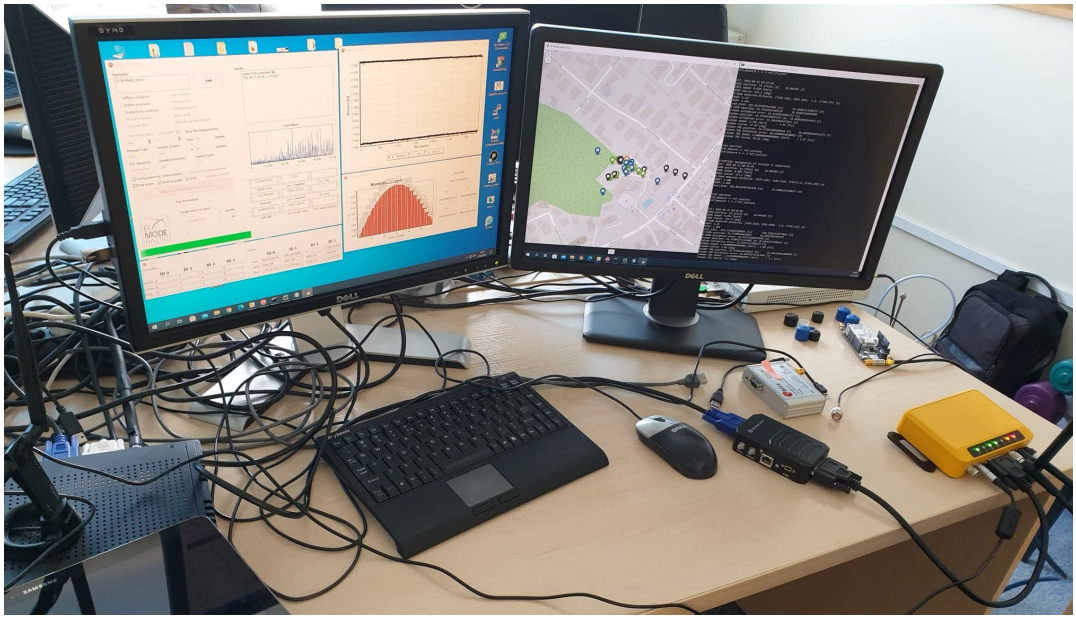

Figure 7-14: R-Mode demonstration stand a)

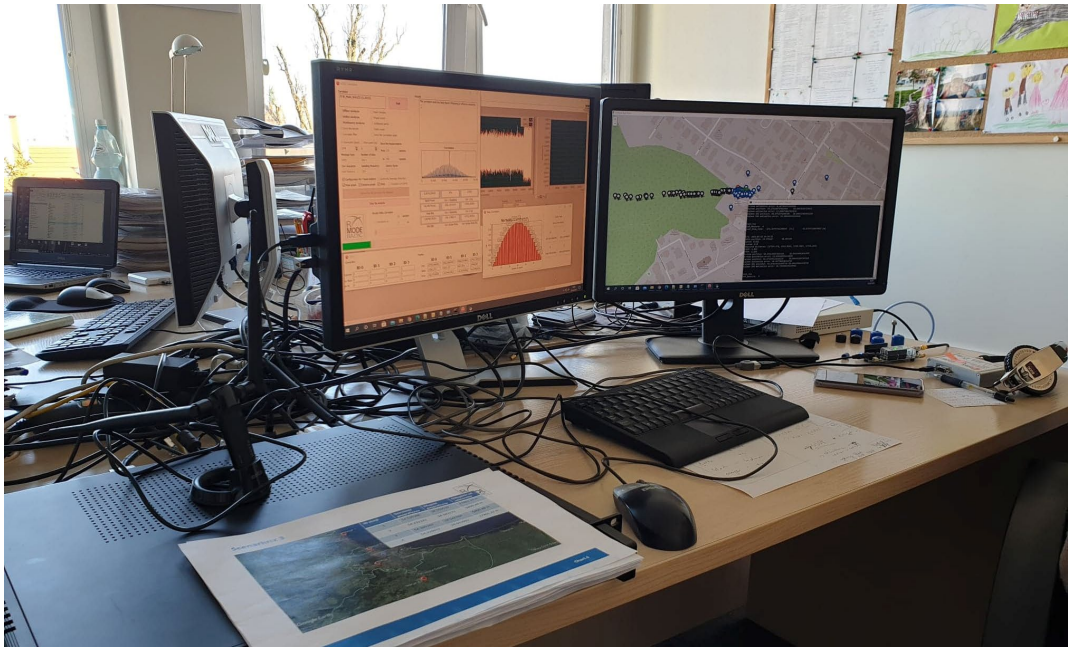

Figure 7-15: R-Mode demonstration stand b)

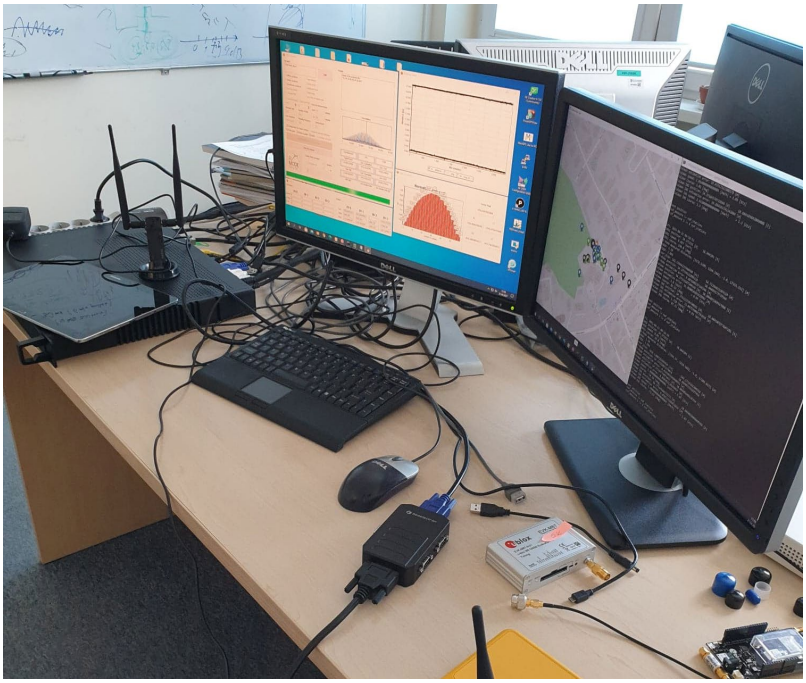

Figure 7-16: R-Mode demonstration stand c)

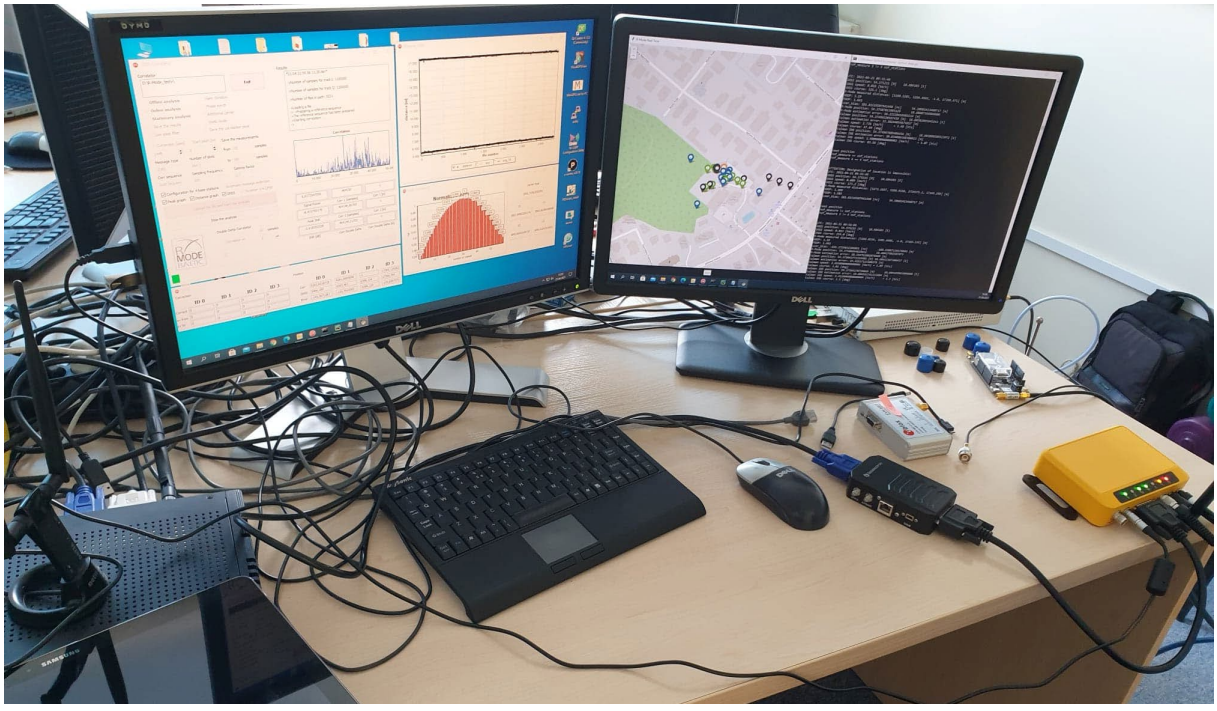

Figure 7-17: R-Mode demonstration stand d)

Figure 7-18: R-Mode demonstration stand e)

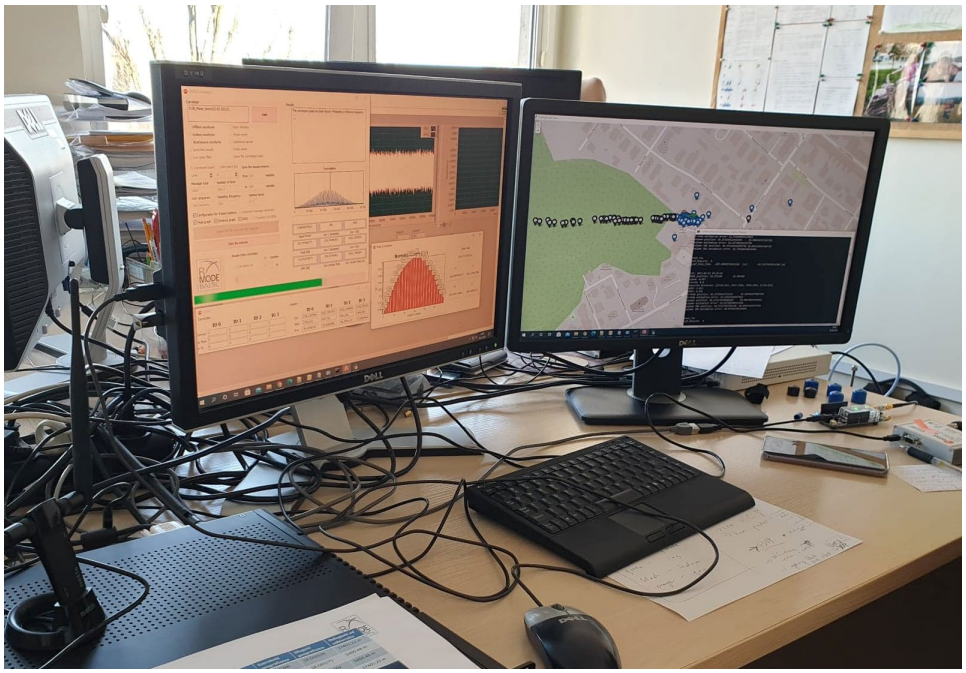

Figure 7-2: R-Mode demonstration stand f)

Table 7-1 below shows the results for all measurement scenarios. Fixed power scenarios mean that the signals from the simulated transmitting stations have the same power regardless of their distance from the receiver. On the other hand, scenarios with variable strengths mean that the signal strength changes proportionally to the distance from a given transmitting station.

Table 7-1: Results of measurement scenarios

scenario	rmode_avg	kalman_avg	ins_avg	nof_measurements	hdop_avg	pdop_avg
Scenario 1 - constant power	15.7753	118.5524	8.696161	186	1.146	1.603
Scenario 1 - variable power	17.04171	18408.79	86.48589	120	1.146	1.603
Scenario 2 - constant power	12.67883	92.52741	7.210433	228	1.063	1.559
Scenario 2 - variable power	13.57581	71.22065	5.979512	144	1.063	1.559
Scenario 3 - constant power	22.21149	80.1648	16.91396	155	1.833	2.194
Scenario 3 - variable power	29.49874	31.41097	24.53933	128	1.833	2.194
Scenario 4 - constant power	79.20474	54.13518	38.23067	243	7.836	8.819
Scenario 4 - variable power	109.6123	74.98872	62.74601	277	7.836	8.82
Scenario 5 - constant power	13.00927	12.91655	12.73657	112	1.182	1.654
Scenario 5 - variable power	15.79613	13.91848	13.78193	197	1.183	1.655
Scenario 6 - constant power	15.12704	11.66721	11.5944	220	1.189	1.66
Scenario 6 - variable power	14.07674	10.22931	10.16125	323	1.189	1.66

The second column of the table shows the results calculated for the R-Mode system itself. The next column shows the results for the R-Mode system along with the Kalman filter. The next column shows the results for the additional inertial module.

As can be seen for the emulated broadcasting stations, where the only broadcasting station was the station in Gdynia - 17.4 km away, very high accuracy of the determined position was obtained: about 15 meters. After a more detailed analysis, it can be seen that for the poor geometry of the distribution of transmitting stations, the determined position accuracy has significantly deteriorated. Of course, it should also be added that the R-Mode demonstrator worked in static mode without any movement.

The screenshot below (Figure 7-20) shows how the signal correlating application processes the samples recorded by the USRP and then the positioning application processes the determined pseudoranges (Figure 7-21).

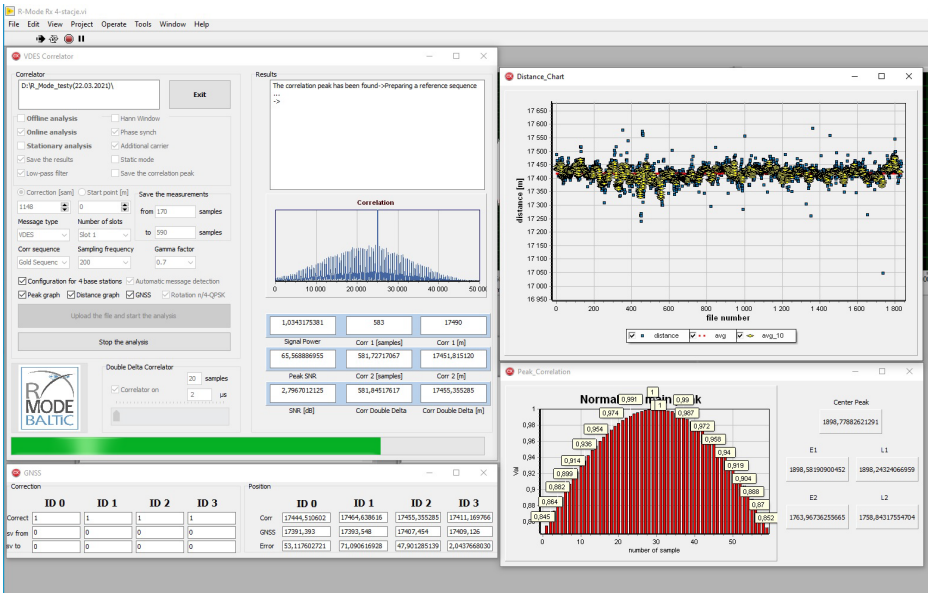

Figure 7-20: A signal correlation application that determines pseudoranges

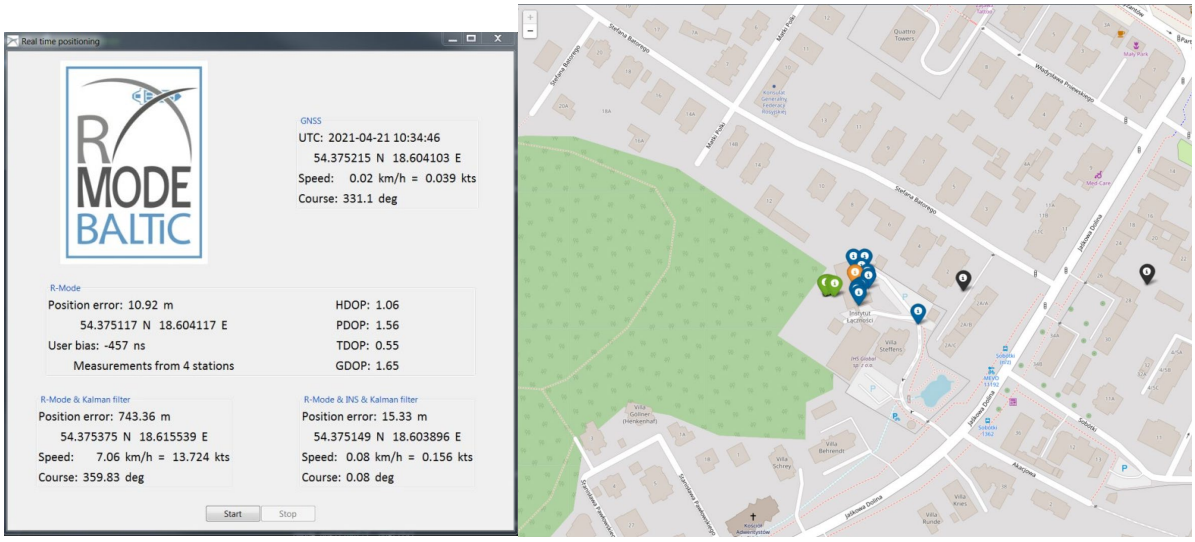

Figure 7-21: Real-time positioning application

8 References

[AAVR20] AIS AND VDES RANGING – MEASUREMENTS RESULTS, GA5.3/5.4 project report, NIT, 2020

[AIS14] Technical Characteristics for an Automatic Identification System Using Time Division Multiple Access in the VHF maritime Mobile Frequency Band, Radiocommunication Sector of the International Telecommunication Union (ITU-R), Feb. 2014, Recommendation ITU-R M.1371-5. [Online]. Available: https://www.itu.int/rec/R-REC-M.1371/en

[CZZ75] D. Chazan, M. Zakai and J. Ziv, "Improved Lower Bounds on Signal Parameter Estimation," in *IEEE Transactions on Information Theory*, vol. 21, no. 1, pp. 90-93, January 1975, doi: 10.1109/TIT.1975.1055325.

[GDZB+18] S. Gewies, and A. Dammann, R. Ziebold, J. Bäckstedt, K. Bronk, B. Wereszko, C. Rieck, P. Gustafson, C. Eliassen, M. Hoppe, and W. Tycholiz, (2018) R-Mode Testbed in the Baltic Sea. In: 19th IALA Conference 2018. 19th IALA Conference 2018, Incheon, South-Korea, https://elib.dlr.de/120702/

[HJZSZ15] Q. Hu, Y. Jiang, J. Zhang, X. Sun and S. Zhang, Development of an Automatic Identification System Autonomous Positioning System, 2015. doi:10.3390/s151128574

[IALA A-124] IALA Recommendation A-124 Appendix 18 “VDL Loading Management”

[IALA G-1139] IALA Guideline G1139, The Technical Specification of VDES, https://www.iala-aism.org/product/g1139-technical-specification-vdes/

[IALA R-129] IALA recommendation R-129 GNSS vulnerability and mitigation measures (edition 3.1), p. 15, December 2012. [Online]. Available: https://www.iala-aism.org/product/gnss-vulnerability-and-mitigation-measures-r-129/

[JS14] G. Johnson, P. Swaszek, Feasibility Study of R-Mode using AIS Transmissions, 2014. [Online]. Available: https://www.iala-aism.org/content/uploads/2016/08/accseas_r_mode_feasibility_study_ais_transmissions_part_2.pdf

[JU97] S. J. Julier and J. K. Uhlmann, “New extension of the Kalman filter to nonlinear systems,” ser. Proceedings Signal Processing, Sensor Fusion, and Target Recognition, vol. 3068, 1997, pp. 182–193. [Online]. Available: https://doi.org/10.1117/12.280797

[Kay93] S. M. Kay, Fundamentals of Statistical Processing, Volume I: Estimation Theory. Prentice Hall, 1993,

[R-MODE19] IALA GUIDELINE, G1139-ANNEX-R-MODE, VDES R-MODE 2019 ITU

[SGWW20] J. Safar, A. Grant, P. Williams, and N. Ward, Performance Bounds for VDES R-mode, Journal of Navigation, vol. 73, no. 1, 2020. https://doi.org/10.1017/S0373463319000559

[UMTS] 3GPP TS 25.213 V15.0.0, 2018, “Technical Specification Group Radio Access Network; Spreading and modulation (FDD)”.

[VDES15] ITU-R, M.2092-0, 2015, "Technical characteristics for a VHF data exchange system in the VHF maritime mobile band"

[VRPSD21] VDES R-MODE POSITIONING SYSTEM DEMONSTRATOR, GA5.3/5.4 project report, NIT, 2021

[WDR19] M. Wirsing, A. Dammann, and R. Raulefs. Investigating R-Mode signals for the VDE system. In OCEANS 2019 MTS/IEEE SEATTLE, Oct. 2019.

[WDR20] M. Wirsing, A. Dammann, and R. Raulefs. Designing a ranging signal for use with VDE R-Mode. In 2020 IEEE/ION Position, Location and Navigation Symposium (PLANS), June 2020.

[WDR21] M. Wirsing, A. Dammann, and R. Raulefs. VDES r-mode performance analysis and experimental results. International Journal of Satellite Communications and Networking, 2021